TECHNISCHE
UNIVERSITÄT
DRESDEN

Studies on polarization in the scattering of two vector bosons with the ATLAS experiment at the LHC

Masterarbeit
zur Erlangung des Hochschulgrades
Master of Science
im Master-Studiengang Physik

vorgelegt von

Jan-Eric Nitschke
geboren am 07.12.1995 in Dresden

Institut für Kern- und Teilchenphysik
Fakultät Physik
Bereich Mathematik und Naturwissenschaften
Technische Universität Dresden
2019

Eingereicht am 1. November 2019

1. Gutachter: Prof. Dr. Michael Kobel
2. Gutachter: Dr. Frank Siegert

Zusammenfassung

Zusammenfassung
Deutsch: Die Streuung zweier Vektorbosonen ist ein Prozess der sich sehr gut für die Untersuchung der elektroschwachen Symmetriebrechung eignet. Ohne ein Higgs-Teilchen oder einen anderen equivalenten Mechanismus verletzt der vorhergesagte Wirkungsquerschnitt der Streuung zweier longitudinal polarisierter Bosonen bei hohen Energien die Unitarität. Eine genaue Messung des Wirkungsquerschnitts dieses Prozesses kann Hinweise darauf geben, ob es sich bei dem beobachteten Higgs-Teilchen um das Standard Modell Higgs handelt oder wie Physik jenseits des Standard Models aussieht. Diese Arbeit untersucht wie die Polarisation der Vektorbosonen aus den mit dem ATLAS Detektor gemessenen Zerfallsprodukten extrahiert werden kann. Dafür werden zwei Arten der Erzeugung von Simulationen mit polarisierten Bosonen untersucht. Es wird gezeigt, dass der Ansatz mit Hilfe der narrow-width-approximation (sinngemäß: Näherung der schmalen Breite) bessere Ergebnisse liefert als die Methode des Umgewichten die in bisherigen ATLAS Publikationen verwendet wurde. Zuletzt wird die Empflindlichkeit verschiedener kinematischer Variablen auf die Polarisation der Bosonen untersucht. Für das Z Boson sind das der Cosinus des Zerfallswinkels sowie Variablen des rekonstruierten Teilchens. Die Polarisation des W Bosons lässt sich am besten durch Observablen seines Leptons oder des fehlenden Impulses bestimmen. Die Balance der transversalen Impulse der Jets ist sogar auf die Kombination beider Bosonen sensitiv.

Abstract
English: The scattering of two vector bosons is a process well suited for studying the mechanism of electroweak symmetry breaking. Without a Higgs boson or an equivalent mechanism the predicted cross section for the scattering of longitudinally polarized bosons violates unitarity at high energies. A precise measurement of the cross section of this process could eventually help us to understand if the observed Higgs boson behaves like a Standard Model one or might give us hints at new physics beyond the Standard Model. This work investigates how the polarization of the vector bosons can be extracted from the decay products measured with the ATLAS detector. To do this two methods of generating simulations of polarized bosons are studied. It will be shown that the approach of using the narrow-width-approximation is superior to the reweighting method used so far in ATLAS publications. Lastly the sensitivity of kinematic variables to the polarization of the bosons is investigated. For the Z boson these are the Cosine of the decay angle as well as variables related to the reconstructed particle. The W's polarization can be best measured with observables of its lepton as well as the missing transverse momentum. The balance of the jets transverse momenta is even sensitive to the combination of both bosons.

Contents

1 Introduction

Physics is the natural science that describes how matter interacts with each other and how these interactions affects their movement through space. Different areas of physics exist that deal with objects of different sizes and interactions. There are applied fields like medical physics[1] and biophysics[2] that deal with the physical aspects of medicine and biology. Condensed matter physics[3] mainly handles the physics of matter that is in its solid or liquid phase. One question these fields of physics don't directly deal with is the question whether or not there are objects, particles, that can not be subdivided into smaller ones and what their properties and interactions with each other are. The field that deals with this question is particle physics. As their name suggests atoms, Greek for 'unable to cut', were the first particles presumed to be fundamental.[4] This eventually proved to be false. As did some later hypothesis regarding fundamental building blocks, like nuclei or protons. Our current and very well tested theory for what these particles are and how they interact is called the Standard Model of particle physics (SM). It lists 18, or more depending on how one counts, elementary particles that make up everything in our universe. Although dark matter[5], dark energy[6] and some other things prove that this is not 100% the case the SM is currently still our best working theory as no alternative candidate has made further measured predictions.

The SM was established in the 1950s and 60s [7, 8, 9, 10, 11] and with the Higgs boson its last predicted particle was found in 2012 [12, 13]. This was done with the Large Hadron Collider (LHC) [14] at CERN. Since this was the last prediction of a particle by the SM, further tests of the theory have to be more precise measurements of the properties of these particles and their interactions. This includes overall cross sections as well as kinematics of particles after the collision. The particle content of the SM may be complete, but all of the predicted interactions of the particles have been observed so far. To gain a deeper understanding of the SM one approach is to try to measure those predictions. One of these ,predicted but rare processes, is the scattering of vector bosons (VBS) and specifically the scattering of the longitudinally polarized modes of the particles.

This process is of special interest because it is deeply linked to the electroweak (EW) symmetry breaking (EWSB) of the SM. The overall process of $W^{\pm}Z$ vector boson scattering has just recently been observed for the first time at the ATLAS[15] detector at the LHC in the final state of a leptonically decayed W and Z boson alongside two jets $W^{\pm}Zjj$ [16].

This works builds upon a previous thesis [17] and studies different methods of generating sim-

ulated data with polarized bosons, compares their results and use them to find the observables most suited to eventually observe the scattering of longitudinally polarized W and Z bosons. In this study on the leptonic decays of the bosons into electrons or muons is considered.
Chapter 2 of this thesis describes the theoretical foundation needed to follow the rest of the descriptions. This includes the above mentioned Standard Model of particle physics, specifically the EW theory and EWSB as well as how to extract measurable predictions out of it. An in depth discussion of polarization and what VBS is and why it is important are also part of this Chapter. In Chapter 3 the LHC and the ATLAS detector are described as the parameters of the simulations used in this work are strongly based on the properties of these two machines. Chapter 4 deals with how the simulated events are generated. Specifically which generators were used, what their strengths and weaknesses are and what exact purpose they served. Additionally it will be explained how exactly polarized events where extracted from these produced events. The explanation how the events were eventually processed and which phase spaces (PS) were used to analyze the data can be found in Chapter 5. The results of this analysis as well as the discussion of those is also part of this chapter. Lastly Chapter 6 gives a summary of this work as well as an outlook on future possibilities.

2 Theoretical Basics

To be able to make predictions and give hints where to look for yet undiscovered phenomena a physical theory has to be more than just a an assortment of measurements and an extrapolation between those but rather a model that combines all these measurements, explains links between those and ideally explains the underlying way according to which the real world functions. Such a theory can then make predictions about what happens in scenarios that could not be tested so far because of technical limitations and possibly predict differences from a simple extrapolation between already done measurements.

2.1 The Standard Model of Particle Physics

The Standard Model of particle physics (SM) is the theory that currently best describes the three fundamental interactions that play a significant role at the level of elementary particle physics. These are the strong interactions, the weak interaction and the electromagnetic one. It does not describe the fourth one, gravity, as it is too weak to probe at the scales we can currently deal with in particle physics.
To describes all of these things quantitatively the SM is a gauge quantum field theory with a local

$$SU(3)_C \times SU(2)_L \times U(1)_Y \tag{2.1}$$

gauge symmetry. This means that any term in the Lagrangian of the SM must be invariant under this symmetry. The invariance under this symmetry leads to conserved quantities as per Noether's theorem [18]. These are the electric charge, the weak hyper charge, the third component of the weak isospin and the (strong) color charge. The part of the SM that is responsible for the strong interaction is the SU(3) subgroup and if viewed separately called QCD [19, 20]. The remaining SU(2)xU(1) group deals with the electroweak interaction, combining the weak and the electromagnetic one. In the SM this symmetry is broken by the Higgs mechanism. How this happens as well as more information on the electroweak interaction in generally will be discussed in the following Section 2.1.1.
In addition the SM addresses which fundamental particles exist in our universe and how they each couple to these interactions.
These particles are separated into two main categories. The first one contains all particles with a half-integer spin. Those are called fermions, follow the Fermi–Dirac statistics and thus

describe 'matter particles'. Although only three of the 12 particles in this category make up the stable matter that we deal with in our everyday lives. These are the electron e^-, the up-quark u and the down-quark d. The last two make up protons p and neutrons n. For each of these particles there are two more with identical quantum numbers. The only differences are the mass. The three particles we encounter in every day live are part of the first generation. The identical ones with a bit more mass are part of the second and the ones with the most mass are in the third generation. The fermions can be divided further. Namely by which charges they hold or equivalently which interactions they take part in. Quarks interact via all three interactions. They have a color charge, an electric charge interact through the weak interaction. The particles that have no strong charge are called leptons. A second significant difference between leptons and quarks is that leptons have an integer electric charge and quarks have electric charges of multiples of $\frac{1}{3}$. However those one-third charges can never be seen directly as quarks can only be observed in color neutral configurations, which also always have integer electric charges. This property is called confinement [21]. The last so far unnamed group of particles in the SM are the neutrinos ν. There is one for each of the charged leptons. Neutrinos also fall into the category of leptons as they do not couple to the strong interaction. They do however have an electric charge of zero which means that they only interact through the weak interaction which also makes them not partake in every day life and also extremely difficult to detect and measure. A list of all the fermions in the SM as well as their properties can be found in Table 2.1. Additionally every Fermion has an associated antiparticle with the same mass and every quantum number reversed. For the electron there is the positron e^+, for the muon there is the antimuon μ^+ and so forth.

Generation	Fermion		Mass in MeV	(el. Charge, T_3)
1st	e^-	electron	0.511	$(-1e, -\frac{1}{2})$
	ν_e	electron-neutrino	$< 1.1 \times 10^{-6}$	$(\ 0e, \ \frac{1}{2})$
	u	up-quark	$2,16^{+0,49}_{-0,26}$	$(\ \frac{2}{3}e, \ \frac{1}{2})$
	d	down-quark	$4,67^{+0,48}_{-0,17}$	$(-\frac{1}{3}e, -\frac{1}{2})$
2nd	μ^-	muon	105.7	$(-1e, -\frac{1}{2})$
	ν_μ	muon-neutrino	< 0.19	$(\ 0e, \ \frac{1}{2})$
	c	charm-quark	93^{+11}_{-5}	$(\ \frac{2}{3}e, \ \frac{1}{2})$
	s	strange-quark	1270 ± 20	$(-\frac{1}{3}e, -\frac{1}{2})$
3rd	τ^-	tau	1776.86 ± 0.12	$(-1e, -\frac{1}{2})$
	ν_τ	tau-neutrino	< 18.2	$(\ 0e, \ \frac{1}{2})$
	t	top-quark	$(172.9 \pm 0.4) \times 10^3$	$(\ \frac{2}{3}e, \ \frac{1}{2})$
	b	bottom-quark	4180^{+30}_{-20}	$(-\frac{1}{3}e, -\frac{1}{2})$

Table 2.1: List of Standard Model fermions. For each one there exists an antiparticle with the same mass but all charges reversed. Values of the masses from [22].

The other major group of particles in the standard model are the bosons. They have integer spins and obey Bose–Einstein statistics. The majority of those are gauge bosons needed to conserve gauge invariance of the theory and mediate the fundamental forces between the fermions. These are the photon γ for the electromagnetic interaction, the W$^{\pm}$ and Z bosons for the weak interaction and the eight gluons g for the strong interaction. They are also called vector bosons as they all have a spin of 1. Throughout this thesis when a particle can be either of the first three it will be denoted by V.

The other one is the Higgs boson H which has a spin of 0 and plays a crucial role in how particles gain mass. Table 2.2 contains all of these particles, some of their properties and which fundamental force they mediate.

Interaction	Boson		Mass in GeV	el. Charge	Spin
electormagnetic	γ	photon	$< 1 \times 10^{-27}$	$0e$	1
weak	$W^{\pm}$	W bosons	80.379 ± 0.012	$\pm 1e$	1
	Z	Z boson	91.1876 ± 0.0021	$0e$	1
strong	g	gluons	0	$0e$	1
-	H	higgs	125.10 ± 0.14	$0e$	0

Table 2.2: Properties of all Standard Model bosons sorted by the interaction their are mediating. Values from [22].

2.1.1 Electroweak Theory and Symmetry Breaking

As proven by experiments the weak interaction violates parity. This means that it treats different chiralities differently [23]. To account for this in the unification of the electromagnetic and weak interaction the fermion fields have to be split into their left- and right-handed parts. This is done via the projections

$$\psi_{L/R} = \frac{1}{2}\left(1 \mp \frac{\gamma^5}{2}\right)\psi. \tag{2.2}$$

Here ψ stands for the four-component spinor of the Dirac field and γ^5 the fifth Dirac matrix (more in Appendix A.1). By construction the chirality projections obey

$$\psi_L + \psi_R = \psi. \tag{2.3}$$

In the SM the parity violation is then realized through the $SU(2)_L$ subgroup with the generators T_a. Each particle is then an eigenstate to T_3. For the left-handed fermions $T_a = \frac{1}{2}\sigma_a$ and for the right-handed fermions $T_a = 0$. Here σ_a stands for the pauli matrices (more in Appendix A.1. This means that the left-handed ones are represented by $SU(2)_L$ with an eigenvalue of T_3 of $\pm\frac{1}{2}$ and the right-handed ones as singles with an eigenvalue of 0. So the first generation leptons can be written as.

$$L_L^j = \begin{pmatrix} \nu_{e,L} \\ e_L \end{pmatrix} \qquad\qquad l_R = e_R. \tag{2.4}$$

For Quarks this works analogously with Q_L^j representing the left-handed doublet and u_R and d_R being the right-handed singlets. On top of that the weak hypercharge Y is introduced for each particle with

$$Q = Y + T_3. \tag{2.5}$$

With all of this the Lagrangian of the EW sector can be written as

$$\begin{aligned} \mathcal{L}_{ew} = &\sum_{j=1}^{3} i\overline{L}_L^j \not{D} L_L^j + i\overline{l}_R^j \not{D} l_R^j \\ &+ i\overline{Q}_L^j \not{D} Q_L^j + i\overline{u}_R^j \not{D} u_R^j + i\overline{d}_R^j \not{D} d_R^j \\ &- \frac{1}{4} W_{a,\mu\nu} W_a^{\mu\nu} - \frac{1}{4} B_{\mu\nu} B^{\mu\nu}, \end{aligned} \tag{2.6}$$

where

$$\not{D} = \gamma^\mu D_\mu \tag{2.7}$$
$$D_\mu = \partial_\mu + i g_W T_a W_\mu^a + i g_Y Y B_\mu \tag{2.8}$$

and

$$B_{\mu\nu} = \partial_\mu B_\nu - \partial_\nu B_\mu \tag{2.9}$$
$$W_{\mu\nu}^a = \partial_\mu W_\nu^a + \partial_\nu W_\mu^a + g_W \epsilon^{abc} W_\mu^b W_\nu^c. \tag{2.10}$$

Here ϵ^{abc} is the Levi-Civita symbol and W_μ^a B_μ and are the gauge fields of the $SU(2)_L$ and $U(1)_Y$ subgroups respectively.

The terms in the first two rows represent kinetic terms as well as terms of interactions with the gauge bosons. Gauge boson self interactions as well as their kinetic terms are described in the third row.

Due to the extra terms in the covariant derivative this Lagrangian is invariant under the transformation

$$\psi \to \exp(i(a(x)Y + \beta_a(x)T_a))\psi. \tag{2.11}$$

For this to hold true the gauge fields have to transform as well according to

$$B_\mu \to B_\mu - \frac{1}{g_Y}\partial_\mu \alpha \tag{2.12}$$

$$W^a_\mu \to W^a_\mu - \frac{1}{g_W}\partial_\mu \beta_a - \epsilon_{abc}\beta_b\beta_c. \tag{2.13}$$

As is this Lagrangian does not directly represent the physical world. This is obvious as at this moment no particle has a mass while in nature all the fermions [1] as well as the $W^\pm$ and Z boson have mass. Another aspect is that none of these particles can be either the photon or the Z boson as all these particles couple to neutrinos while the photon does not and all of these particles either treat left- and right-handed particles the same or do not couple to right-handed particles the same while the Z boson does neither.
To solve the first problem the one could naively introduce mass terms as

$$\mathcal{L}_{fermionmass} = m\overline{\psi}\psi \qquad \mathcal{L}_{bosonmass} = -\frac{1}{2}M_V^2 V_\mu V^\mu. \tag{2.14}$$

These however are not gauge invariant. To generate these mass terms a complex scalar $SU(2)_L$ doublet with $Y = \frac{1}{2}$ is introduced

$$\Phi = \begin{pmatrix} \Phi^+ \\ \Phi^0 \end{pmatrix}. \tag{2.15}$$

It has the gauge transformation

$$\Phi \to \exp(i\alpha(x)Y + i\beta_a(x)T_a)\Phi. \tag{2.16}$$

Additionally a potential is introduced with

$$V(\Phi) = -\mu^2\Phi^\dagger\Phi + \lambda(\Phi^\dagger\Phi)^2, \tag{2.17}$$

with the two real free parameters $\lambda, \mu > 0$ This makes the total Lagrangian for this field

$$\mathcal{L}_{Higgs} = |D_\mu\Phi|^2 + \mu^2\Phi^\dagger\Phi - \lambda(\Phi^\dagger\Phi)^2. \tag{2.18}$$

The minimum of this potential can be found as

$$|\Phi^0|^2 + |\Phi^+|^2 = \frac{\mu^2}{2\lambda}. \tag{2.19}$$

If one chooses $\Phi^+ = 0$ then

$$\Phi^0 = \sqrt{\frac{\mu^2}{2\lambda}} =: \frac{v}{\sqrt{2}}, \tag{2.20}$$

[1]It is still possible that one neutrino is massless. However, this is not expected.

which means that the vacuum expectation value for this field is

$$\Phi_0 = \frac{1}{\sqrt{2}} \begin{pmatrix} 0 \\ v \end{pmatrix} \tag{2.21}$$

This vacuum state however is not invariant under the full $SU(2)_L \times U(1)_Y$ symmetry. It is however invariant under the transformation

$$\Phi_0 \to \Phi_0' = \exp\left\{ i\theta(x) \begin{pmatrix} 1 & 0 \\ 0 & 0 \end{pmatrix} \right\} \Phi_0 \tag{2.22}$$

$$\approx (\mathbb{1} + i\theta(x) \begin{pmatrix} 1 & 0 \\ 0 & 0 \end{pmatrix} + ...)\Phi_0 \tag{2.23}$$

$$= \begin{pmatrix} 1 + i\theta(x) & 0 \\ 0 & 1 \end{pmatrix} \begin{pmatrix} 0 \\ \frac{v}{\sqrt{2}} \end{pmatrix} = \frac{1}{\sqrt{2}} \begin{pmatrix} 0 \\ v \end{pmatrix} = \Phi_0 \tag{2.24}$$

This matrix however is the sum of T_3 and $Y \times \mathbb{1}$

$$Q := \begin{pmatrix} 1 & 0 \\ 0 & 0 \end{pmatrix} = \frac{1}{2} \begin{pmatrix} 1 & 0 \\ 0 & -1 \end{pmatrix} + \frac{1}{2} \begin{pmatrix} 1 & 0 \\ 0 & 1 \end{pmatrix} = T_3 + Y \tag{2.25}$$

So it is invariant under the new subgroup

$$SU(2)_L \times U(1)_Y \to U(1)_Q \tag{2.26}$$

If one expands this doublet around it vacuum value one generally gets

$$\Phi = \begin{pmatrix} \theta_2(x) + i\theta_1(x) \\ \frac{1}{\sqrt{2}}(v + H(x)) + i\theta_3(x) \end{pmatrix}, \tag{2.27}$$

with H and $\theta_1, \theta_2, \theta_3$ as real scalar fields. Using gauge invariance this can be transformed into

$$\Phi = \frac{1}{\sqrt{2}} \begin{pmatrix} 0 \\ v + H(x) \end{pmatrix}. \tag{2.28}$$

Inserting this into Equation 2.18 yields

$$\mathcal{L}_{Higgs} = |D_\mu \begin{pmatrix} 0 \\ \frac{v+H(x)}{\sqrt{2}} \end{pmatrix} |^2 + \mu^2 \begin{pmatrix} 0 & \frac{v+H(x)}{\sqrt{2}} \end{pmatrix} \begin{pmatrix} 0 \\ \frac{v+H(x)}{\sqrt{2}} \end{pmatrix} - \lambda(\begin{pmatrix} 0 & \frac{v+H(x)}{\sqrt{2}} \end{pmatrix} \begin{pmatrix} 0 \\ \frac{v+H(x)}{\sqrt{2}} \end{pmatrix})^2. \tag{2.29}$$

Focusing on the first term results in

$$|D_\mu\Phi|^2 = \frac{1}{2}|(\partial_\mu + ig_W\frac{\sigma_a}{2}W_\mu^a + ig_Y Y B_\mu)\begin{pmatrix}0\\ v+H(x)\end{pmatrix}|^2 \tag{2.30}$$

$$= \frac{1}{2}|\begin{pmatrix}\partial_\mu + \frac{i}{2}(g_W W_\mu^3 + g_Y Y B_\mu) & \frac{ig_W}{2}(W_\mu^1 - iW_\mu^2)\\ \frac{ig_W}{2}(W_\mu^1 + iW_\mu^2) & \partial_\mu - \frac{i}{2}(g_W W_\mu^3 - g_Y Y B_\mu)\end{pmatrix}\begin{pmatrix}0\\ v+H(x)\end{pmatrix}|^2 \tag{2.31}$$

$$= \frac{1}{2}(\partial_\mu H)^2 + \frac{1}{8}g_w^2(v+H)^2|W_\mu^1 - W_\mu^2|^2 + \frac{1}{8}(v+H)^2|g_W W_\mu^3 - g_Y B_\mu|^2 \tag{2.32}$$

Here the first term obviously represents the kinetic term for the Higgs boson and the other two represent some sort of mass and interaction terms for the gauge bosons. To get physical mass states this mass matrix has to be diagonalized. The result of that are the four particles defined as

$$W_\mu^\pm = \frac{1}{\sqrt{2}}(W_\mu^1 \mp iW_\mu^2) \tag{2.33}$$

$$Z_\mu = \frac{g_W W_\mu^3 - g_Y B_\mu}{\sqrt{g_W^2 + g_Y^2}} \tag{2.34}$$

$$A_\mu = \frac{g_W W_\mu^3 + g_Y B_\mu}{\sqrt{g_W^2 + g_Y^2}}. \tag{2.35}$$

This changes the last two terms to

$$(v+H)^2(\frac{g_W^2}{4}W_\mu^+ W^{-\mu} + \frac{g_W^2 + g_Y^2}{8}Z_\mu Z^\mu + 0A_\mu A^\mu). \tag{2.36}$$

The Terms proportional to v^2 represent the mass terms of the particles while those proportional to vH and H^2 deal with coupling of one or two Higgs bosons to a pair of the vector bosons. The masses are now easily read off as

$$m_W = \frac{1}{2}g_W v \tag{2.37}$$

$$m_Z = \frac{1}{2}v\sqrt{g_W^2 + g_Y^2} \tag{2.38}$$

$$m_A = 0. \tag{2.39}$$

These particles now represent the physically measured particles with their masses. This means that they also have to correctly describes their interactions with other particles. One example that this is the case is that the A field does not couple to neutrinos at all just like the real photon.

The last part left to discuss is the potential.

$$\mathcal{L}_{HiggsPot} = \mu^2\Phi^\dagger\Phi - \lambda(\Phi^\dagger\Phi)^2. \tag{2.40}$$

With $\Phi = \frac{1}{\sqrt{2}} \begin{pmatrix} 0 \\ v+H \end{pmatrix}$ and $v^2 = \frac{\mu^2}{\lambda}$ this results in

$$\frac{\lambda v^2}{2}(v+H)^2 - \frac{\lambda}{4}(v+H)^4 \tag{2.41}$$

$$\rightarrow \frac{\lambda v^2}{2}H^2 - \frac{\lambda}{4}(6v^2H^2 + 4vH^3 + H^4) \tag{2.42}$$

$$= -\lambda v^2 H^2 - \lambda v H^3 - \frac{\lambda}{4}H^4 \tag{2.43}$$

Here the first term corresponds to $\frac{m_H^2}{2}$ and the other two to triple and quartic Higgs self coupling.
This means the mass of the Higgs boson can be written as

$$m_H = \sqrt{2\lambda} v \tag{2.44}$$

The value of the vacuum expectation value v can be measured in Muon decays using Equation 2.37 is determined to approximately 246 GeV. Combined with the measured Higgs mass of (125.10 ± 0.14) GeV a value for λ can be calculated. With that all the values of the Higgs self coupling are know whose measurement can be another test of the SM that will however not be discussed in this thesis.
Finally Yukawa couplings are introduced by hand to account for the fermion masses as

$$\mathcal{L}_Y = \sum_{j=1}^{3} y_l^j \overline{L}_L^j \Phi l_R^j + y_u^j \overline{Q}_L^j i\sigma_2 \Phi u_R^j + y_d^j \overline{Q}_L^j \Phi d_R^j + h.c. \tag{2.45}$$

Those combined with the not discussed Lagrangian of QCD gives the total SM Lagrangian as

$$\mathcal{L}_{SM} = \mathcal{L}_{ew} + \mathcal{L}_{Higgs} + \mathcal{L}_Y + \mathcal{L}_{QCD}. \tag{2.46}$$

2.1.2 Cross Sections and Event Numbers

To test whether the SM or any other theory is the one realized in nature we can not directly test if the Lagrangian is the true one since we can not measure it in any experiment. To get measurable prediction we have to find all Feynman graphs that connect our initial state with our finale state. After that one has to employ Feynman rules to convert these into matrix elements $\mathcal{M}$. For every process there exist an infinite number of feynman diagrams. These can be ordered by the number of fundamental couplings $\alpha_s, \alpha W, \alpha em$. As long as these couplings are smaller than 1 diagrams of a higher order in these couplings will contribute less and less to the final matrix element. If one only considers diagrams of the lowest order these predictions are of 'leading order' (LO).

From these matrix elements one can obtain the cross section for the process of interest as

$$d\sigma \propto |\mathcal{M}^2| d\Phi. \tag{2.47}$$

Here $d\Phi$ is the differential volume of the phase space one is considering and $d\sigma$ the differential cross section.

From that one can finally calculate an event rate which is what can be observed in experiment. This even rate is given by

$$\dot{N} = \sigma \cdot \mathscr{L}. \tag{2.48}$$

$\mathscr{L}$ stand for the Luminosity which involved accelerator and detector effects.

Since this thesis is based on the LHC accelerator the Luminosity of this machine is needed to calculate the measured event rates. It is given by[14]

$$\mathscr{L} = \frac{N_B^2 n_b f_{rev} \gamma_r}{4\pi \epsilon_n \beta^\star} F, \tag{2.49}$$

where N_b is the number of particles per bunch, n_b the number of bunches per beam, f_{rev} the revolution frequency, γ_r the relativistic gamma factor, ϵ_n the normalized transverse beam emittance, β^* the beta function at the collision point and F the geometric reduction factor due to the crossing angle at the interaction point.

2.2 Polarization

Polarization describes the alignment of a particle's spin with a given direction. Here this direction is chosen as the one defined by the momentum of the particle. This is quantified using the helicity h defined as the projection of the spin S onto said direction of the particle's momentum $\vec{p}$

$$h = \vec{S} \cdot \frac{\vec{p}}{|p|}. \tag{2.50}$$

The helicity of a particle is only Lorentz invariant if that particle is massless and thus always travels at the speed of light. If it has a mass then one can boost into a frame where the particle is moving in the opposite direction while the spin retains its. This means that the helicity of the particle switches. Due to this one has to be careful to keep track of the frame in which the helicity was defined in. The laboratory frame is a common choice for this frame but it will not be the only frame considered in this work.

For a particle with spin S and a mass greater than 0 there are $2S + 1$ possible eigenvalues for its helicity. Massless particles can only have a helicity of $\pm S$. Since $W^\pm$ and Z bosons are massive and have spin 1 the three possible values for h are 0 and ± 1. The first one means that the spin is orthogonal to the direction of the momentum and is called longitudinally polarized and particles with this helicity will be denoted by V_L. A helicity of ± 1 corresponds to a spin aligned/antialigned with the direction of momentum. These are called right and left-handed polarizations or taken together referred to as transversal polarization. Particles with either of these helicities are written as V_T.

2.3 Vector Boson Scattering

As discussed in Section 2.1.1 Equation 2.6 contains terms describing triple and quartic gauge boson self interactions. This chapter deals with a special set of processes that not only contain the triple couplings like some other processes but also crucially the quartic gauge boson self interactions.

2.3.1 Definition

The process of massive vector bosons scattering off each other many interesting aspects of the SM. The cross section for VBS as predicted by the SM is very small, making this process particularly challenging to measure experimentally. The reason why it has just now become a big focus is because with the LHC there is enough statistics to measure it.
The process of interest of this thesis is the direct scattering of a $W^{\pm}$ and a Z boson. There is a variety of feynman diagrams contributing to this interaction.
There are two diagrams involving the triple vertex, one containing the quartic vertex and lastly one with the Higgs. These are shown in Figure 2.1.

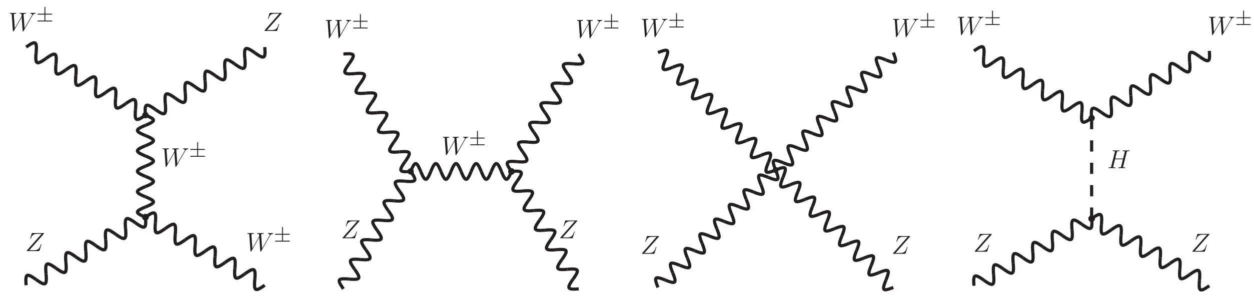

Figure 2.1: Feynman diagrams for the scattering of a $W^{\pm}$ and a Z boson.

Since the LHC can not produce and accelerate the gauge bosons directly and because they decay before they can reach any detector the actually studied processes and diagrams are not as simple.
To generate a $W^{\pm}$ or a Z boson at a $p-p$ accelerator like the LHC they have to be radiated off the initial state quarks. These quarks propagate through to the final state where the detector will eventually see them as jets. Since the jets are produced only via through the weak force they are deflected only slight and thus have a very tight angular separation from each other as well as an extremely high invariant mass. Both of these are very characteristic

to VBS and allow for a good separation of signal and background, which is a reason for why these processes can be studied despite their tiny cross sections. On top of that the bosons have to decay. They can do this either hadronically into quarks or into one of the three lepton flavours. In this thesis only the decay into electrons or muons and their corresponding antiparticles and neutrinos will be studied. Including other channels would add a considerable amount of cross section. However each additional channel would also introduce other problems either in form of more jets and/or more missing energy which would complicate the complete event reconstruction even further.
This means that the total final state that will be looked at is $\ell_1^{\pm}\nu_{\ell_1}\ell_2^{-}\ell_2^{+}jj$. Whether the neutrino is a particle or antiparticle can be easily identified by the charge of the corresponding lepton. Due to this and for readability reason the distinction will not be made in this thesis. A depiction of this whole process is shown in Figure 2.2. Hereby the black blob represents the diagrams shown in Figure 2.1.

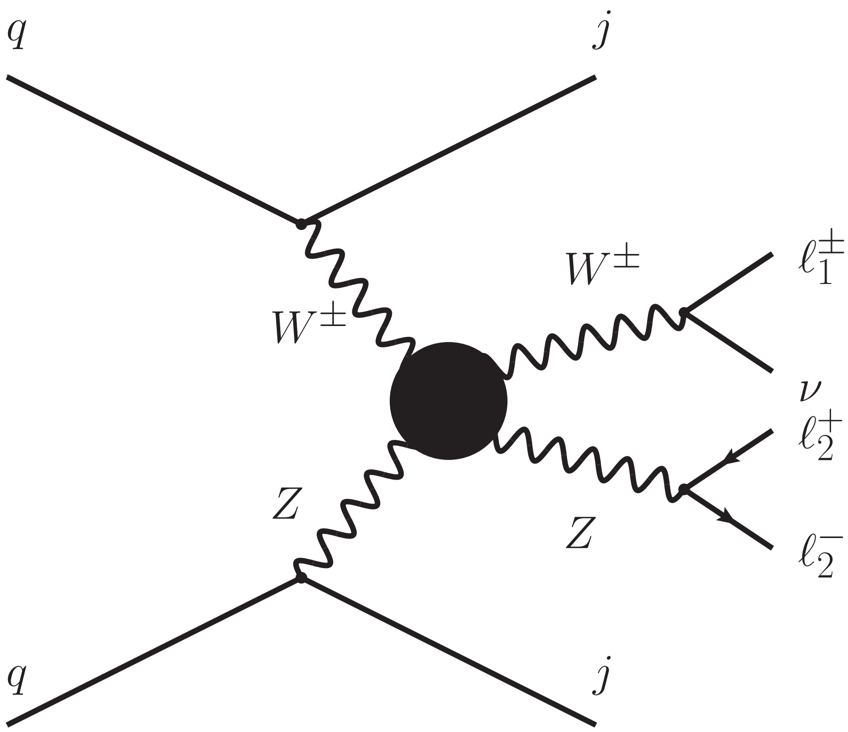

Figure 2.2: Feynman diagram for the scattering of a $W^{\pm}$ and a Z boson as realized at the LHC. All initial state quarks are denoted with 'q' but do not have to have the same flavour or charge.

Given a final state it is not possible to know which diagram lead to it as they all play a partial role and interfere with each other. For this reason other diagrams have to be considered when trying to study VBS. The first big group of other diagrams are those that share the coupling order of the VBS processes, which is $\mathcal{O}(\alpha_{EW}^6)$. Since not all of these diagrams, some are shown in Figure 2.3, can be separated from the VBS diagrams in a gauge invariant way they have to be considered as signal and are denoted by $WZjj - EW$.

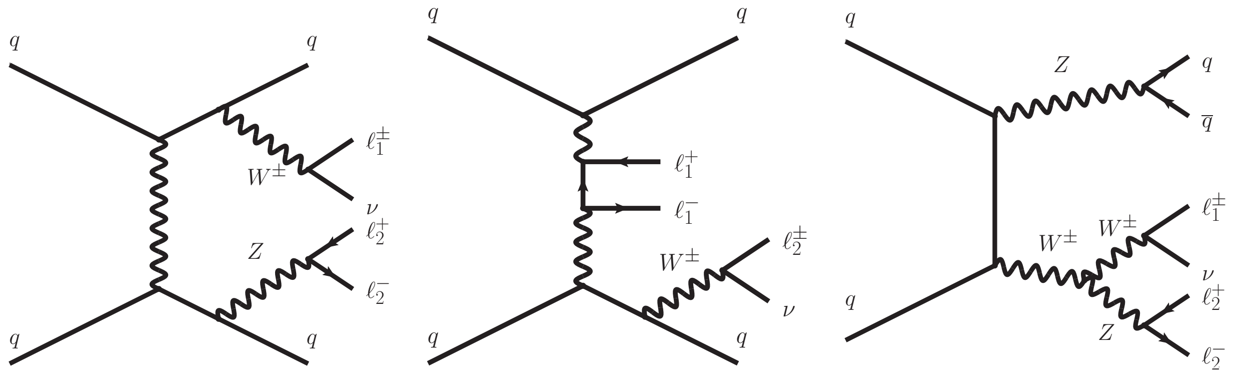

Figure 2.3: Non-VBS diagrams with the same coupling order and final state. All initial and final state quarks are denoted with 'q' but do not have to have the same flavour or charge.

To increase the proportion of the VBS diagrams another restriction is applied. Neither the intial- nor the final state can not contain any b quarks. This is because b quarks in the initial state lead to a top quark resonance that contributes a considerable amount to the final cross section but does not contain any scattering of vector bosons. This process is often called tZj and depicted in Figure 2.4.

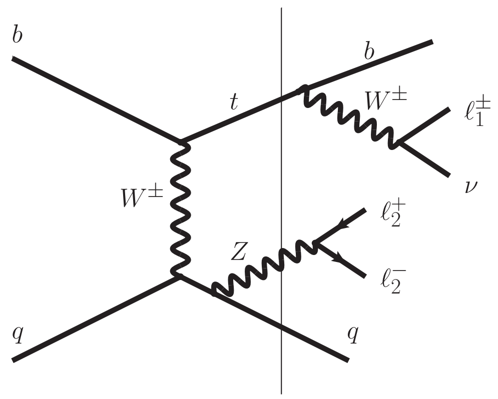

Figure 2.4: Feynman diagram of the tZj process (left of the vertical line) with subsequent decays (right of the line). The 'b' and 't' quarks are allowed to have both charges.

Diagrams of the order $\mathcal{O}(\alpha_{EW}^4\alpha_s^2)$ can also result in the same final state as can be seen in Figure 2.5. These can be separated from the other ones in a gauge invariant way and are thus not counted as signal but as background. Since there is no difference between their final states this is part irreducible background. This contribution is called $WZjj-QCD$. Other processes that are part of the irreducible background all that do not share the same 'true' final state but the same detector final state with three leptons, two jets and missing energy. This happens in the process $ZZ \to 4\ell$ where one lepton is outside the detector acceptance, the previously mentioned tZj, WWW and

Additionally there is reducible background which happens due to falsely reconstructed objects. In principle this background can be reduced with a better detector or better object

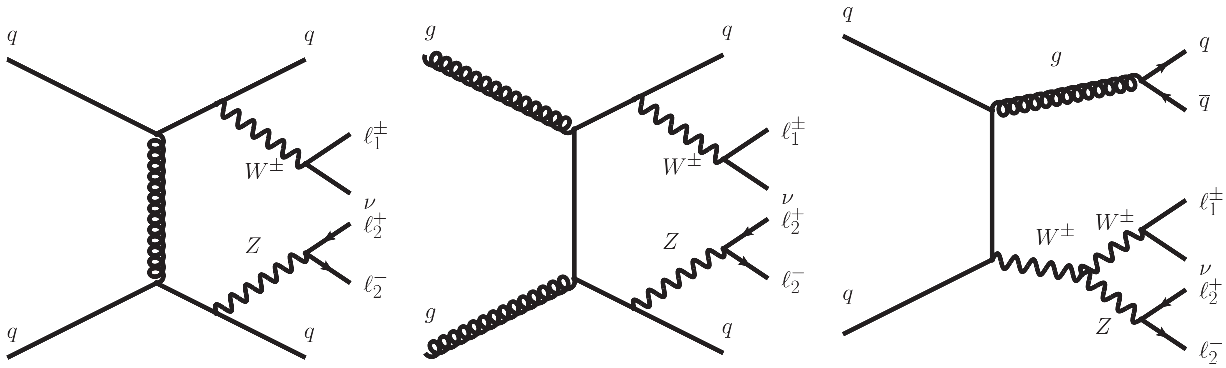

Figure 2.5: Feynman diagrams with the same final state but a different coupling order. All initial and final state quarks are denoted with 'q' but do not have to have the same flavour or charge.

reconstruction. A more in depth discussion can be found in [24].

2.3.2 Polarization in VBS

$W^{\pm}Z$ VBS is extremely sensitive to the exact mechanism by which EWSB takes place. This is because without the contributions from the SM Higgs the scattering of these bosons grows steadily with the center of mass energy of the initial particles. For large enough energies this would violate the unitarity limit. Which would mean that the scattering has a probability larger than 1. It is very interesting to study polarization in this process because this unitarity violation is solely due of the scattering of the longitudinal modes, specifically $W_L^{\pm}Z_L \rightarrow W_L^{\pm}Z_L$. This can be seen in Figure 2.6.

To study longitudinal VBS it is necessary to draw conclusions about the polarization of the bosons based on the observed final state.

The parity violating nature of the weak interaction provides for a couple of possibly sensitive observables. One that is easy to visualize is the angular distribution of the finale state leptons. Since a W^+ only couples to right-handed antiparticles this means that the positron that results from its decay is right-handed. Since it has such a small mass compared to the W boson it can basically be viewed as massless and will thus also have a right-handed helicity. Which means that it will travel in the direction of its spin. Due to conservation of angular momentum this will also align with the boson spin. Thus, if the boson was polarized in a right-handed way the positron will be emitted in the boson's direction of flight. A depiction of this can be found in Figure 2.7.

To properly quantify this the decay angle θ_V^* is introduced. It describes the angle between the lepton's momentum in the boson's rest frame and the direction of the boson's momentum boosted into the boson's rest frame. For Z bosons the negatively charged lepton is considered. A visualization of this definition can be seen in Figure 2.8.

If the momentum of the boson is considered in the same frame as its helicity has been defined

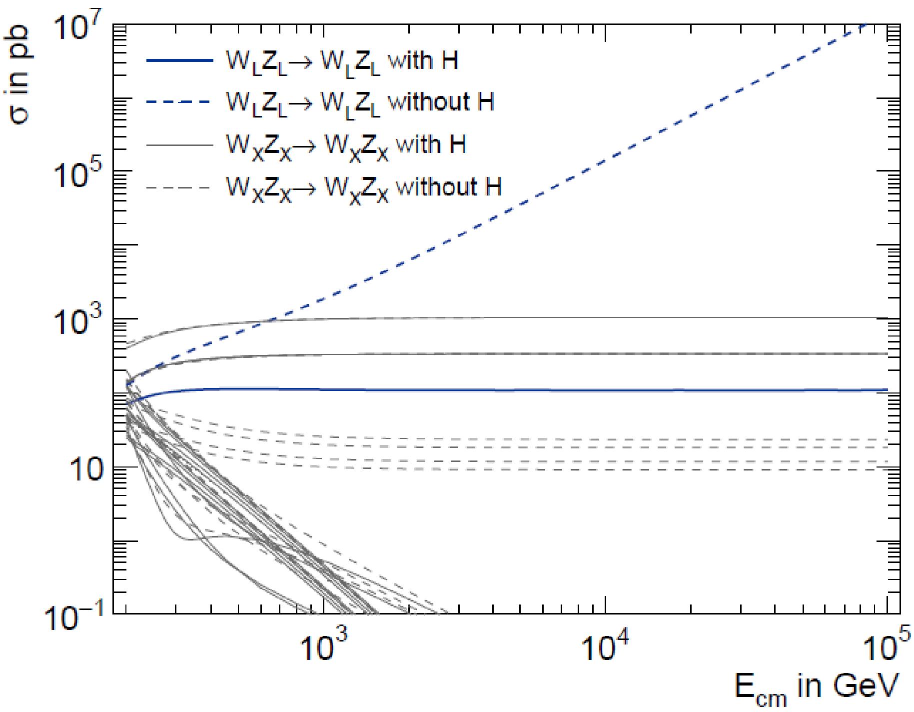

Figure 2.6: Cross section for the scattering $WZ \to WZ$ depending on the center-of-mass energy [17]. The blue lines depict the cross section for the scattering of two longitudinal bosons to longitudinal bosons while the gray line show all other possible combinations.

the analytically expected distribution for θ_V^* for a mixture of polarized bosons can be given as [25]

$$\frac{1}{\sigma}\frac{\mathrm{d}\sigma}{\mathrm{d}\cos\theta_W^*} = \frac{3}{8}\left(1 \mp \cos\theta_W^*\right)^2 f_{-1} + \frac{3}{8}\left(1 \pm \cos\theta_W^*\right)^2 f_{+1} + \frac{3}{4}\sin^2\theta_W^* f_0 \tag{2.51}$$

and

$$\begin{aligned}\frac{1}{\sigma}\frac{\mathrm{d}\sigma}{\mathrm{d}\cos\theta_Z^*} = &\frac{3}{8}\left(1 + \cos^2\theta_Z^* - \frac{2(c_L^2 - c_R^2)}{(c_L^2 + c_R^2)}\cos\theta_Z^*\right) f_{-1} \\ &+ \frac{3}{8}\left(1 + \cos^2\theta_Z^* + \frac{2(c_L^2 - c_R^2)}{(c_L^2 + c_R^2)}\cos\theta_Z^*\right) f_{+1} + \frac{3}{4}\sin^2\theta_Z^* f_0\end{aligned} \tag{2.52}$$

for a $W^\pm$ and a Z boson respectively. Here f_i denoted the fraction of each polarization in the mixture of helicities and c_L and c_R the right- and left-handed couplings of the fermion to the Z. As can be seen in Figure 2.9 the reasoning above holds as for right-handed W^+ bosons the positron is primarily emitted in the forward direction.

In general it is not enough to consider the helicity fractions if one is dealing with quantum mechanical spin systems. The use of the full spin density matrix is necessary to properly include statistical and quantum mechanical effects. For the system of two massive vector bosons the spin density matrix is a 9×9 matrix. The diagonal elements correspond to the combination of the helicity fractions of the two bosons. Currently there is no format or program that can

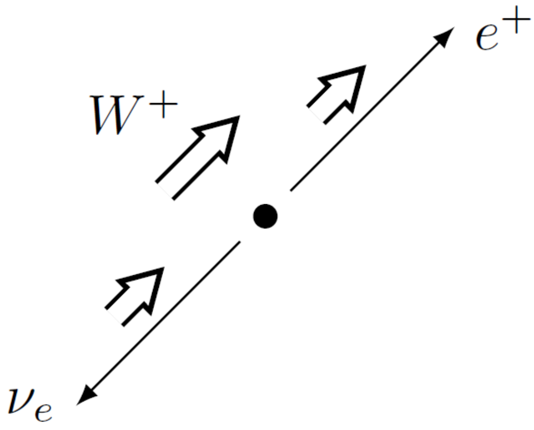

Figure 2.7: Visualization of the spins and momenta in the decay of a W^+ boson [17].

handle polarized decays using the full spin density matrix in a way where the polarization is known at the end. Due to this Equations 2.51 and 2.52 are sufficient for this thesis. A slightly more in depth discussion of the spin density matrix can be found in [17].

Just as the polarization leads to measurable differences in the decay process of the bosons there are equivalent effects in their production. As with the leptons a W^+ also only couples to left-handed quarks and right-handed antiquarks. This means that the spin of quarks is antialigned with the direction of their momentum. Since the deflection of the quarks is small for VBS processes their spin vector does not change much at all. Thus, the boson's spin vector is orthogonal to the quark's direction of movement. If the boson is also emitted orthogonally then it will be left- or right-handed. If it is emitted forward or backward it will be longitudinally polarized. Due to this those tend to have a higher absolute rapidity and lower transverse momenta. Energy and momentum conservation cause a similar effect on the momenta of the jets. If the boson has a low transverse momentum so does the jet.

The last point only holds true if the bosons do not change helicity between production and decay. This however does not have to be the case as the scattering of the bosons can change their helicity. For the direct scattering of on-shell bosons with defined helicity states going into the scattering this was discussed in Reference [17]. The cross sections for scattering into longitudinal bosons depending on the helicity of the particles going into the scattering can is listed in Table 2.3. While the cross section of other production modes it not negligible the most likely initial state is still $W_L Z_L$. For VBS as it happens at the LHC it has been shown that

	Initial state			
	$WLZL$	$WTZL$	$WLZT$	$WTZT$
σ [pb]	94.46 ± 0.03	12.81 ± 0.03	14.810 ± 0.003	6.648 ± 0.003

Table 2.3: List of cross sections of $W_X Z_X \to W_L Z_L$ scattering for all initial state helicity combination at a center-of-mass energy of the di-boson system of 250 GeV [17].

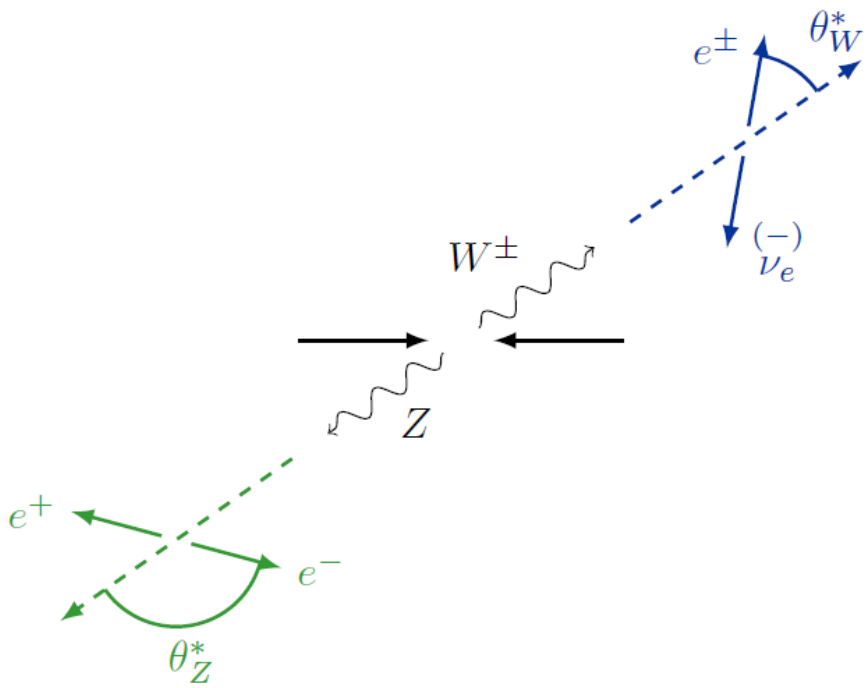

Figure 2.8: Visualization of the definition of the decay angle. The black lines are in the frame the helicity was defined in. The coloured lines are then boosted from there to the rest frame of the boson [17].

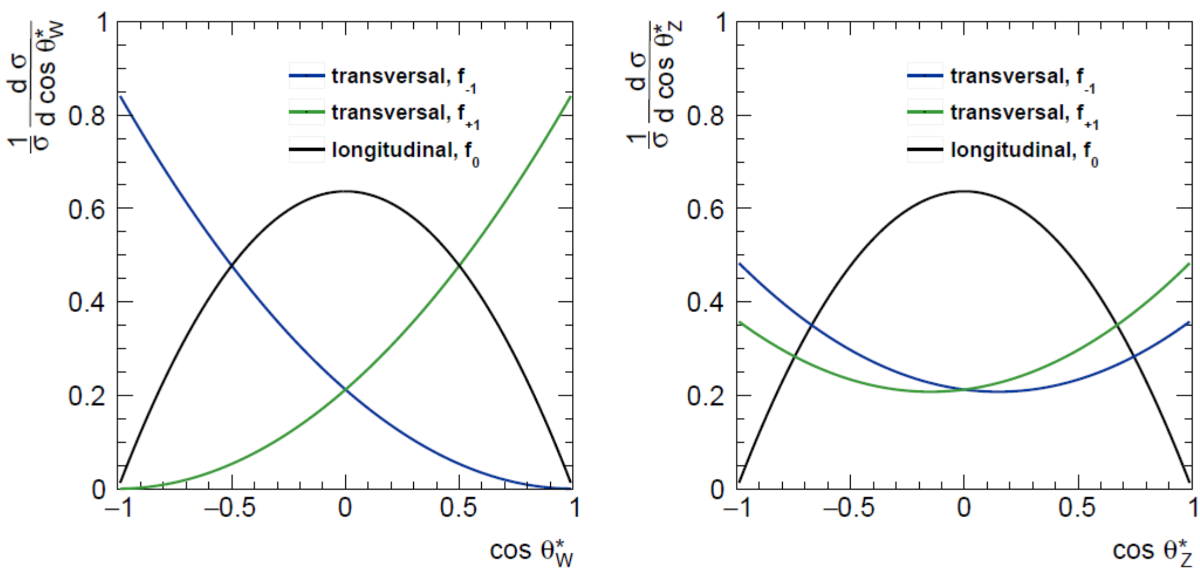

Figure 2.9: Normalized distributions of the cross section over the decay angle for a given helicity. W^+ boson on the left and Z boson on the right [17].

separating the helicities of the bosons going into the scattering proves problematic as most diagrams in $WZjj - EW$ do not have initial bosons [26]. Choosing a specific polarization for the initial bosons in the VBS diagrams has a strong effect on the interferences with these diagrams causing faulty predictions. For this reason the helicity of initial bosons is not studied in this work. Only the polarization of the final state bosons and its effect on kinematic observables of leptons, bosons and jets is investigated.

3 Experiment

This thesis is based purely on simulated results and does not use any data taken at the LHC or with the ATLAS detector. Nevertheless, the simulation of the collisions as well as the phase space used to analyse the generated events are heavily based on the actual setup of the LHC and those used in ATLAS analysis. That is why the basics of how the LHC and the ATLAS detector work are explained in this chapter.

3.1 LHC

The LHC [14] is the most powerful particle accelerator in the world. Its construction was approved in 1994 and eventually built between 2000 and 2008. It reuses the 26.7 km long tunnel originally designed and built for the Large Electron-Positron collider (LEP). Due to this it resides at the European Organization for Nuclear Research (CERN French: Organisation Européenne pour la Recherche Nucléaire) close to Geneva. The majority of the ring was built under french territory and can be found in a depth of 45 to 170 m under ground. The accelerator has a total slope of 1.4 %. The original tunnel had eight crossing points surrounded by Radio Frequency cavities to accelerate the particles again since they loose a lot of energy to synchrotron radiation. For protons this energy loss is significantly less. Thus it was decided to only use 4 of those interaction points. These hosts the four main experiments at the LHC. The general purpose detectors ATLAS [15] and CMS [27] and the two more specialized ones ALICE [28] and LHCb [29]. A total of 9593 magnets are used to accelerate the particles, keep them on their track and to focus the bunches of particles in the beam pipe. 1232 of those constitute the main dipole magnets used for acceleration. These superconducting magnets are operated at a temperature of 1.9 K. The LHC collides two beams of protons with 6.5 TeV each of which corresponds to a velocity of 99.999 999 1 % the speed of light. It is not possible for a single accelerator to bring the particles from rest to this velocity. This means that the protons have to enter the LHC at a velocity that is already fairly close to the speed of light. To achieve this a couple of pre accelerators are used. Firstly the linear accelerator LINAC 2 accelerates the protons that come form a simply hydrogen bottle to 50 MeV and hands them off to the Proton Synchrotron Booster (PSB) where the energy is increased to 1.4 GeV. From there they are fed into the Proton Synchrotron (PS) and then into the Super Proton Synchrotron where they reach energies of 26 GeV and 450 GeV respectively. Lastly the protons enter the LHC itself. They do so in 'bunches' of 1.2×10^{11} protons per bunch. At each point in time there are 2808 bunches in each of the two beams of the LHC. These are then made to cross at the four collision points whereby roughly 20 to 40 protons collide in each crossing. They do so with a total center of mass energy of 13 TeV. This high number of collision causes interesting high-energy collisions to be contaminated by multiple one with lower energy. This is known as pile-up. A schematic view of the LHC as well as the pre-accelerators and positions of the experiments can be found in Figure 3.1

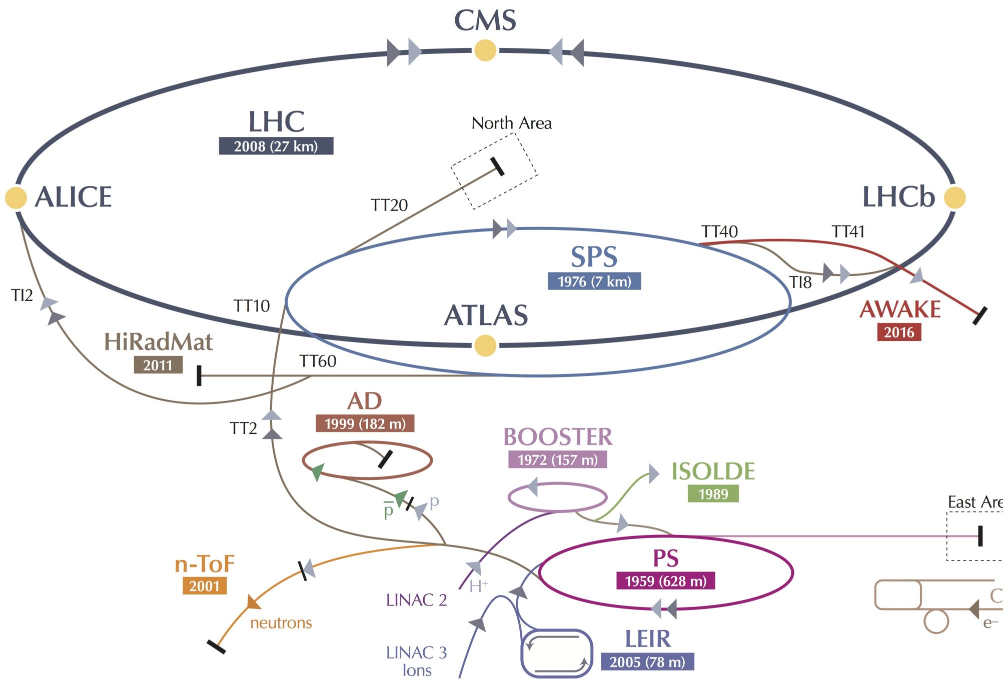

Figure 3.1: Schematic view of the LHC and its main experiment. Also shown are the pre-accelerators and other experiments at CERN [30].

3.2 ATLAS

The ATLAS detector is one of the four total detectors at the LHC and one of the two main purpose detectors. It is 25 meters high and 44 meters long and is build to study a plethora of different physics processes, from almost all SM effects to supersymmetry to searches for dark matter.

A cut-away view of the ATLAS detector can be found in Figure 3.2. To be able to fulfill all of these requirements the ATLAS detector consists of a multitude of separate detectors, each optimized to detect and measure specific particles and their properties. These is discussed in this Chapter. Information is taken from reference [15].

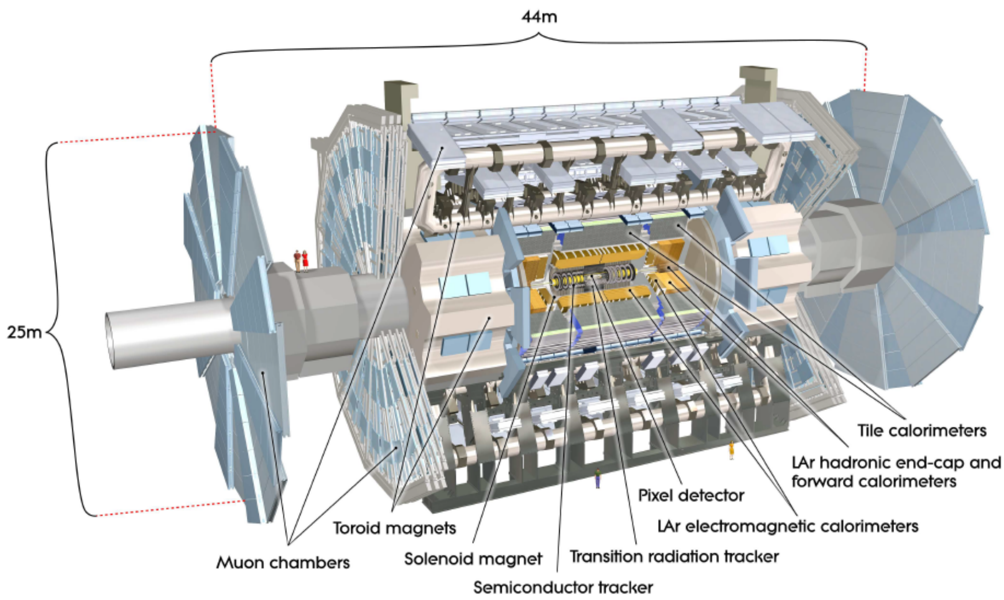

Figure 3.2: Cut-away view of the ATLAS detector [15].

3.2.1 Coordinate system

To be able to compare results between different groups and processes the ATLAS detector uses a specific coordinate system. A right-handed Cartesian coordinate system is used. The x-axis points towards the center of the LHC, the y-axis points upwards and the z-axis point along the beam axis. Additionally ϕ,θ and R are used as well. Here ϕ is the angle from the projection onto the transverse plane to the x-axis. θ is the angle between the point and the z axis. Lastly R is smallest distance between the z axis and the point. Since the LHC is a proton proton collider the total momentum of the event along the z axis is not known. This is due to each quark containing a random fraction of the momentum of the proton. This leads to the need to use observables that are invariant under boosts along the z axis. One way to do this is to use observables that only deal with the transverse plane and completely disregard the z axis to begin with. For example the transverse momentum p_T which is the projection of the momentum onto said plane. The other option is to build more complicated variables. To properly describe the angles or particles one needs to use this approach. The commonly used one is the rapidity y

$$y := \frac{1}{2}\ln\left(\frac{E+p_z}{E-p_z}\right). \tag{3.1}$$

While rapidity itself is not invariant under said boosts differences in rapidity are. A common replacement for the rapidity is the pseudo-rapidity η

$$\eta := -\ln\tan\left(\frac{\theta}{2}\right). \tag{3.2}$$

It has the advantage of being easier to calculate but the disadvantage that it is only equal to the actual rapidity for particles that can be treated as massless. A combination of these two angles is used regularly as well. Namely the angular distance δR

$$\Delta R := \sqrt{(\Delta\phi)^2 + (\Delta\eta)^2} \tag{3.3}$$

Although the ATLAS detector has many different system to detect a wide range of different particles it is unable to detect neutrinos as they only interact via the weak force and thus basically do not deposit any energy in the detector material what so ever. The initial partons of a collision have negligible transverse momentum. Conservation of momentum can be used to sum up the transverse momenta of the final state particles to zero. If this is not the case there was either a mistake in the measurement of the particles momenta or a particle passed the detector without being measured at all. This discrepancy in the transverse momentum is called p_T^{miss} or missing transverse momentum. In processes like VBS with one neutrino this can be used to infer its transverse momentum. However this can not be used to reconstruct their full momenta due to the already mentioned fact that an events total momentum in the z axis is not accessible at the LHC.

3.2.2 Tracking

Since the LHC operators at such a high center of mass energy and $20 - 40$ protons collide at each bunch crossing the detector has to deal with thousands of particles every couple of nanoseconds. To be able to do proper analysis each particle has to be traced back to which of the initial proton collisions it comes from. To achieve this ATLAS has an Inner Detector (ID) (see Figure 3.3)that contains Pixel and silicon microstrip (SCT) trackers as well as a Transtition Radiation Tracker (TRT) which are embedded in a 2 T magnetic field generated by a central solenoid. The inner detector spans a length of 6.2 m and has a height of 2.1 m. The pixel detectors and the SCT cover a region of $|\eta| < 2.5$. In the barrel region the pixel detectors are laid out on concentric cylinders around the beam axis. In the end-cap region they are placed on disks perpendicular to it. Each track usually crosses three layers of the pixel detectors. In the barrel region they offer an accuracy of 10 µm in the $R - \phi$ plane and 115 µm in the z direction. In the disks the 115 µm apply to the R direction.
Additionally each track crosses eight layers of the SCT. In the barrel regions the strips are placed parallel to the beam direction. At the end-caps there are some running radially and some placed at an angle of 40 mrad. Their accuracy is 17 µm$(R - \phi)$ and 580 µm(z/R)
Surrounding these two are the straw tubes of the TRT measuring 4 mm in diameter. Each track leaves roughly 36 hits in this detector. The TRT spans a smaller angle of only up to $|\eta| = 2.0$. It provides information about the $R - \phi$ planes with an accuracy of 130 µm
All of these detector types are needed to achieve a maximum track resolution needed for pile-up

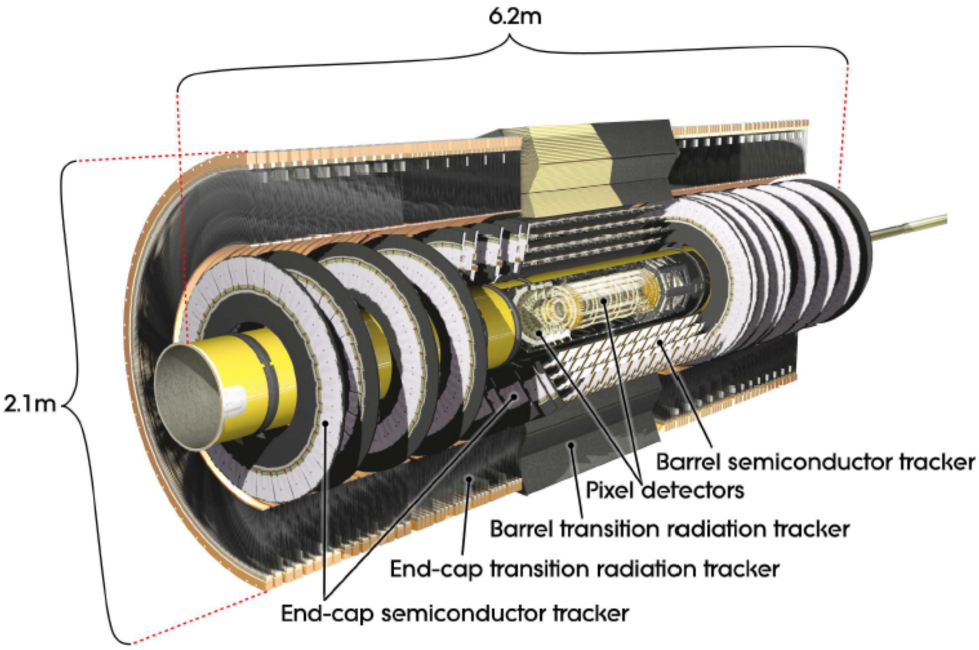

Figure 3.3: Cut-away view of the ATLAS inner detector [15].

rejection, b/τ-tagging and proper charge identification.

3.2.3 Calorimetry

The calorimeters are used to ensure proper energy measurements for all the particles resulting from a collision. One reason this is needed is to have accurate measurements of particle's energies and to be able to properly identify them. The other is that in order to draw conclusion about possible neutrinos one has to accurately measure all particles and their momenta. If a particle is not measured at all because it escapes the acceptance region of the detector or its momentum is measured inaccurately then p_T^{miss} can not be identified with the neutrino momentum.

To make sure this does not happen the calorimeters cover a total range of $|\eta| < 4.9$. The first part of the calorimeter is the electromagnetic one. It is divided into the barrel part $|\eta| < 1.475$ and the end-cap components $., 375 < |\eta| < 3.2$ and is a lead-liquid argon (LAr) detector. The end-cap calorimeter is further divided into an outer wheel region covering $1.375 < |\eta| < 2.5$ and an inner wheel region covering $2.5 < |\eta| < 3.2$. The region of $|\eta| < 2.5$ is the one devoted to precision physics as it has the finer granularity. The electromagnetic calorimeter provides full coverage of the azimuthal angle ϕ.

Not all particles are completely stopped in the electromagnetic calorimeter. These are heavy particles that are usually bound states of quarks. To make sure these are also stopped completely so their whole energy can be measured the electromagnetic calorimeter is surrounded by the hadronic calorimeters. The first one of these is the tile calorimeter which is placed di-

rectly outside the EM calorimeter. Its barrel covers a region of $|\eta| < 1.0$ and its two extended barrels additionally measure particles with $0.8 < |\eta| < 1.7$. It consists of steel absorbers and scintillating tiles as active material. The LAr hadronic end-cap calorimeter further extends the coverage between $1.5 < |\eta| < 3.2$.
The also LAr based forward calorimeter consists of three modules per end-cap. The first one is made of copper and deals with electromagnetic measurements while the other are made from tungsten and measure hadronic reactions. It covers the range $3.1 < |\eta| < 4.9$.
A cut-away view of the calorimetry system is depicted in Figure 3.4

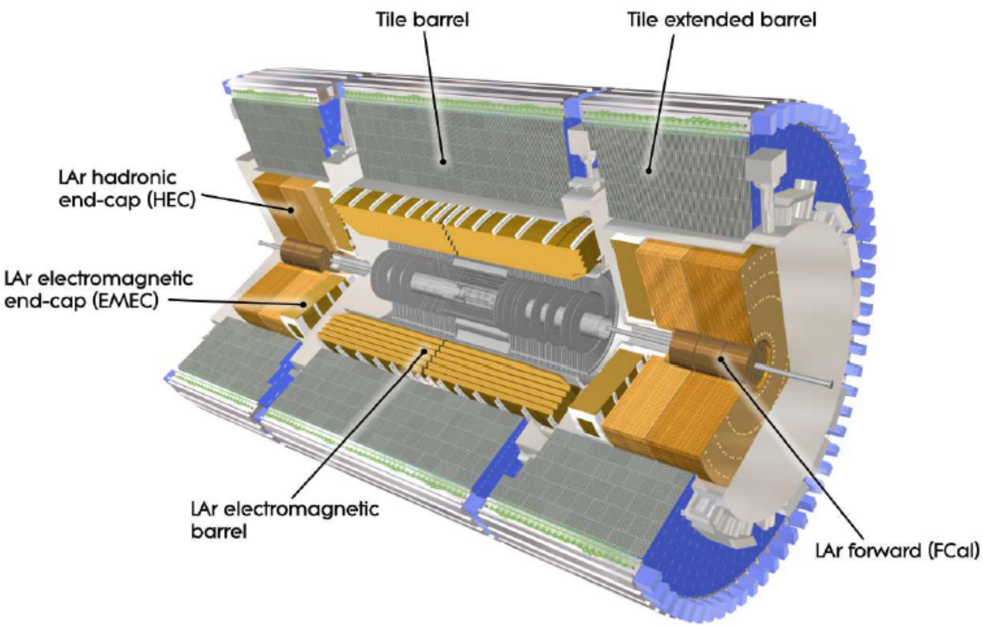

Figure 3.4: Cut-away view of the ATLAS calorimeter system [15].

3.2.4 Muon system

Neither the EM calorimeter nor the hadronic one can properly stop and measure muons. This is because their mass is significantly higher then the one of the electron which reduces bremsstrahlung significantly. It is also not stopped by the absorbers of the hadronic calorimeters. Due to this a special system is build to accurately measure the energy and momentum of muons. The Muon system (see Figure 3.5) is based on the deflection of the muon tracks in the magnetic field of large superconducting magnets. It covers a region of $|\eta| < 2.7$. Over the largest part of the η-range the tracking measurement is done via Monitored Drift Tubes (MDT's). Cathode Strip Chambers are used for $2 < |\eta| < 2.7$.
The triggers system works for a slightly smaller range of $|\eta| < 2,4$ In the barrel region Resistive Plate Chambers are used and Thin Gap Chambers proved the information for the end-caps.
Since other particles are typically stopped in the calorimeters and do not make it to the Muon system muons are generally identified extremely well.

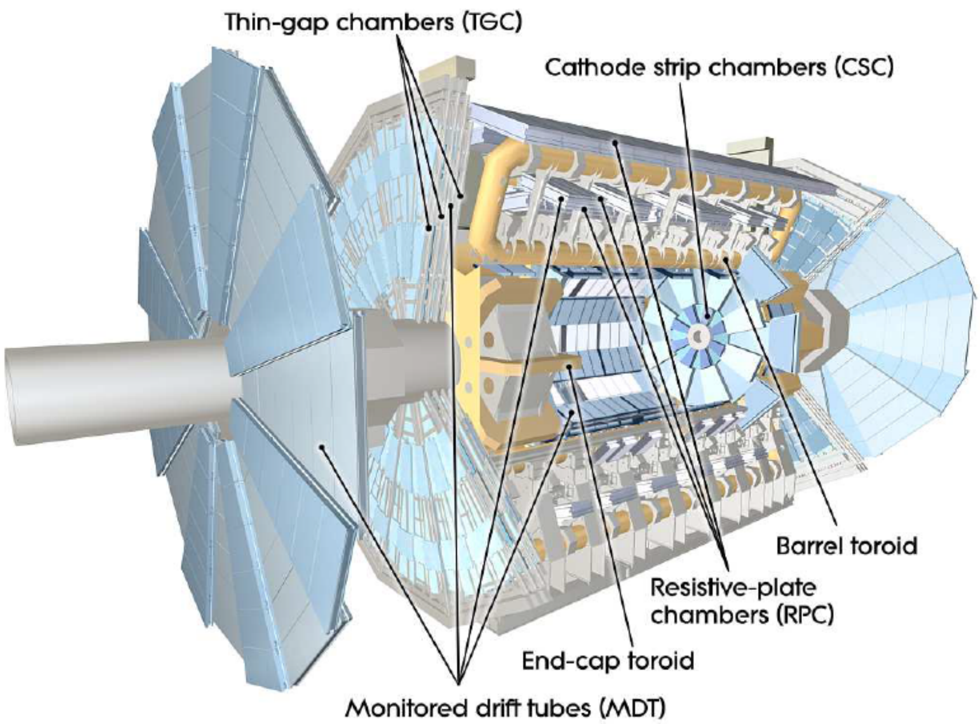

Figure 3.5: Cut-away view of the ATLAS muon system [15].

3.2.5 Forward detectors

Additionally to the parts that make up the main detector and determine the momentum and energy of particles there are three smaller detectors that provide ATLAS with luminosity information or play an important role for heavy-ion collisions. LUCID (Luminosity measurement using Cerenkov Integrating Detector) which placed at ± 17 m from the interactions point and ALFA (Absolute Luminosity for ATLAS) which resides at ± 240 m fulfill the first role and the Zero-Degree Calorimeter plays a key role for the second one. It is located at ± 140 m and measures neutral particles at $|\eta| > 8.2$.

3.2.6 Trigger

In most collisions that happen at the ATLAS detector nothing of interest happens. Due to this and because it is infeasible to save the data for every single collision a system of triggers is put in place that reduces the amount of data that has to be saved by a significant portion. Collisions happen every 25 ns which corresponds to a frequency of 40 MHz. The Trigger and Data Acquisition System (TDAS) consists of three levels that each build on the information of the one before.

The first level $L1$ is a hardware based system that uses information of a subset of detectors. It does however use data from almost all regions of the detector. However it do so with reduced granularity and precision. It generally looks for particles with high p_T. Additionally $L1$ defines regions of η and ϕ which are called Regions-of-Interest (RoI's). These are the areas where it

has identified interesting features. This first trigger level makes its decision in less than 25 µs reduces the frequency of events passed onto the next level to 75 kHz.
The second stage $L2$ uses full all the available detector data in the RoI's as defined by $L1$. A major difference is that it uses the data at 100 % of the available precision. This amounts to approximately 2 % of the total event data. $L2$ is software based, takes 40 ms to make its decision about an event and reduces the trigger rate to roughly 3.5 kHz.
The final decision is done by the event filter. It utilizes offline analysis procedures which take on the order of four seconds. The final rate of events that are properly saved and distributed for further offline analysis is 200 Hz. With a size of $\approx$ 1.3 MB this still results in $\approx$ 15 GB per minute of data that has to be saved.

4 Event Generation

To validate whether a theory correctly describes nature one has to calculate what it predicts for quantities that are measurable. In the scenario of the LHC this means to calculate with which frequency one expects specific particles to occur after a collision and what kinematic features these should have. To do this one simulates a large amount of collisions as predicted by the theory to then compare those to actual measurements at detectors. This chapter describes how simulated events are obtained from theories in particle physics.

4.1 Generators

To properly generate simulated events of collisions at accelerators like the LHC multiple steps have to be done to get results that can actually be compared with measured data.
Programs that do this are called event generators or Monte Carlo generators.
A rough visualization of the simulation process without detector effects can be seen in Figure 4.1 with the example being a $pp \to t\bar{t}H$ process.
The first step that has to be taken in simulating collisions at the LHC is the hard process. In Figure 4.1 it is represented by the big red circle. For this the program calculates the matrix element of all the possible Feynman diagrams connecting the initial and final state up to a given order in pertubation theory. Then the phase space integral is performed and the events are simulated accordingly. The calculated Feynman diagrams consider quarks or gluons as their initial state particles. To conciliate the fact that the LHC accelerates protons parton density functions (PDF's) are introduced. They parametrize the chance to find a parton with a specific fraction of the proton's momentum. These can not be calculated from first principle yet and are thus acquired through fits to data. At this stage even unobservable quarks are allowed in the final state, which is why a simulation to this stage is described as parton level.
The next step in the simulation are the decays of unstable particles in the matrix element final state. In Figure 4.1 these are the small red circles representing the decays of the top quarks and the Higgs boson. After this step QCD bremstrahlung is simulated which describes the additional radiation of quarks and gluons off all color charged particles. This step is described by parton showers. Then all the particles that are not color neutral have to be grouped into colorless hadrons. These might then decay further to reach particles that have a long enough lifetime to be observable by the detector. All effects after the hard scattering and decays of

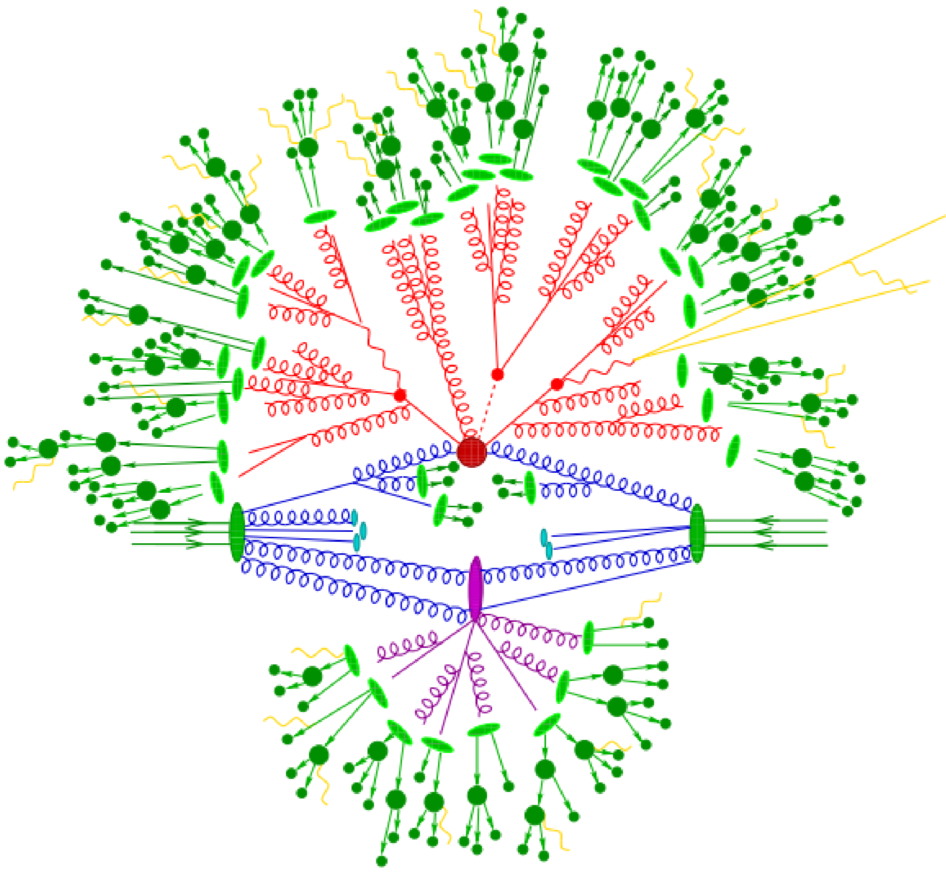

Figure 4.1: Pictorial representation of a $t\bar{t}H$ event as produced by an event generator. The hard interaction (big red blob) is followed by the decay of the top quarks and the Higgs boson (small red blobs). Additional hard QCD radiation is produced (red) and a secondary interaction takes place (purple blob) before the final-state partons hadronise (light green blobs) and hadrons decay (dark green blobs). Photon radiation occurs at any stage (yellow) [31].

those particles can generally not be described properly by pertubation theory as the couplings are not small enough. Instead one relies on approximations and phenomenological models. Additionally initial state radiation has to be considered as well as photon radiation at all stages of the process.

A further complication of hadron colliders is the fact that protons consist of more than the one quark or gluon that participates in the hard interaction. The other partons of the proton can participate in less energetic collisions themselves. This is shown by the purple oval in Figure 4.1. These are called underlying event and pose issues because they can be at energy scales where pertubation theory does not give good predictions and are also color connected to the hard process which complicates things even further. At this stage the identity, momentum, energy, and origin of each particle is known exactly. Due to this, the events generated up to now are called particle level. The final step needed to directly compare the generated events to data is to simulate the detector response. These simulations incorporate the detector materials and geometry. Lastly the 20 to 40 other proton-proton collision causing the pile-up are calculated.

Now the simulated events, just like the data, are described by the energy deposited in each part of the detector. From then on the analysis trys to reconstruct the actual event from these detector hits. For the studies done in this thesis generators were needed that could simulate events for the finale state $\ell\ell\ell\nu jj$ and also generate events for $WZjj$ with polarized gauge bosons. In total four programs were necessary to generate the samples used in this work. These will be introduced here.

4.1.1 Whizard

Whizard [32] is an event generator that is able to do all the processes needed to generate partonic samples. This includes computing tree-level matrix elements via the in house generator O'Mega [33], integrating over the phase space and evaluating the distributions of observables and finally writing out the events in a variety of formats like lhef [34] or hepmc [35]. The other steps like showering and hadronization are done by external code. While Whizard can cover physics at multiple different accelerator types and of a range of physics models only the setup of the LHC and the SM were used in this thesis. In principle Whizard is able write out the helicity of gauge bosons in the final state as well as having the possibility to utilize decay chains with different configurations for the spin density matrix. Due to problems in the production of the decay chain events and the samples with gauge bosons in the final state, Whizard was mainly used to evaluate the validity of the approximations needed to generate events with polarized W's and Z's. Whizard is controlled through the command language SINDARIN (Scripting Integration, Data Analysis, Results display and Interfaces). It allows the definition of complex phase space or scale definitions.

4.1.2 MadGraph5_aMC@NLO

Just like Whizard MadGraph5_aMC@NLO [36] (Madgraph/MG) is a Monte Carlo event generator able to do all steps of partonic event generation for all possible processes. It is only limited by the available computing power and time. Showering and detector simulations are done via the available interfaces to external programs. A significant difference between Madgraph and Whizard is that Madgraph is steered not through a dedicated scripting language but through simple runcards. This makes the usage easier but provides significantly less flexibility. While Madgraph is able to produce events at next to leading order only leading order ones were used for this thesis due to time constraints and complications with writing out the helicity of the bosons in NLO samples. Madgraph ist able to produce samples with final state gauge bosons in the lhef file format. This includes the spin for all final state particles including the bosons. They can then be decayed according to their helicity. Different options were studied in Reference [17] with one eventually giving good results. On top of that Madgraph is able to directly produce the $\ell\ell\ell\nu jj$ finale state using different or no approximations at LO.

One of these is the utilization of a decay chain syntax. This separates the whole generation process into a production and a decay. For this thesis this means the production and decay of the W and Z bosons. This means that only W and Z resonant diagrams are considered. For this Madgraph takes full spin correlations and off-shell effects into account. However, the virtuality of the decaying particles m_V^* is forced to be in the range $|m_V^* - m_V| \leq \text{bwcutoff}\ \Gamma_V$, where bwcutoff is a user defined number. This does not fix the helicity of the intermediate particle but can still be used to test the validity of the approximation used in the final polarized samples.

4.1.3 Pythia8

Pythia 8 [37] able to do the whole process needed for generating particle level events. The simulation of detector effects has to be done via external software. However it is most commonly used in conjunction with other programs like Whizard or Madgraph. Thereby those programs produce the parton level events which are then fed into Pythia to simulate the other effects like initial- and final-state radiation. In this thesis Pythia is used to simulate the parton shower, hadronisation, multiparton interactions, which include the underlying event, beam remnants, and the decays of unstable particles. Pythia decays most particles, including W's and Z's isotropically. Therefore, it is not used for that purpose but only for processing the parton level events after the bosons have already been decayed. Pythia is also able to do matching and merging, supports a variety of BSM physics and physics at lepton-lepton and other hadron-hadron colliders. However neither of these options are used in this work.

4.1.4 Herwig7

Herwig [38, 39] is a general purpose Monte Carlo event generator. Like Pythia it can handle collisions at lepton-lepton and hadron-hadron colliders. On top of that it also supports lepton-hadron collisions. Some important hard scattering processes can be simulated by Herwig itself at parton level. However even more processes can be included through dedicated matrix element generators and the lhef format. It also provides simulations of BSM physics but as with all the other generators this option is not used here. Herwig can then be used to simulate inital- and final-state QCD radiation via parton showers. This includes color coherence effects with a special emphasis on the correct description of radiation from heavy particles. For this work Herwig was used to simulate the effects necessary to go from the partonic to the particle level events after the boson decays have already been simulated separately. This is because a test showed that Herwig does not reproduce the expected decay angle distribution for the decays of longitudinally polarized bosons. Overall Herwig was used for the simulation of the parton shower, the underlying event and beam remnants, hadron decays and hadronization.

4.2 Polarized Samples

In order to be able to study the nature of the EWSB using VBS as accurately as possible it is necessary to study the polarization of the bosons involved in the scattering process. For that samples are needed where one has knowledge of the helicity of the gauge bosons that decayed into the observed leptons. This section studies the two main ways this can be accomplished.

4.2.1 Reweighting

The way that polarized samples used to be generated was to implement a reweighting approach [40, 41]. The most recent analysis to do so was one measuring the $W^{\pm}Z$ production cross section alongside the boson polarization at $\sqrt{s} = 13\,\text{TeV}$ with the ATLAS detector [42]. Besides measuring the fraction of longitudinal bosons f_0 the difference between the left- and right-handed fractions $f_L - f_R$ was also determined. Most importantly the longitudinal helicity fraction of the Z boson was measured with an observed significance of 6.5σ. For the W boson the presence of its longitudinal polarisation was established with an observed significance of 4.2σ.

To use this reweighting approach the first step is to generate a general sample of the full $\ell\ell\ell\nu jj$ final state. Using this to generate samples corresponding to polarized bosons requires two steps to be taken. The first is to analyze the generated events and calculate the decay angle θ^*_V as described in Section 2.3.2 as well as the transverse momentum and the rapidity of the bosons, that is of the $\ell^+\ell^-$ and $\ell\nu$ pairs. The last two variables are needed because the polarization of the bosons is predicted to depend on the p_T and rapidity of the bosons [43]. The bosons are then grouped depending on their p_T and $|y|$ and the analytical decay angle formulas are fitted to the measured one. For each boson this results in a value for the three helicity fractions for each bin of p_T and $|y|$. Afterwards each event is looked at again. Depending on the variables of the bosons in that event the helicity fractions for that bin are chosen and the event is reweighted according to

$$\frac{\left.\frac{1}{\sigma}\frac{\mathrm{d}\sigma}{\mathrm{d}\cos\theta^*_W}\right|_{-1,0,+1}}{\frac{3}{8}\left(1\mp\cos\theta^*_W\right)^2 f_{-1} + \frac{3}{8}\left(1\pm\cos\theta^*_W\right)^2 f_{+1} + \frac{3}{4}\sin^2\theta^*_W f_0}, \tag{4.1}$$

where

$$\left.\frac{1}{\sigma}\frac{\mathrm{d}\sigma}{\mathrm{d}\cos\theta^*_W}\right|_{-1,0,+1} = \begin{cases} \frac{3}{8}\left(1\mp\cos\theta^*_W\right)^2 f_{-1}, & for\ h=-1 \\ \frac{3}{4}\sin^2\theta^*_W f_0, & for\ h=0 \\ \frac{3}{8}\left(1\pm\cos\theta^*_W\right)^2 f_{+1}, & for\ h=+1 \end{cases} \tag{4.2}$$

The same is done for each event depending on the desired Z boson helicity. The formula is analogous. In this thesis the pseudo-rapidity η was used instead of the rapidity. While these two observables are strongly correlated, which can be seen in Figure 4.2, the pseudo-rapidity

distributions of longitudinal bosons show features that are interesting to try to reproduce via the reweighting method.
This effectively produces samples where the leptons have decay angles that are predicted to come from a specific combination of the helicities of the two bosons. Due to the binning in the transverse momentum and pseudo-rapidity of the bosons these variables should be modelled correctly. The exceptions are the edges of the chosen bins. At those unphysical steps are expected. Other variables are not guaranteed to be reproduced correctly. Additionally this procedure only works in a phase space without lepton cuts as those have an effect on the analytically expected distributions. Equations 2.51 and 2.52 only hold without those [40].
Effects of non-resonant diagrams as well as interference effects between the different helicity states are split up and forced into the polarized samples. This means in turn that using this approach one can not model these correctly afterwards nor can they be determined through a subtraction of the polarized samples from a general one.
In this work to study the reweighting approach the boson transverse momentum $p_T(V)$ and the pseudo-rapidity of the bosons $\eta(V)$ were used. The $p_T(V)$ was binned in $[0, 30), [30, 60), [60, 90), [90, \infty)$ and $|\eta(V)|$ was binned as $[0, 1), [1, 2), [2, 3), [3, \infty)$. For the decay angle of the bosons $\cos\theta^*_V$ twenty equidistant bins between minus and plus one were used.

4.2.2 WZDecay

An alternative to the reweighting technique described above is to produce events with polarized boson in the final states and then decay these. This was done using the program WZDecay [44] which was developed specifically for this purpose and maintained and improved in the course of this thesis [45]. Using this approach requires the use of some approximations. These approximations as well as the way this method is implemented in WZDecay are explained in this section.

4.2.2.1 Narrow-width-approximation

The production of vector bosons in the final state requires them to be on-shell and means that only resonant diagrams are considered. They can then be decayed according to their helicity. This factorization approach is equivalent to using the narrow-width-approximation [46] which substitutes the propagator of an intermediate boson with one where the particle is at its pole using

$$\frac{1}{q^2 - M^2 + iM\Gamma} = \delta(q^2 - M^2)\frac{\pi}{M\Gamma}. \tag{4.3}$$

This approximation is only valid if $\Gamma \ll M$. Using this approach includes neither off-shell effects nor non-resonant diagrams and interferences with those.
As shown in Reference [47] full spin correlations can be taken into account when using the narrow-width-approximation. To do so only the spin density matrix has to be propagated

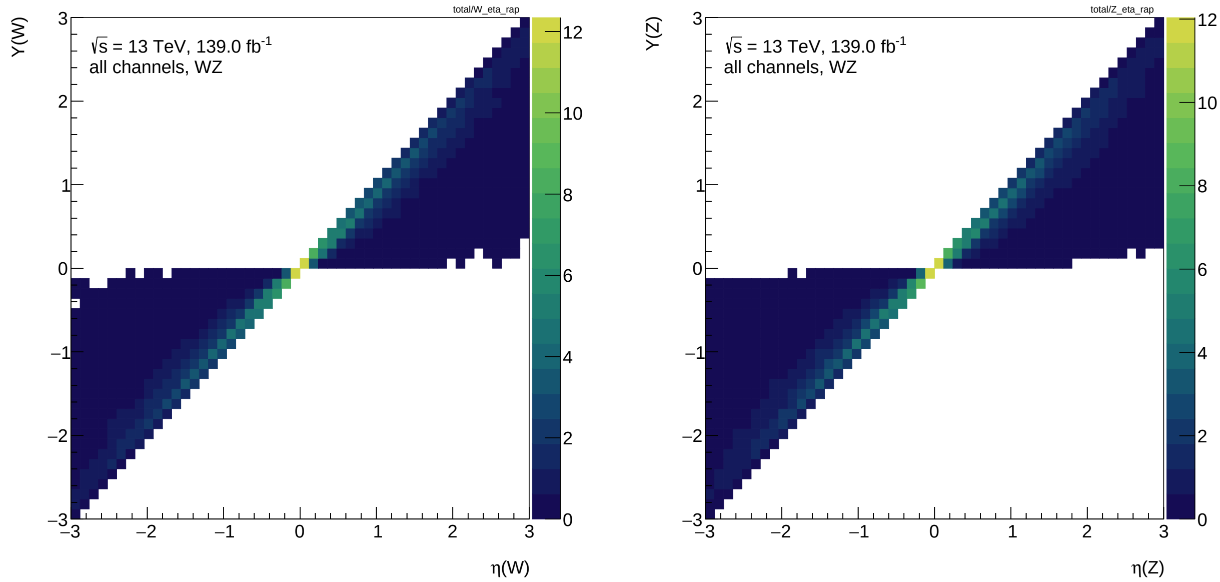

(a) **(b)**

Figure 4.2: Visualization of the dependency of the bosons's transverse rapidity on its pseudo-rapidity. Depicted are the distributions for a sample with on-shell bosons in the total phase space. On the left it is shown for the W boson and on the right for the Z boson.

from the production to the decay process. Since no format allows the transfer of that full information a diagonal spin density matrix is another approximation required for the use of this method. These diagonal elements correspond to the helicity fraction of the two bosons.

4.2.2.2 Implementation

WZDecay requires the input of partonic events with polarized gauge bosons in the final state. These where generated with Madgraph in the .lhef file format. This means that it is Madgraph that determines the helicity fractions in the generated samples. WZDecay parses these files and for each event finds the W and Z bosons. The first step in generating their decays is the determination of the decay angles. This is done based on the analytical functions in Equation 2.51 and 2.52 using a hit-or-miss procedure. A random value for the cosine of the decay angle cos_{rdm} is generated along side a random number between 0 and 1 x_{rdm}. If the random number is smaller than $F(_{cos_{rdm}})$ the angle is calculated from the cosine and kept. Here $F(cos_{rdm})$ corresponds to the functions in front of the f_i in Equations 2.51 and 2.52. This depends on which boson is being decayed and which helicity it has. So for a longitudinal W boson $F(cos_{rdm}) = \frac{3}{4}(1 - cos^2_{rdm}) = \frac{3}{4}sin^2_{rdm}$. The lepton momenta are finally determined based on the mass of the boson, the determined decay angle and a random azimuthal angle. Then the momenta are rotated so that the z-axis aligns with the boson's momentum in a chosen frame. This frame should be chosen such that it is the one that the helicity of the boson was defined in. For this WZDecay supports the laboratory frame (LabFrame) , the partonic center of mass

frame (PCoMFrame) and the center of mass frame of the WZ system. Lastly they are boosted from the boson's rest frame to the laboratory frame.
The so generated leptons are written to the file and the boson's status is switched to that of an intermediate particle. In principle WZDecay supports the decays of the bosons to any of the leptons. The branching ratios are given by hand. If multiple channels are enabled these are used to determine the fraction with which each of them show up in the final state. Additionally they are used to reduce the cross section of the process to the proper amount.
Finally output files are produced containing events with the desired combination of boson helicities. For this thesis left- and right-handed helicites were grouped as transversal polarization and not investigated further. Thus, four output files were produced. WZDecay supports output to hepmc and lhef files. These can either by analyzed as partonic samples or processed further using Pythia or Herwig.

5 Study of Generated Events

For this study samples were produced at both the particle as well as the parton level. This was done using Madgraph and Whizard to produce the partonic events. These were studied directly using RIVET [48]. In a second step additional Madgraph samples with different settings were produced. All of the Madgraph samples were then showered using either Pythia or Herwig and studied further. All relevant parameters needed to produce these results are shown in Table 5.1. All samples that were used are listed in Table 5.2 as well as how exactly their were produced. In this chapter these samples are studied and compared. For the study at the partonic level one sample of the $WZjj$ finale state was generated using Madgraph. It was then decayed and split into four samples with specific helicities via WZDecay. Additionally two samples of the $2 \rightarrow 6$ process were generated with Whizard to check the validity of the approximations used for the first sample. For the particle level study two validation samples were produced with Madgraph. Additionally two more samples of the $2 \rightarrow 4$ process were generated. These were then decay and split via WZDecay. Lastly all of the samples for the particle level study were showered with Pythia or Herwig.

Table 5.1: List of parameters and their values used to generate the events with Whizard and Madgraph. The strong coupling α_S as well as the masses of all not listed particles were either zero for both generators or they were not used in final analysis.

Parameter	**Value**	
	Whizard	**Madgraph**
$\sqrt{s}$	13 TeV	
PDF	NNPDF30_nnlo_as_0118	
renorm. scale	$M_{\ell\ell\ell\nu}$	default dynamical '-1'
fact. scale	$M_{\ell\ell\ell\nu}$	default dynamical '-1'
α_{EW}^{-1}	132.3479	132.506 98
M_W	80.399 GeV	80.419 GeV
Γ_W	2.085 GeV	2.047 599 51 GeV
M_Z	91.1876 GeV	91.188 GeV
Γ_Z	2.4952 GeV	2.441 403 51 GeV
M_H	126 GeV	125 GeV
Γ_H	0.004 18 GeV	0.006 382 339 34 GeV

Table 5.2: List of all samples generated for this work. Above the double line the samples include only positive W^+ bosons but all flavour combinations of electrons and muons. Cross sections and event numbers are given after the removal of τ's and b quarks. These events were directly analyzed with Rivet at parton level. Samples below the double line include both charges and all electron/muon flavour combinations, but only one option is shown. Cross sections and event numbers are those after the shower.

ID	Generator	Helicity	Shower	#Events	σ in fb	Process definition	additional Information
1	Whizard	mixed	-	63 470	8.616	qf, qf => qf qf e2 E2 E1 n1	full process
2	Whizard	mixed	-	59 436	4.462	qf, qf => qf qf e2 E2 E1 n1	only resonant diagrams
						{$restrictions="5+6~Z&& 7+8 ~W+" }	off-shell effects included
3	Madgraph	WTZT	-	71 859	2.431	generate p p > W+ Z j j	WZDecay in LabFrame
4	Madgraph	WTZL	-	21 427	0.702	generate p p > W+ Z j j	WZDecay in LabFrame
5	Madgraph	WLZT	-	20 191	0.675	generate p p > W+ Z j j	WZDecay in LabFrame
6	Madgraph	WLZL	-	6428	0.206	generate p p > W+ Z j j	WZDecay in LabFrame
7	Madgraph	mixed	Pythia	1 000 000	61.640	generate p p > mu+ mu- e- ve~j j	full process
8	Madgraph	mixed	Pythia	999 866	8.264	generate p p > W+ Z, jj,	only resonant diagrams
						W+ > e+ ve, Z > mu+ mu-	bw_cutoff=15
9	Madgraph	WTZT	Herwig	230 889	3.956	generate p p > W+ Z j j	WZDecay in LabFrame
10	Madgraph	WTZL	Herwig	68 088	1.173	generate p p > W+ Z j j	WZDecay in LabFrame
11	Madgraph	WLZT	Herwig	66 042	1.125	generate p p > W+ Z j j	WZDecay in LabFrame
12	Madgraph	WLZL	Herwig	20 968	0.360	generate p p > W+ Z j j	WZDecay in LabFrame
13	Madgraph	WTZT	Herwig	230 889	3.956	generate p p > W+ Z j j	WZDecay in PCoMFrame
14	Madgraph	WTZL	Herwig	68 088	1.173	generate p p > W+ Z j j	WZDecay in PCoMFrame
15	Madgraph	WLZT	Herwig	66 042	1.125	generate p p > W+ Z j j	WZDecay in PCoMFrame
16	Madgraph	WLZL	Herwig	20 968	0.360	generate p p > W+ Z j j	WZDecay in PCoMFrame
17	Madgraph	WTZT	Herwig	1 144 818	3.957	generate p p > W+ Z j j	WZDecay in PCoMFrame
18	Madgraph	WTZL	Herwig	338 262	1.1768	generate p p > W+ Z j j	WZDecay in PCoMFrame
19	Madgraph	WLZT	Herwig	324 170	1.115	generate p p > W+ Z j j	WZDecay in PCoMFrame
20	Madgraph	WLZL	Herwig	103 683	0.358	generate p p > W+ Z j j	WZDecay in PCoMFrame

5.1 Parton Level

At the partonic level samples were generated using Madgraph and Whizard. While Whizard is in principle able to produce samples with polarized bosons as was studied in Reference [17] none could be produce for this thesis due to technical difficulties where the samples took too long to produce. Instead Whizard was used to generate the full $pp \to \ell\ell\ell\nu jj$ process directly both in full and with restrictions. This was done to verify that the approximations that are required for a polarized sample have a reasonably small effect in the final phase space. The individual helicity samples were produced by generating events with polarized bosons in the final state using Madgraph. These were then processed using WZDecay as described in Section 4.2.2. All events require three leptons at least two of which have the same flavour and opposite charge. Generators cuts are necessary to avoid divergences in the integration. Analysis cuts are used to reduce backgrounds and thus enhance the fraction of signal in this phase space. The total phase space has no analysis cuts at all because the reweighting has to be done without those. To reduce some background the inclusive phase space, which is optimized to simply enhance the fraction of events with massive gauge bosons, has some general cuts on the lepton momenta and their separation. The cuts that are most easily understood to help with enhancing the boson fraction are the cut on the invariant mass of the same flavour opposite charge leptons and the one on the transverse mass of the W boson. The latter is defined as

$$m_T(W) = \sqrt{2 \cdot p_T(\ell^W) p_T^{miss} \cdot \left(1 - \cos\left(\Delta\phi(\vec{\ell^W}, \vec{p_T^{miss}})\right)\right)}. \tag{5.1}$$

The VBS phase space is used for investigating vector boson scattering. Since the jets only participate a single weak interaction each, they should only deviate very slightly from their incoming trajectory causing a large rapidity separation between the two jets. This also leads to a high invariant mass of the two jets M_{jj}. The generator level cuts as well as those of the studied phase spaces are shown in Table 5.3 and Table 5.4 respectively.

Table 5.3: Cuts used for the integration in the Monte Carlo generators. Note that for Whizard only two of the leptons are required to have a p_T larger than 5 GeV. Only objects and events that pass these criteria are produced.

	Whizard	**Madgraph+WZDecay**
$min\ p_{T\ell}$ [GeV]	5.0	0
$min\ p_{Tj}$ [GeV]	15.0	30.0
$max\ \|\eta\|_\ell$	5.0	∞
$max\ \|\eta\|_j$	5.0	5.5
$min\ \Delta R_{\ell\ell}$	0.3	0
$min\ \Delta R_{jj}$	0.4	0.4

Table 5.4: List of selection criteria for the three phase spaces studied with rivet. In the analysis only events that pass all of these criteria are considered.

	total PS	**inclusive PS**	**VBS PS**
$min\ p_{T\ell Z}$ [GeV]	0	15	15
$min\ p_{T\ell W}$ [GeV]	0	20	20
$max\ \|\eta\|_\ell$	∞	2.5	2.5
$max\ \|\eta\|_j$	∞	4.5	4.5
$min\ N_{\text{leptons}}$	3	3	3
$min\ \Delta R_{\ell\ell}$	0	0.3	0.3
$min\ \Delta R_{jj}$	0	0.4	0.4
$min\ \Delta R_{j\ell}$	0	0.3	0.3
$min\ \Delta R_{Z\ell\ell}$	0	0.2	0.2
$min\ m_{\ell\ell}$ [GeV]	0	0.1	0.1
$max\ Z-$ Window [GeV]	∞	10	10
$min\ m_T\,(W)$ [GeV]	0	30	30
$min\ p_{Tj}$ [GeV]	0	5	40
$min\ \Delta Y_{jj}$	0	0.4	1.5
$min\ m_{jj}$ [GeV]	0	0	500
$min\ n_{\text{jets}}$	0	0	2

5.1.1 Influence of Approximations

It is necessary to use approximations when investigating the effect of polarized gauge bosons in VBS. This is because in general non-resonant diagrams contribute. In those cases a distinction of boson polarization makes no physical sense. Due to that a restriction to resonant diagrams is necessary. The fact that helicity can only easily be defined for on-shell particles requires the use of the narrow-width-approximation on top that. Finally technical constraints make it impossible to include interference effects between the different polarizations. If these effect have a large contribution a fit of the polarized events to a full sample will give inaccurate or unphysical results. In Figure 5.1 to Figure 5.3 a comparison of the three different samples is shown for a variety of observables in the used phase spaces. The sample with name 'Madgraph' is the sum of the samples with Ids 3 to 6 as listed in Table 5.2. 'Whizard_full' corresponds to sample 1 and 'Whizard_restr.' to sample 2. In most of them it is obvious that the approximations have a significant effect in the total phase space. This is to be expected since there non-resonant diagrams should have a larger influence. However, a direct comparison between the Whizard and Madgraph samples are not straight forward due to the different generator level cuts shown in Table 5.3. In the total phase space this has a significant effect on all variables. The effects of the non-resonant diagrams can still be seen clearly in Figure 5.1a and the effect of the off-shellnes is obvious in Figure 5.1c.

The different generator cuts still have a relevant effect in the inclusive phase space. That is if one looks at jets variables like in Figure 5.2. The inclusive phase space is shown in the

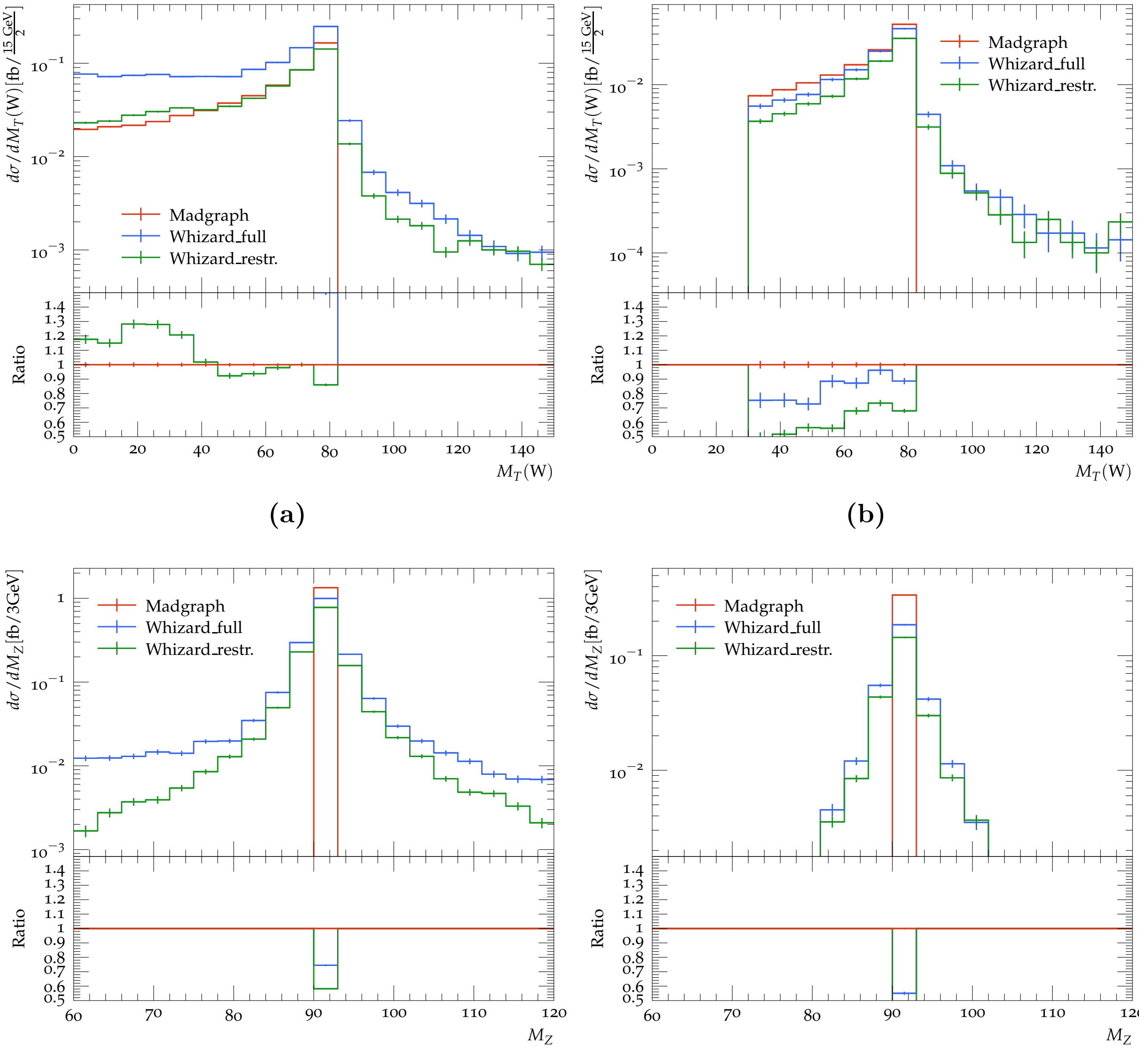

Figure 5.1: Comparisons of distributions for the samples with no approximation (blue), restriction to resonant diagrams (green) and using the narrow-width-approximation (red). The first two samples were generated using Whizard, the other one with Madgraph and WZDecay. On the left side the distributions in the total phase space are shown while the right side shows the VBS phase space. On the top the mass of the Z boson M_Z is considered while at the bottom the transverse mass of the W $m_T(W)$ is looked at.

middle column in Figures 5.2b, 5.2e and 5.2h. This is because the jet cuts of the inclusive phase space are weak than the ones at generation level. The generator cut effects on the leptons, however, are removed by the stronger analysis cuts. This means that the differences in Figures 5.3b and 5.3e are purely due to the used approximations. These are significantly smaller but still exist. Especially the normalization difference have been reduced a lot and the shapes are more similar as well. In the VBS phase space the differences become even smaller. However, they have not disappeared completely. These deviations can not be ignored when doing a fit to determine the helicity fractions via these variables. Especially those that are the most sensitive to the mass of the intermediate boson still show significant differences as can be seen in Figures 5.1b and 5.1d. However, for the decay angle of the W boson the shapes look exactly the same in the VBS phase space. This is demonstrated in Figure 5.3i. While both shapes and normalization are clearly distinct in the total phase space as seen in figure 5.3g both differences get significantly smaller with the shapes becoming basically identical within uncertainties in the VBS phase space. It is to note that the bosons were decayed with their momenta considered from the laboratory frame. Later it was found that the helicity of the bosons was defined in the partonic center-of-mass frame. Due to that the decay angles are not expected to fit exactly. The effect of this switch on observables of the sum of ploarized samples is small. This is discussed in more detail in Section 5.2.2. It still has to be kept in mind when analyzing the results here.

What remains are the curious normalizations. The expectation is that regardless of the phase space the full sample should have the largest cross section, followed by the resonant sample with the on-shell sample having the smallest one. Only the fraction of the cross sections should get closer to one. However, in the VBS phase space it seems that the sample with the most restrictions has the highest overall cross section. That this is actually the case can be seen in Table 5.5. For the Whizard sample with the restricted diagrams the reason could be traced back to how exactly those are handled. In Figure 5.4 it can be seen that the problem arises from the same flavour channels. Whizard forces each of the final state leptons to come from a specific intermediate particle. In the case where all particles are electrons or muons this disregards same diagrams. For example in the finale state $e^+e^-e^+\nu_e$ with the particles numbered from 1 to 4 from left to right. In this case Whizard only considers diagrams where

Table 5.5: Cross sections of the different samples for W^+Z scattering in three phase spaces. These are the values without τ leptons and b quarks.

	total PS σ [fb]	**inclusive PS** σ [fb]	**VBS PS** σ [fb]
Whizard_full	8.62	1.97	0.94
Whizard_restrictions	4.46	1.63	0.73
Madgraph+WZDecayALL	4.01	1.65	1.01

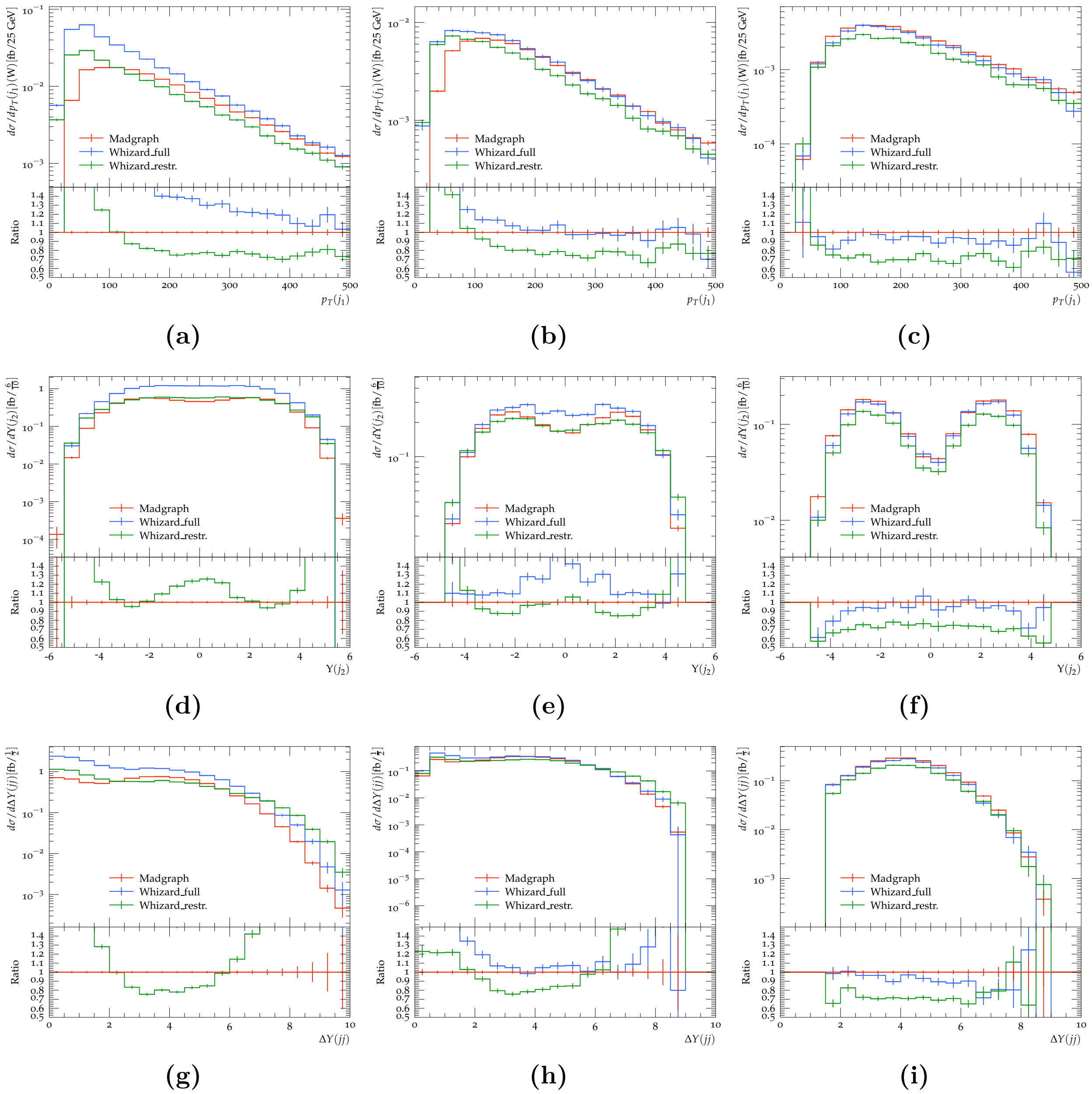

Figure 5.2: Comparisons of distributions for the samples with no approximation (blue), restriction to resonant diagrams (green) and using the narrow-width-approximation (red). The first two samples were generated using Whizard, the other on with Madgraph and WZDecay. On the left side the distributions in the total phase space are shown while the middle shows the inclusive phase space and the right side shows the VBS phase space. From top to bottom the transverse momentum of the leading jet $p_T(j_1)$, the pseudo-rapidity of the subleading jet $\eta(j_2)$ and difference in the rapidity of the two leading jets $\Delta Y(jj)$ are shown.

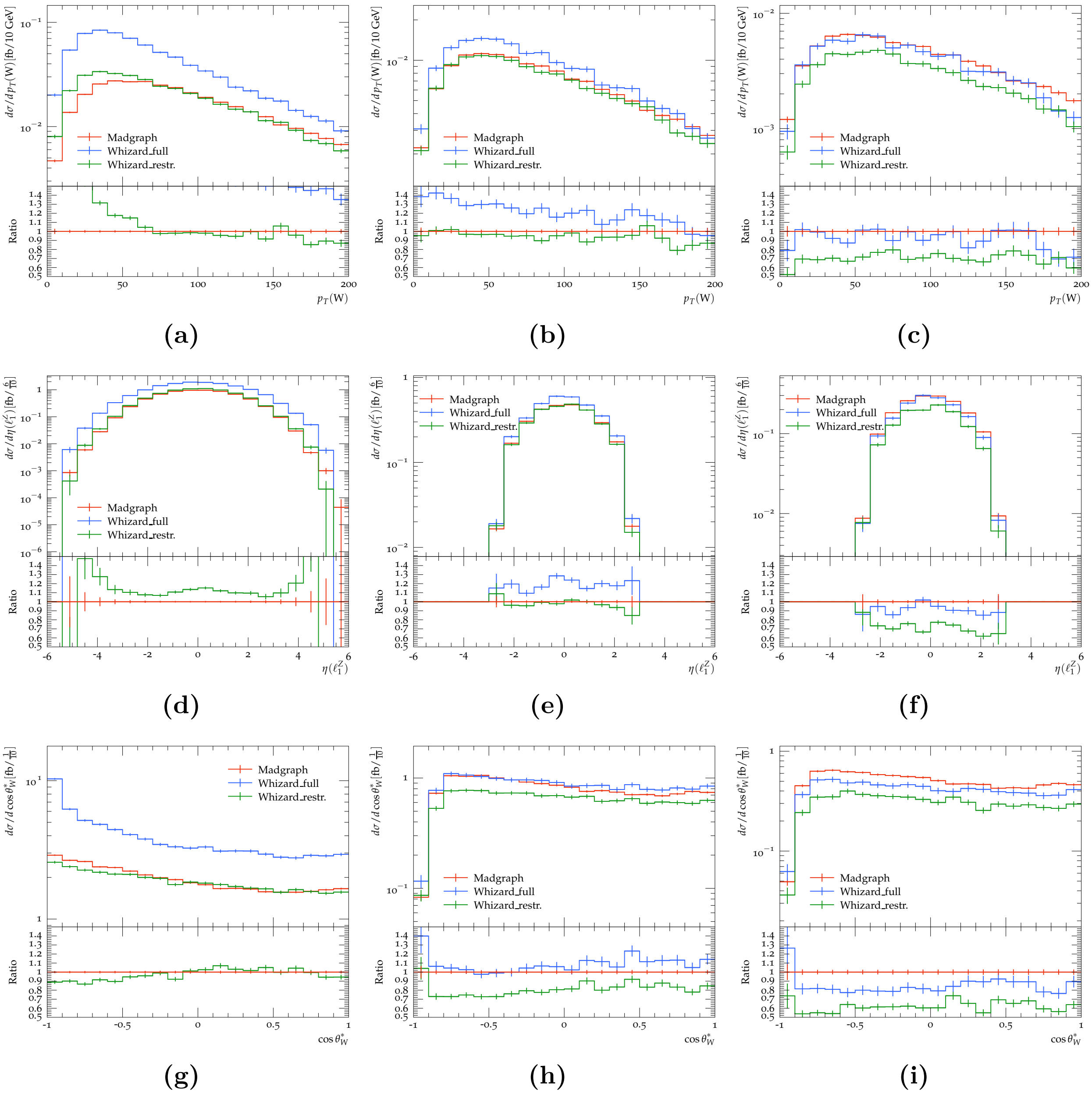

Figure 5.3: Comparisons of distributions for the samples with no approximation (blue), restriction to resonant diagrams (green) and using the narrow-width-approximation (red). The first two samples were generated using Whizard, the other one with Madgraph and WZDecay. On the left side the distributions in the total phase space are shown while the middle shows the inclusive phase space and the right side shows the VBS phase space. On top the transverse momentum of the W boson $p_T(W)$, in the middle the pseudo-rapidity of the leading Z lepton $\eta(\ell_1^Z)$ and on the bottom the decay angle of the W $\cos\theta_W^*$ are shown.

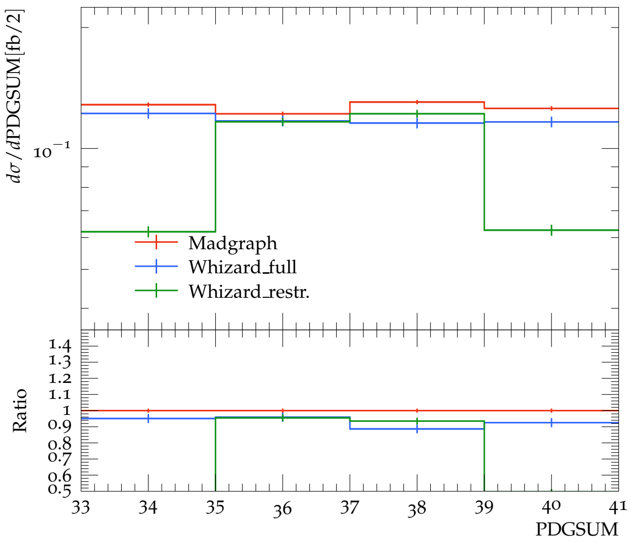

Figure 5.4: Differential cross section over the sum of the lepton's absolute pdg ids. The electron has an id of 11 and the muon's id is 13. This means that 33 corresponds to the channel where both bosons decay into electrons, 35 to the one where the W decays to a muon and the Z to an electron positron pair and so on. This means that 35 and 37 are the opposite flavour channels while 33 and 39 the same flavour channels.

1 and 2 come from a Z bosons while the other two come from the W. However, it is possible that 3 and 2 originate from the Z and 1 and 4 from the W. The second case is ignored by Whizard causing a different cross section in the same flavour channels. Differences between the full Whizard sample and the Madgraph one can not be explained by that. There the difference could be due to the branching ratios that are put in by hand and effect the final cross section, negative interferences between the resonant and non-resonant diagrams. The most likely reason is that the differences come from the different settings listed in Table 5.1, especially from the different sacles. This is because the issue did not appear in the particle level studies where all samples were produced with madgraph. For this reason the issue was also not investigated further.

5.1.2 Study of Polarizations

To eventually do a fit determining the helicity fractions suitable observables have to be found first. Based on theoretical considerations the decay angle seems to be the most obvious one. However, it is not clear how exactly the phase space cuts influence this observable as well as other potential candidates. Especially for the W boson other observables have to be considered as the decay angle is difficult to reconstruct due to the neutrino which can not be measured directly. In this thesis this part is reduced to a minimum as an extensive study has already been done in Reference [17]. The samples considered in this section are those with Ids 3 to 6 in Table 5.2. The main purpose for this work is to verify that the implementation of the decay angle works correctly in WZDecay and to again visually identify some variables that are good candidates. Another reason is to possibly identify significant differences that arise after showering that make some variables better or worse than one would assume from the partonic events. This is discussed in Section 5.2.4.

The first and most important step is to verify that WZDecay produces the correct decay angles for the polarized gauge bosons. For that purpose the normalized decay angle is plotted alongside the analytical functions.This can be seen in Figure 5.5a. The agreement between the black lines for the analytical distributions and the coloured lines representing the distributions of the samples is perfect withint statistic. In Figure 5.5b it can be seen that while the decay angle distribution is affected by the phase space cuts in a fairly significant way the differences between transversal and longitudinal helicities are still clearly visible.

Figure 5.6 shows some boson variables both in the total and in the VBS phase space. The transverse momentum and the transverse mass of the W boson seem to be sensitive to its polarization in both phase spaces. The rapidity however shows different behaviour. In the total phase space the transversal and longitudinal modes show the exact same shape over the majority of the range, never deviating more than 10 % until an absolute rapidity of 1 and not more than 20 % until 4. When looking at the VBS phase space longitudinal bosons show strongly deviating behaviour of up to 20 % in the area with a lot of events around $|Y| < 1$ and up 30 % for absolute rapidities below 3, although the statistical fluctuations already become large at those values. While some lepton and boson observables show significant differences between the helicities as was predicted in Section 2.3.2 the jet variables shown in Figure 5.7 seem to only exhibit minimal changes. Non of the variables show significant differences if only the polarization of one boson is changed In the VBS phase space the differences to the sum never cross 20 % in a statistically significant way. Only the comparison between the cases where both bosons are longitudinal or transversal shows deviations. However, the distribution where both bosons are longitudinal shows differences of up to 30 % for the rapidity difference and rapidity and more than 50 % for the transverse momentum. Reduced sensitivity can be partially explained by the spin flips mentioned in Section 2.3.2.

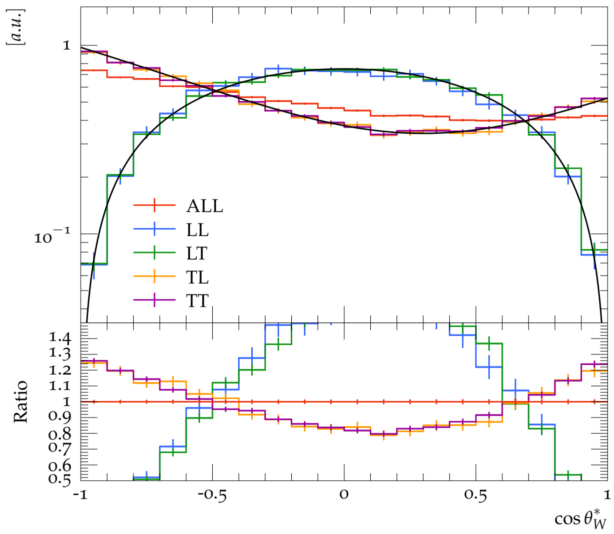

(a)

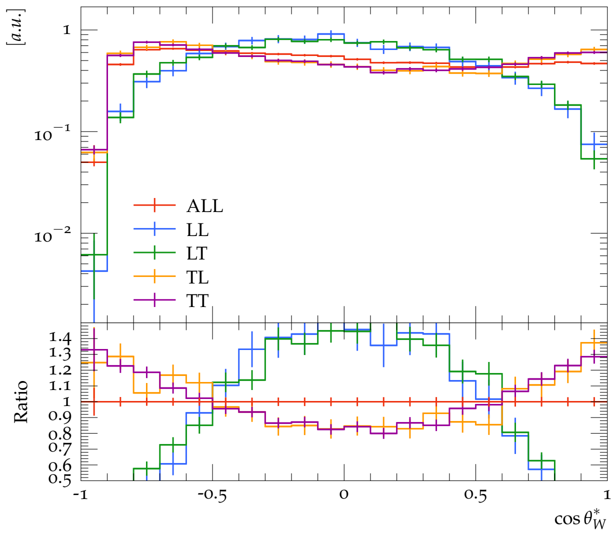

(b)

Figure 5.5: Comparison of the decay angle distribution of the W $\cos\theta^*_W$ between the different helicities. In purple the distribution is shown for the sample where both bosons are transversally polarized, in yellow the W is polarized transversally while the Z has a longitudinal helicity. For the green distribution this if flipped and for the blue one both bosons have a longitudinal helicity. Red is then simply the sum of all the other samples. One the left side the distribution for the total phase space is shown while the right side depicts the same for the VBS phase space. The black line in Figure 5.5a represent the analytical functions.

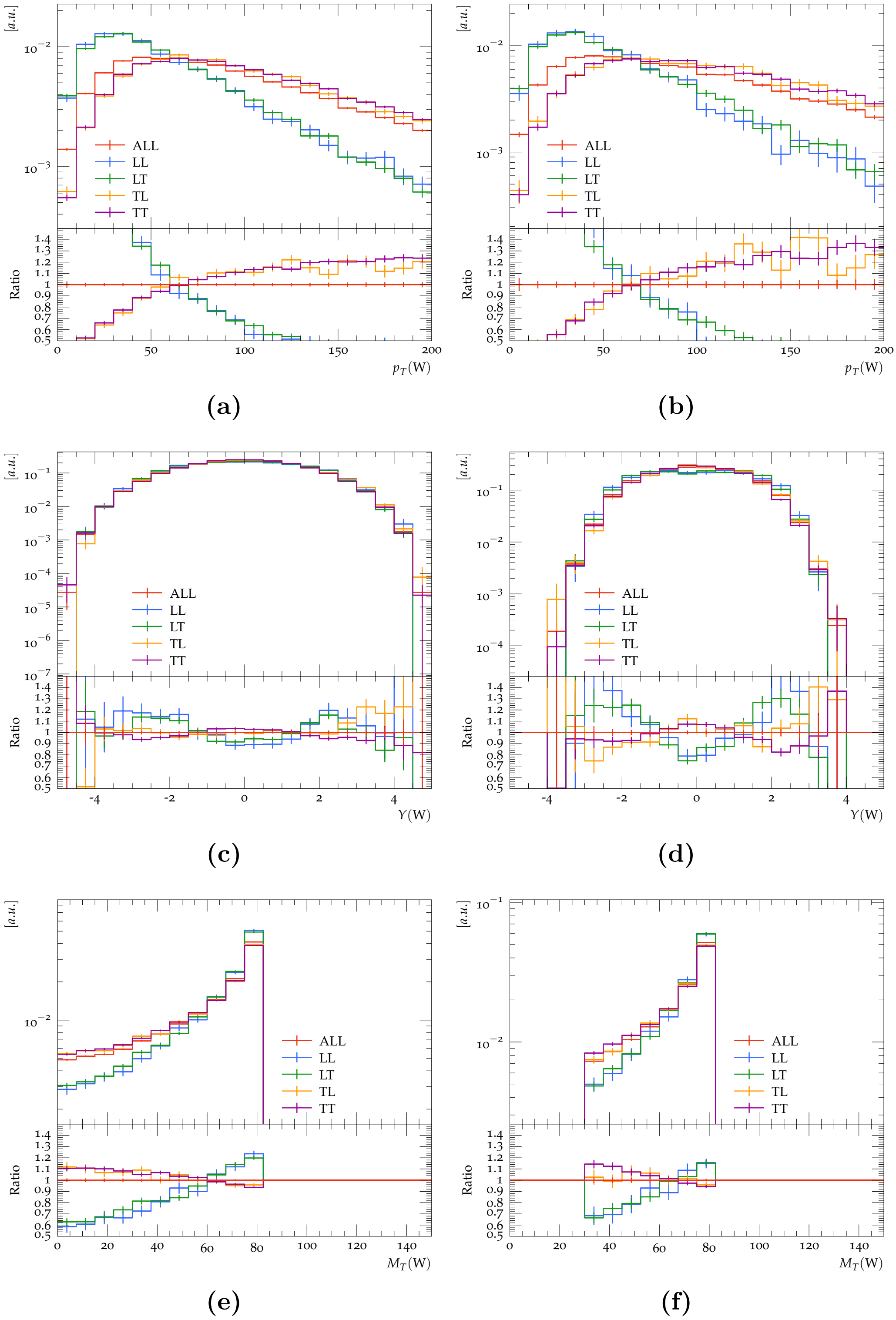

Figure 5.6: Comparison of distributions between the different helicities. In purple the distributions are shown for the sample where both bosons are transversally polarized, in yellow the W is polarized transversally while the Z has a longitudinal helicity. For the green distribution this if flipped and for the blue one both bosons have a longitudinal helicity. Red is then simply the sum of all the other samples. One the left side the distributions for the total phase space are shown while the right side depicts the same for the VBS phase space. From top to bottom the transverse momentum, the rapidity and the transverse mass of the W boson are considered.

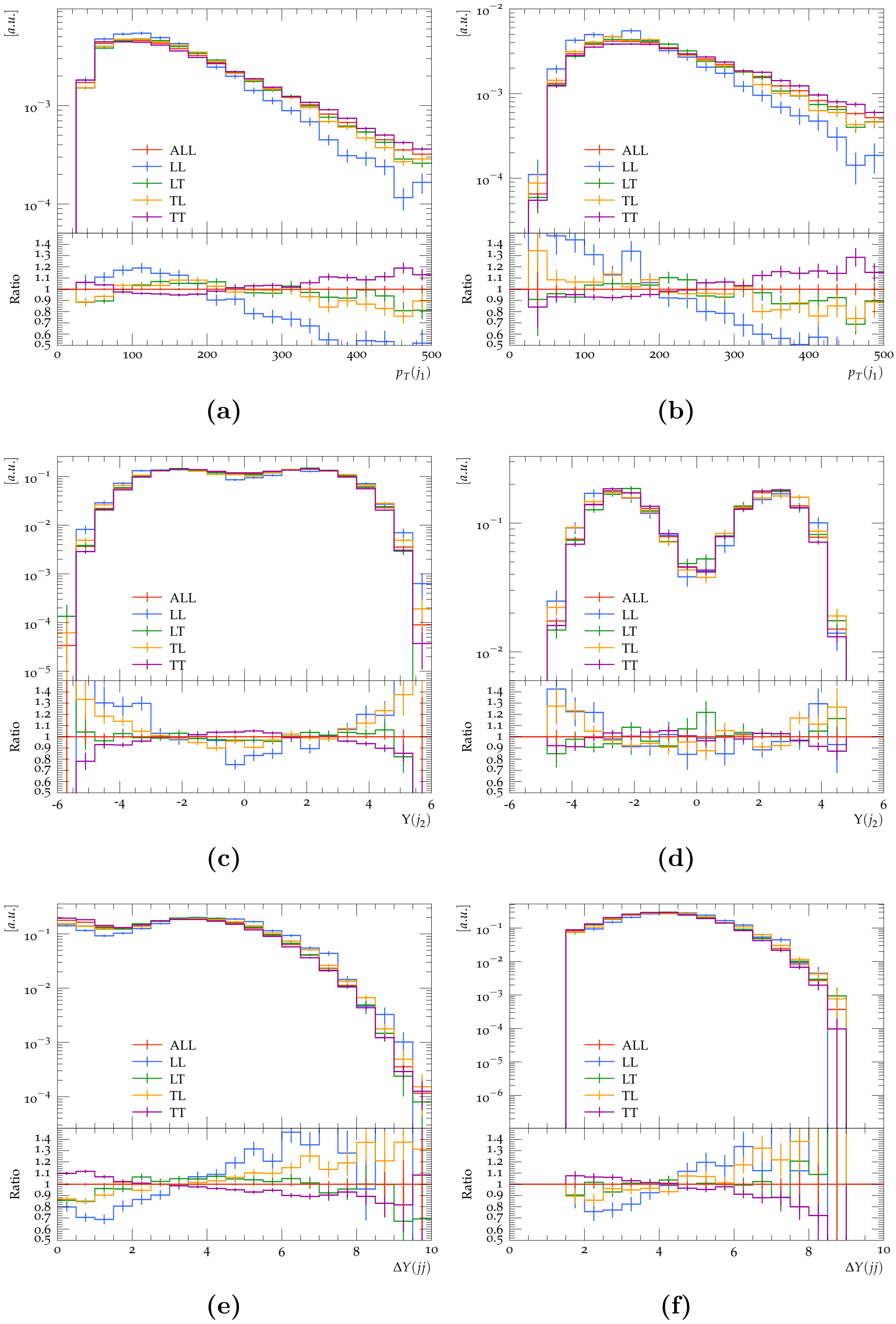

Figure 5.7: Comparison of distributions between the different helicities. In purple the distributions are shown for the sample where both bosons are transversally polarized, in yellow the W is polarized transversally while the Z has a longitudinal helicity. For the green distribution this if flipped and for the blue one both bosons have a longitudinal helicity. Red is then simply the sum of all the other samples. One the left side the distributions for the total phase space are shown while the right side depicts the same for the VBS phase space. From top to bottom the transverse momentum of the leading jet, the rapidity of the subleading jet and the rapidity difference between those two are considered.

5.2 Particle Level

Since so far in this work there have only been rough qualitative estimates as to which observables could be interesting and these were solely based on parton level a more thorough quantitative study is done with events after showering in this section.

The cuts for both the sample generation as well as the phase spaces that are looked at are slightly different for this study. Since they are still very similar to those before they will not be explained again but are just listed in Tables 5.6 and 5.7 respectively.

Table 5.6: Cuts used for the integration in the Monte Carlo generators. Only objects and events that pass these criteria are produced.

	Full	**Chain**	**WZDecay**
$min\ p_{T\ell}$ [GeV]	$5,0$	$5,0$	0
$min\ p_{Tj}$ [GeV]	$15,0$	$15,0$	$30,0$
$max\ \|\eta\|_\ell$	$5,0$	$5,0$	∞
$max\ \|\eta\|_j$	$5,0$	$5,0$	$5,5$
$min\ \Delta R_{\ell\ell}$	$0,3$	$0,3$	0
$min\ \Delta R_{jj}$	$0,4$	$0,4$	$0,4$

Table 5.7: List of selection criteria for the two phase spaces studied at particle level. In the analysis only events that pass all of these criteria are considered. In the VBS phase space the two leading jets are also required to be in opposite hemispheres.

Cut	**total PS**	**VBS PS**
$min\ p_{T\ell Z}$ [GeV]	0	15
$min\ p_{T\ell W}$ [GeV]	0	20
$max\ \|\eta\|_\ell$	∞	2,5
$max\ \|\eta\|_j$	4,5	4,5
$min\ n_{leptons}$	3	3
$min\ \Delta R_{\ell\ell}$	0	0,3
$min\ \Delta R_{j\ell}$	0,3	0,3
$min\ \Delta R_{Z\ell\ell}$	0	0,2
$max\ Z-Window$ [GeV]	25	10
$min\ m_T\,(W)$ [GeV]	0	30
$min\ p_{Tj}$ [GeV]	25	40
$min\ \Delta Y_{jj}$	0	2,0
$min\ m_{jj}$ [GeV]	0	500
$min\ n_{jets}$	0	2

5.2.1 Influence of Approximations

For this part three different samples were used. The first is the one with Id 7, called 'Full', and simulated the complete $2 \rightarrow 6$ process with no approximations used at all. The second one, with Id 8 and shorthand 'Chain', employed Madgraphs decay chain syntax of producing the gauge bosons and decaying them. This restricts the diagrams to resonant ones and employs a condition where the decay products have to have an invariant mass close to that of the on-shell intermediate particle [36]. For this the standard setting of 15 particles widths were used. The third sample is the one of interest and consists of those with Ids 17 to 20.It is called 'WZPart' and was produced with Madgraph and WZDecay. Madgraph generated events with polarized on-shell bosons in the final state and WZDecay was used to split the sample and decay the bosons based on their helicity. For the study of the validity of the approximations the correct setting for the decay frame were used. Namely the center of mass frame of the initial partons as dictated by Madgraph. In Figure 5.8 it can be seen that just like without the shower the distributions that are the most sensitive to the mass of the bosons show significant differences between the samples with and without the narrow-width-approximation.

Figure 5.9 shows some jet variables both in the total and in the VBS phase space. For almost all observables the differences in the total phase space are very significant. The transverse momentum of the leading jet shows very significant deviations especially as small values, where the removal of the non-resonant diagrams causes a difference of around 30 %, which is increased even further to more than 50 % by the restriction to the narrow-width-approximation. This is depicted in Figure 5.9a and corresponds to the jets in the on-shell samples generally having higher transverse momenta. Figure 5.9c that the removal of non-resonant diagrams causes fewer of the subleading jets to be emitted both orthogonal and parallel to the beam axis. The effect of the approximation on the rapidity difference of the leading jets in the total phase space is shown in Figure 5.9e. The the restriction to resonant diagrams causes fewer events where these two jets are very close to each other. For the WZDecay sample the number of event where the jets are very strongly separated from each other declines also. The addition of of the cut on the transverse momentum of the jets as well as the rapidity difference eliminates the region where those two variables differed the most between the full sample and the one produced with WZDecay. This is visible in the Figures 5.9b and 5.9f. Coincidentally the deviation in the subleadings jet pseudo-rapidity are also reduced. Nevertheless $p_T(j_1)$ and $\Delta Y(jj)$ still show significant differences for lower and high values respectively. While the deviations of the pseudo-rapidity of the second jet are reduced they still remain in the low and high regions. When trying to determine the polarization fractions via these variables one has to be careful so the result is not affected too much by these effects.

Similar things can be observed for observables related to the bosons, some of which are depicted in Figure 5.10. In the total phase space the transverse momentum of the W shows behaviour very similar to that of the jet with strong deviations at low values which can be seen in Figure

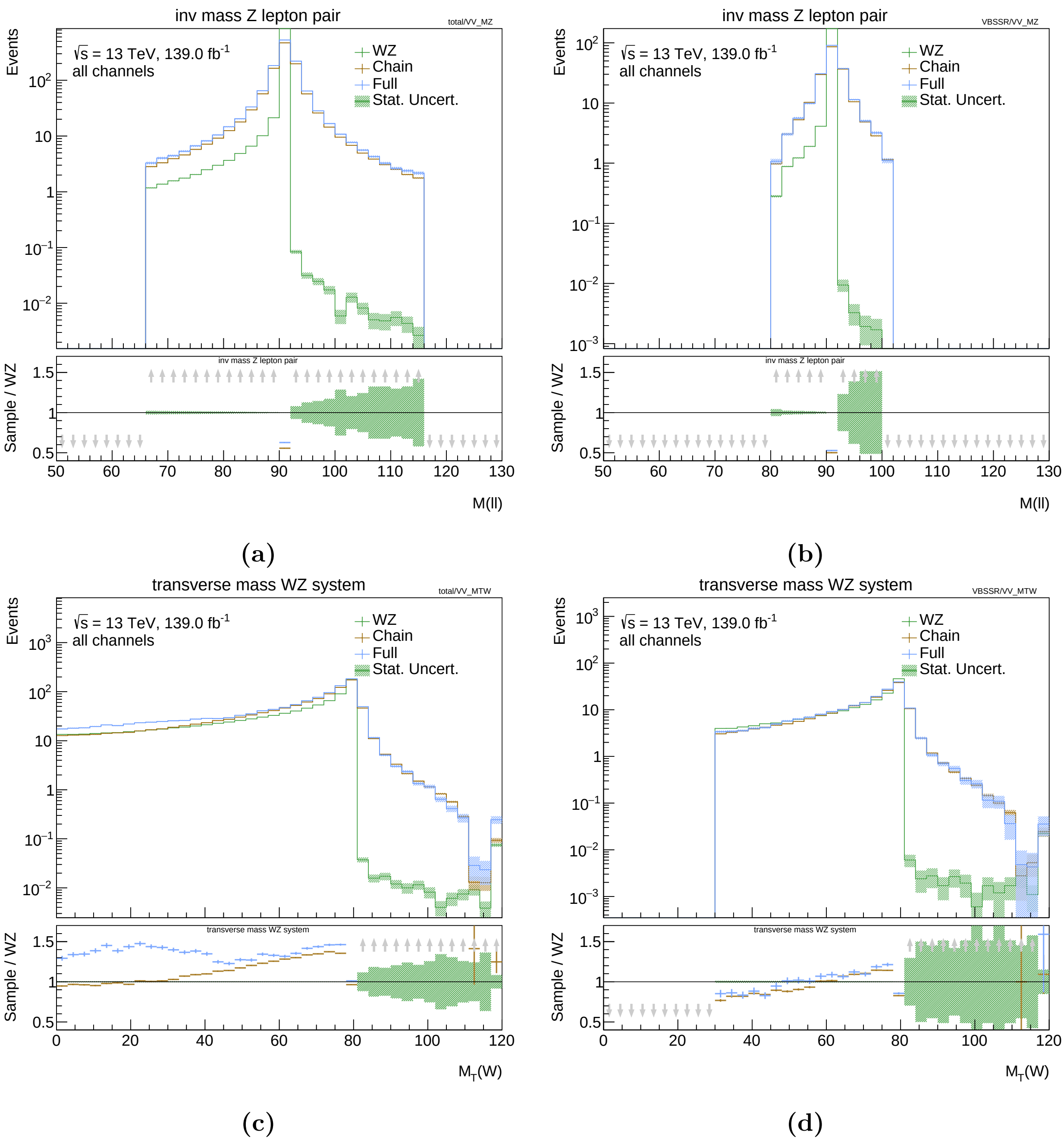

Figure 5.8: Comparisons of distributions for the samples with no approximation (blue), restriction to resonant diagrams (brown) and using the narrow-width-approximation (green). On the left side the distributions in the total phase space are shown while the right side shows the VBS phase space. On the top the mass of the Z boson M_Z is considered while at the bottom the transverse mass of the W $m_T(W)$ is looked at.

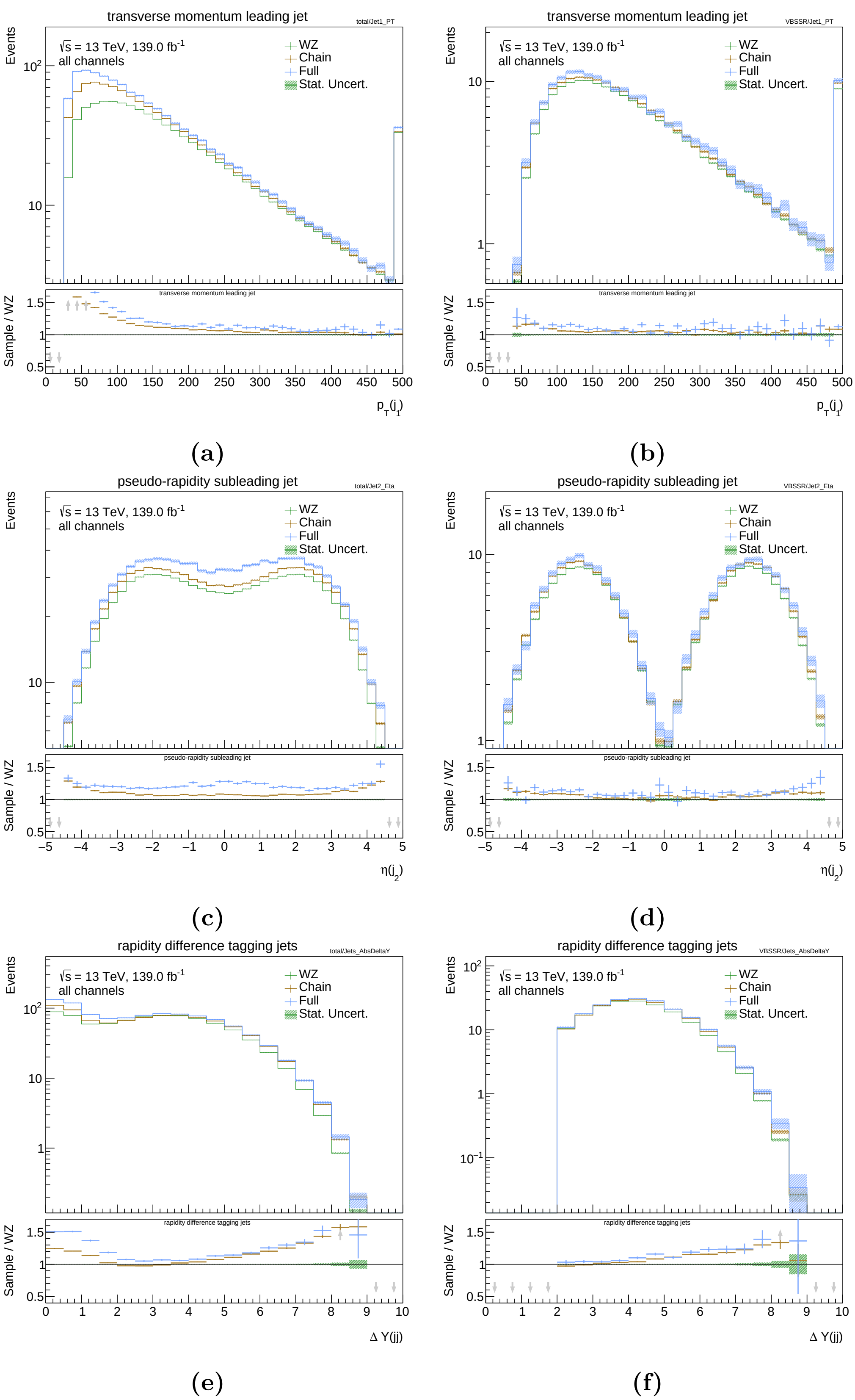

Figure 5.9: Comparisons of distributions for the samples with no approximation (blue), restriction to resonant diagrams (brown) and using the narrow-width-approximation (green). On the left side the distributions in the total phase space are shown while the right side shows the VBS phase space. From top to bottom the transverse momentum of the leading jet, the pseudo-rapidity of the subleading jet and the rapidity differences between those two are shown.

5.10a. Unlike with the jets no differences are present in the VBS phase space shown in Figure 5.10b. The only variable of these that shows a significant shape difference in the total phase space is the decay angle of the W. The shape differences that can still be seen in the total phase space in Figure 5.10c disappear completely in the VBS phase space in 5.10d.
The only major deviation that remains into the VBS phase space is the transverse momentum of the leading lepton of the Z boson shown in Figure 5.10f. There the samples do not agree for values below 40 GeV and the difference is up to 50 %. This means that when doing the fit with most lepton and boson variables the results should be easy to interpret without many problems but care has to be taken for the few exceptions that remain. More observables then the ones shown here can be found in Appendix A.2.
The differences in normalization can also be seen in Table 5.8. There the cross sections can be seen for both phase spaces scaled to a luminosity of $139\,\text{fb}^{-1}$. While the on-shell samples only has about 72 % of the full cross section in the total phase space this increases to $\approx 91\,\%$ in the VBS phase space. Overall it can be noted that the approximations do have some effect on a lot of variables even the the VBS phase space. However, the effect on those observables that are most likely well suited for the study of polarization fractions are minimal. This means that these samples can be used for the study of the polarization fractions.

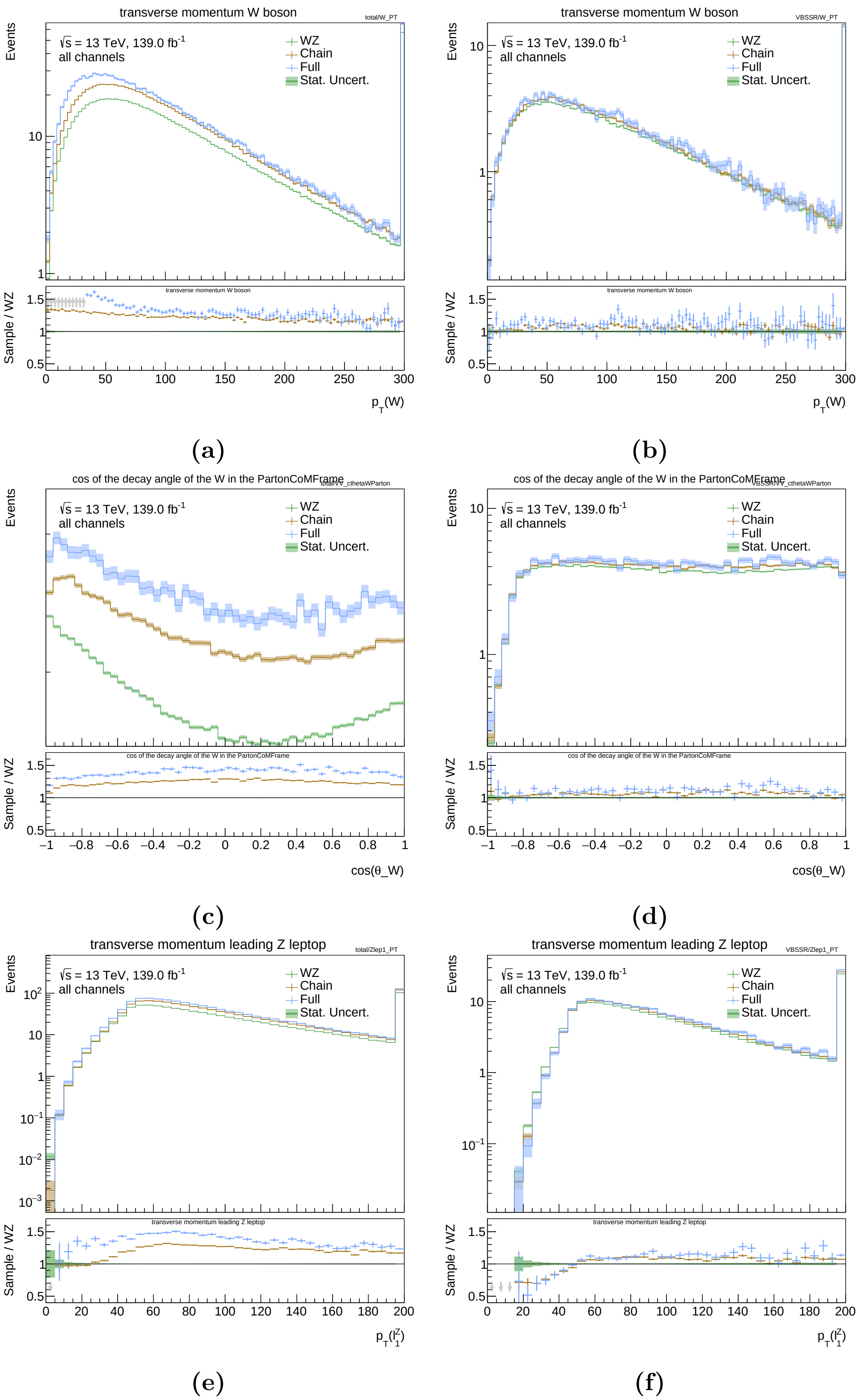

Figure 5.10: Comparisons of distributions for the samples with no approximation (blue), restriction to resonant diagrams (brown) and using the narrow-width-approximation (green). On the left side the distributions in the total phase space are shown while the right side shows the VBS phase space. From top to bottom the transverse momentum of the W boson, the pseudo-rapidity of the leading Z lepton and the decay angle of the W boson are shown.

Full	1257.8	± 3.5
Chain	1117.6	± 1.2
WZ	904.0	± 0.7
Ratio:Chain/Full	0.8886	± 0.0028
Ratio:WZ/Full	0.7187	± 0.0024
Ratio:WZ/Chain	0.8088	± 0.0012

Full	199.3	± 1.4
Chain	191.3	± 0.5
WZ	180.43	± 0.30
Ratio:Chain/Full	0.960	± 0.007
Ratio:WZ/Full	0.905	± 0.007
Ratio:WZ/Chain	0.9431	± 0.0030

Table 5.8: Event numbers of the three samples scaled to a luminosity of 139 fb^{-1} . Also depicted are their ratios. On the top they are shown for the total phase space while the table on the bottom depicts them for the VBS phase space.

5.2.2 Influence of the Chosen Decay Frame

Important for those studies is the decay angle of the boson decay products. For physically meaningful samples the bosons have to be decayed with respect to the frame their helicity was defined in. In Section 5.1 this was not done. This was due to the assumption that Madgraph used the laboratory frame for that purpose while it actually used the partonic center-of-mass frame. Since even with the wrong frame the results in Section 5.1 seemed to not be off and because this frame might not always be known it is interesting to study the effects of the choice of this frame.

This was done by using one sample produced by Madgraph with polarized bosons in the final state. These were then decayed once with the correct choice of frame and once using the laboratory frame. This means that samples 17 to 20 are used and referred to by the same name as in the previous chapter, 'WZPart' as well as samples 9 to 12 which will be called 'WZLab'. The events were subsequently showered with Herwig.

Some distributions can be seen in Figure 5.11.

The choice of frame for the decay as no effect on observables of jets (see Appendix A.3) and reconstructed bosons, which can be seen in Figures 5.11a and 5.11b. This is expected as the decay angle only has an effect on single leptons. For the sum of all polarized samples the transverse momenta of the individual leptons and the decay angles only show minimal differences as can be seen in Figures 5.11c and 5.11e. Figure 5.11d shows that for the polarized samples there is a small effect on the observables related to the individual leptons but it is still extremely small and effectively within statistics. Where the difference plays the biggest

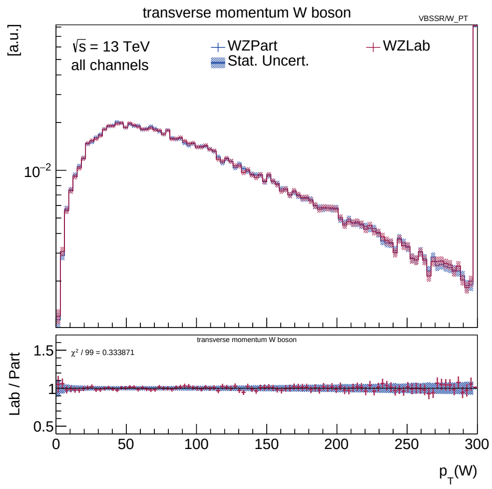

(a)

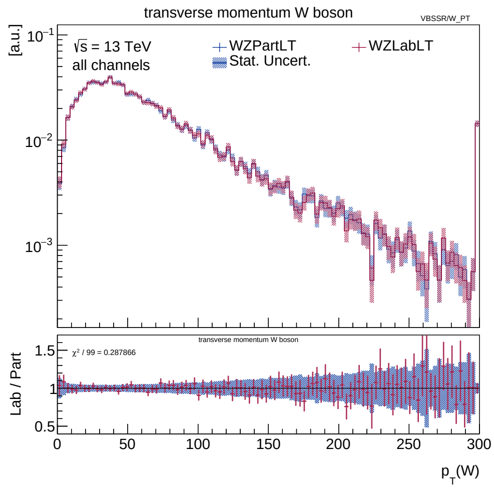

(b)

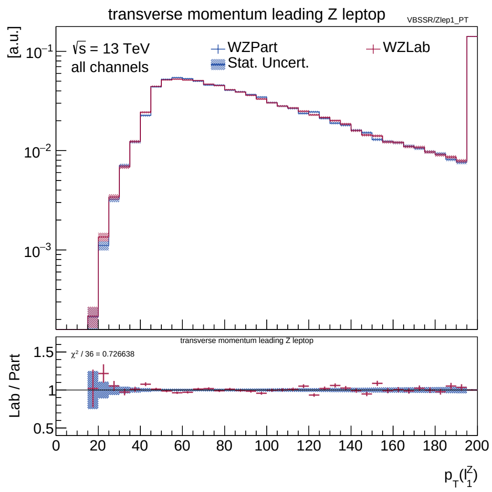

(c)

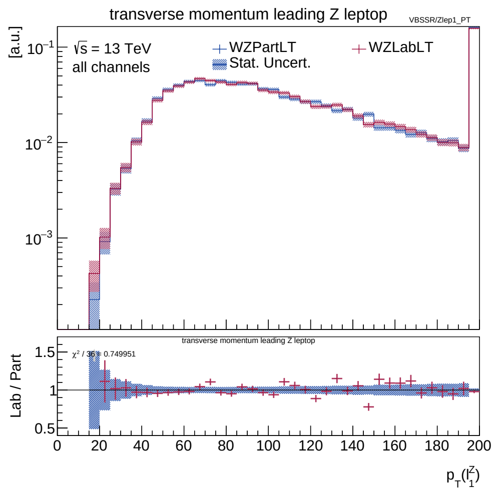

(d)

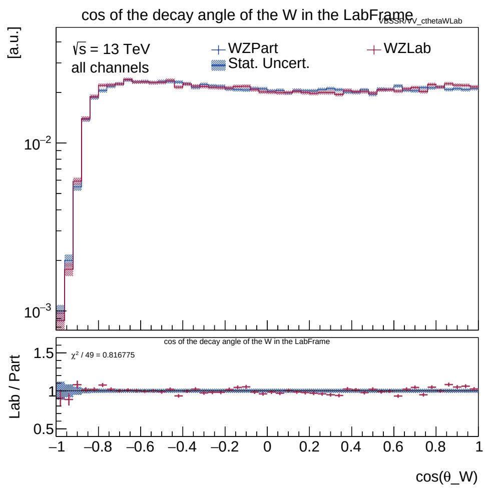

(e)

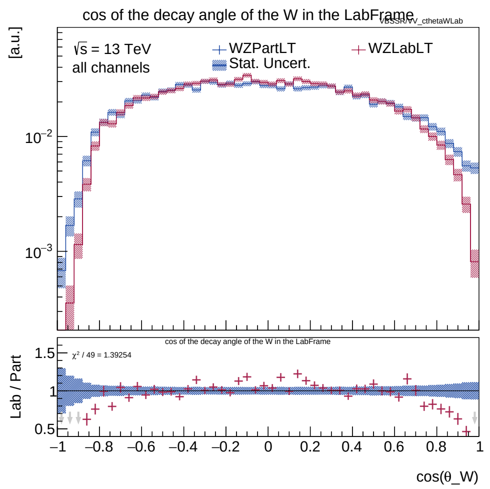

(f)

Figure 5.11: Comparison of normalized distributions between the samples decay with respect to the laboratory frame (red) and the partonic center-of-mass frame (blue) in the VBS phase space. On the left side the distributions is shown for the sum of all helicites while the right side shows it for longitudinal W and transversal Z bosons. From top to bottom the transverse momentum of the W, the transverse momentum of the leading Z lepton and the W's decay angle are depicted.

role is for the decay angles of the individual polarized samples shown in Figure 5.11f. This is exactly as expected.
The difference between the two studied frames is a boost along the z-axis that should peak at and also be symmetric about zero. This causes a similar effect for the difference between the two decay angles. That this is almost, but not exactly, the case can be seen in Figure 5.12. The dependency of $\Delta \cos\theta^*_V$ on the helicity combination comes from the differences in transverse momentum and rapidity of the bosons depending on their polarizations. However, even a symmetric decay angle difference would not explain the identical lepton observables by itself. Depending on the rapidity and decay angle distributions of the bosons even a symmetric decay angle difference around zero can lead to differences in the lepton observables. For example if both the bosons rapidity and the nominal decay angle were 0 then the rapidity of the lepton would also be 0. Any change of the decay angle would reduce the leptons transverse momentum and increase its absolute rapidity. It is unclear whether the distributions are not affected by the change in decay frame or if the deviations are just too small be differentiable from statistical fluctuations. It can be concluded that the decay angle should not be used for fitting the polarization fractions when it is not known in which frame the helicity of the bosons was defined in or when it is known that the decay was simulated in the wrong one. Other variables can, however, still be used for this frame as long as one is not sensitive to deviations significantly smaller than the statistical fluctuations of the samples used for this comparison. If the production frame is completely unknown the only save observables are those of the jets and the reconstructed bosons. Of course one still has to make sure they are sensitive to the helicity in the first place and that they are not heavily affected by the used approximations. Table 5.9 shows that the overall cross section is also not significantly affected by the choice of decay frame. The small differences most likely come from differences in the transverse momenta of the leptons in each event. The different choice of decay angle might make it so that the p_T of the lepton is too small to pass the minimum cut of 15 GeV/ 20 GeV as listed in Table 5.7.
In the future Madgraph will allow users to chose the frame in which the matrix element is calculated. This will also be the frame in which the final state bosons helicities are going to be defined in. From a physical point of view it should make no difference which frame the helicity was defined in as long as the decay happens with respect to that frame, if one adds up all of the polarizations. When this option is available a cross check should be done where the bosons are produced and decayed in the laboratory frame and also in the partonic center-of-mass frame. The resulting samples should be identical within statistic. Unlike the decay frame, the change in production frame should have a significant effect on the cross sections of the individual polarizations. The option was, however, not available within the time frame of this thesis.

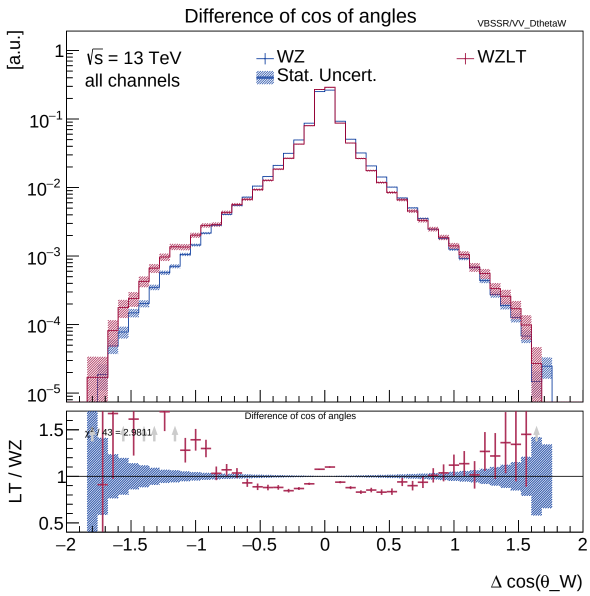

Figure 5.12: Differences of the cosines of the decay angle in the PCoM frame and in the lab frame $\left(\cos\theta_W^{part} - \cos\theta_W^{lab}\right)$ of the W boson.

WZPart	189.3 ± 0.7
WZLab	189.1 ± 0.7
WZPartLT	37.24 ± 0.31
WZLabLT	36.99 ± 0.31
Ratio:LT-Part	0.197 ± 0.004
Ratio:LT-Lab	0.196 ± 0.004

Table 5.9: Comparison of the event number of the polarized samples in the VBS phase space scaled to a luminosity of 139 fb^{-1}. 'Part' refers to the samples decayed with respect to the correct partonic center-of-mass frame and those with 'Lab' to the ones decayed with respect to the laboratory frame. 'L' and 'T' refer to the polarization of the W and Z boson in the sample in that order. The first two are the sum of all the individual ones produced with the same frame. Also depicted are the ratios of the individual polarized samples to the sum of the ones produced in that specific frame.

5.2.3 Comparison between WZDecay and Reweighting Methode

The reweighting approach was used in previous analyses. In this part of the thesis the old approach with compared with the newer on using the narrow-width-approximation to find advantages and disadvantages of each approach to make sure the right one is used in the future depending on what the goal is.

5.2.3.1 Fit of Helicity Fractions

The first step in generating polarized samples with the reweighting methode is to get values for the helicity fractions by fitting the analytically expected decay angle distributions shown in Equations 2.51 and 2.52 to the measured ones. For this the bosons are grouped depending on their transverse momentum and pseudo-rapidity. Then a weighted log likelihood [49] fit is performed in each of these bins using the ROOT software framework [50]. As cuts on the leptons distort the analytical functions these fits are performed in the total phase space. The used fitting method constrains each parameter to be between 0 and 1. It does not, however, constrain the sum to be equal to 1 as then the former constraint could not be guaranteed. The difference between these two options has already been studied in [17] with the result being that it is preferable to constrain the individual parameters. To make sure that the fit works properly in the first place a closure test is done by applying it to the WZDecay sample. Since the total WZDecay sample is a sum of samples that were produced with the proper distributions put in the fits should reproduce them exactly as long as there is enough statistics for a good fit. Table 5.10 shows this. Additional tables can be found in Appendix A.6. The polarizations fractions of the fit and the ones produced by Madgraph are identical within statistic. Figure 5.13 shows the decay angle distributions as well as the fit for the Z boson in the bins with the absolute value of the pseudo-rapidity larger than 3.0. The full set of figures is depicted in Appendix A.7. The differences in the shape as well as the declining number of events is clearly visible.

Another consistency check is done by considering the p-values of the fits. For this the χ^2 value as well as the number of degrees of freedom are used. It represents the probability to obtain a larger χ^2 value assuming a χ^2-distribution for that number of degrees of freedom. A total of 48 fits was done. If the fit performs well the p-values should be distributed uniformly over the $[0, 1]$. This distribution is shown in Figure 5.14.

While the distribution is not directly compatible with a uniform one it will still be used. The same fit was then used for the sample with the complete process as well as the one utilizing the decay chain syntax. The Table 5.11 shows the values generated by the fit for all three samples in the different bins of boson pseudo-rapidity and transverse momentum. This time events with both positively and negatively charged W's were used. Figure 5.15 also shows the p-value distributions for both of those fits.

While the p-value distribution for the full sample is compatible with a uniform one the one

Table 5.10: List of $f_0(Z)$ helicity fractions for the W^+Z WZDecay sample in different $(p_T/|\eta|)$-bins of the vector boson in %. The left column represent the root fits in the first step of the reweighting and the right one the actual fractions as produced by madgraph.

		Z			
		Fit	MG	Fit	MG
$p_T(V)$ \ $\lvert\eta\rvert(V)$		$0-1$		$1-2$	
$0-30$	[GeV]	49.4 ± 1.8	50.4 ± 0.6	50.8 ± 1.3	52.1 ± 0.4
$30-60$	[GeV]	33.8 ± 0.8	33.4 ± 0.2	37.0 ± 0.7	36.7 ± 0.2
$60-90$	[GeV]	23.3 ± 0.7	22.7 ± 0.2	25.6 ± 0.7	25.6 ± 0.2
$90-\infty$	[GeV]	12.2 ± 0.3	12.3 ± 0.1	13.4 ± 0.4	13.8 ± 0.1
		$2-3$		$3-\infty$	
$0-30$	[GeV]	55.5 ± 1.1	55.6 ± 0.3	59.5 ± 0.9	59.3 ± 0.3
$30-60$	[GeV]	40.1 ± 0.7	40.9 ± 0.2	39.4 ± 0.9	40.0 ± 0.3
$60-90$	[GeV]	29.2 ± 0.8	27.9 ± 0.2	24.0 ± 1.3	23.7 ± 0.3
$90-\infty$	[GeV]	14.0 ± 0.6	14.6 ± 0.1	12.8 ± 1.4	12.0 ± 0.3

Table 5.11: List of $f_0(Z)$ helicity fractions for the three samples in different $(p_T/|\eta|)$-bins of the vector boson in %. The values are as produced by the root fit. This is true even for the WZDecay sample.

		Z					
		Chain	Full	WZ	Chain	Full	WZ
$p_T(V)$ \ $\lvert\eta\rvert(V)$		$0-1$			$1-2$		
$0-30$	[GeV]	50.7 ± 2.0	49.0 ± 4.9	49.8 ± 1.3	53.3 ± 1.5	42.9 ± 3.8	50.8 ± 0.9
$30-60$	[GeV]	38.9 ± 0.9	39.3 ± 2.4	33.4 ± 0.6	39.6 ± 0.8	37.4 ± 2.1	36.1 ± 0.5
$60-90$	[GeV]	30.9 ± 0.8	31.7 ± 2.1	23.0 ± 0.5	29.2 ± 0.7	31.1 ± 2.0	25.0 ± 0.5
$90-\infty$	[GeV]	21.7 ± 0.4	22.2 ± 1.0	12.4 ± 0.2	21.2 ± 0.4	20.5 ± 1.1	13.5 ± 0.3
		$2-3$			$3-\infty$		
$0-30$	[GeV]	51.9 ± 1.2	48.1 ± 3.3	54.5 ± 0.8	55.7 ± 1.0	52.7 ± 2.5	57.1 ± 0.6
$30-60$	[GeV]	38.5 ± 0.8	39.6 ± 2.1	39.4 ± 0.5	33.3 ± 1.0	30.2 ± 2.5	37.5 ± 0.7
$60-90$	[GeV]	24.7 ± 0.9	24.6 ± 2.3	27.6 ± 0.6	16.5 ± 1.3	15.9 ± 3.5	23.1 ± 1.0
$90-\infty$	[GeV]	17.8 ± 0.6	17.8 ± 1.6	13.7 ± 0.4	12.0 ± 0.6	22.0 ± 4.9	12.5 ± 1.0

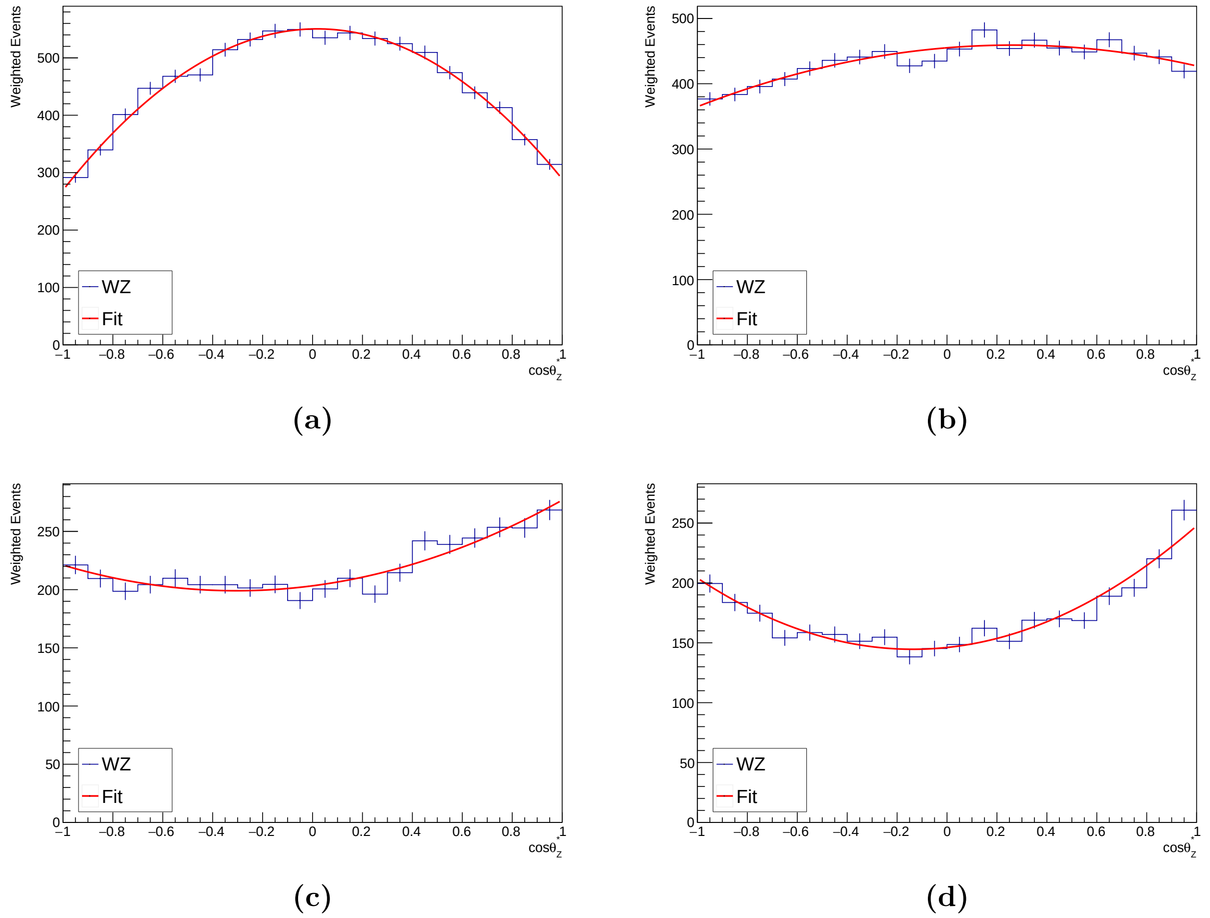

Figure 5.13: Decay angle distribution of the Z boson in W^+Zjj events (blue) alongside the fit of the analytical distributions to it (red). Depicted are the bins where the absolute pseudo-rapidity of the bosons is larger than 3. From top left to bottom right the transverse momentum of the Z was between $0-30$, $30-60$, $60-90$ and $90-\infty$ GeV. The distributions are for the sample produced with on-shell bosons.

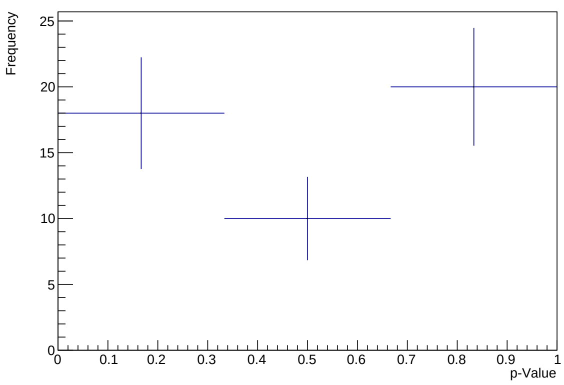

Figure 5.14: Distribution of the p-values for the fits of the analytical decay angle distributions to the measured ones for the sample produced with WZDecay.

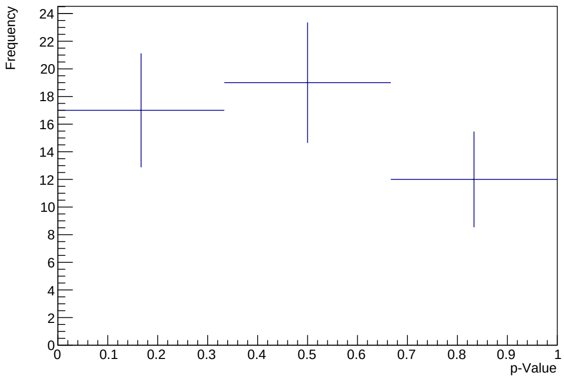

(a)

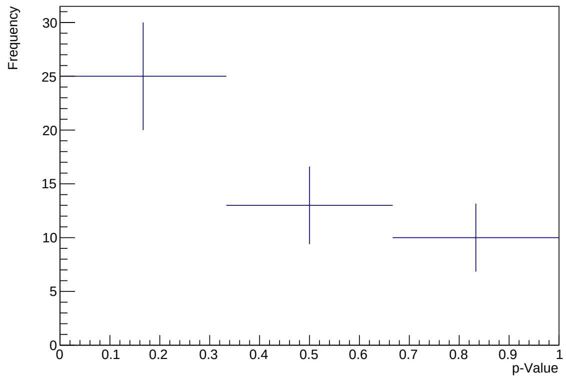

(b)

Figure 5.15: P-value distribution for the fits of analytical decay angle distributions to the measured ones for the full sample (left) and the decay chain sample (right).

for the chain sample deviates from that significantly. On top of that it is shifted towards lower values which corresponds to worse fits. As no systematic cause for these bad fit results could be found they were still used for the reweighting. The table shows that while all three samples display similar behaviour in that the fraction of longitudinal bosons decreases with higher p_T the Full and Chain samples do not reproduce the dependency on the rapidity nor do they reproduce the absolute values very well. This is especially visible in the bin with a transverse momentum larger than 90 GeV where the values for the two samples with no on-shell approximations are up to 80 % higher than the ones with the approximation present. This can also be seen in Figure 5.16 It shows the angle distributions of the Z boson for the three samples in three different bins. For bins in the upper two rows the fit to the WZDecay sample predicts lower fractions of longitudinal bosons while for the third one it predicts a larger one. This can be seen by the facts that for lower longitudinal fractions there are fewer events close to $|\cos\theta| = 1$ compared to those around zero. It is more obvious in the bin with the transverse momentum between $30 - 60$ GeV and the absolute value of the pseudo-rapidity in the range $0 - 1$. While the distributions in the Figures 5.16i and 5.16b are lower at the edges, Figure 5.16c is basically flat.

The different determination of the helicity fractions in each bin also has an effect on the overall helicity fraction combined over all of the bins. All of the helicity fraction a produced by the reweighting of the three samples and as produced by Madgraph directly are shown in Table 5.12.

The values for the total phase space show that the reweighting of the Full and Chain samples did not only produce wrong fractions in each bin but that they are also incorrect if summed over all of the bins. The reweighting of the samples produced with Madgraph and WZDecay, however, reproduces the correct values in the total phase space. In the VBS phase space the fractions for the samples with fewer approximations still remain significantly different from

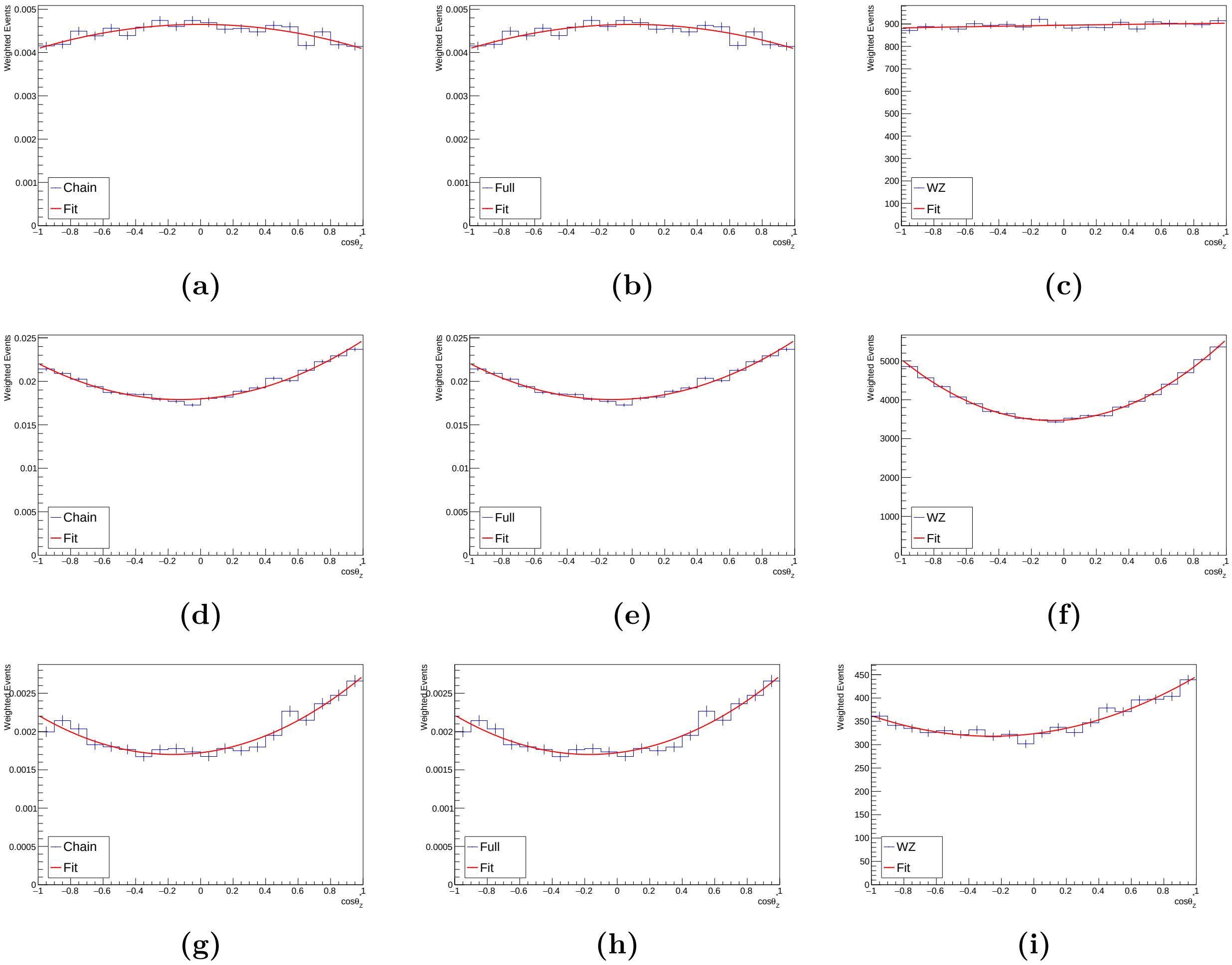

Figure 5.16: Decay angle distributions of the Z boson in $W^{\pm}Zjj$ events (blue) alongside the fit of the analytical distributions to it (red). From left to right are the sample with the decay chain syntax, with the full process and lastly the one using WZDecay. On top the $p_T/|\eta|$-bin $30-60\,\text{GeV}/0-1$, in the middle $90-\infty\,\text{GeV}/1-2$ and on the bottom $60-90\,\text{GeV}/3-\infty$ are shown.

	total phase space			
Sample	LL	LT	TL	TT
Full	7.85 ± 0.11	19.43 ± 0.19	20.33 ± 0.19	52.39 ± 0.29
Chain	7.70 ± 0.05	19.04 ± 0.07	20.59 ± 0.07	52.68 ± 0.11
WZReweight	5.38 ± 0.03	16.85 ± 0.05	17.77 ± 0.05	60.00 ± 0.08
WZ	5.42 ± 0.08	16.89 ± 0.08	17.80 ± 0.08	59.90 ± 0.10
	VBS phase space			
Sample	LL	LT	TL	TT
Full	8.25 ± 0.34	19.9 ± 0.5	20.6 ± 0.6	51.2 ± 0.7
Chain	8.50 ± 0.12	20.20 ± 0.18	20.81 ± 0.18	50.50 ± 0.26
WZReweight	5.57 ± 0.07	18.09 ± 0.12	17.29 ± 0.11	59.05 ± 0.19
WZ	6.68 ± 0.17	19.58 ± 0.18	17.82 ± 0.18	55.92 ± 0.21

Table 5.12: Total helicity fractions as determined by the reweighting of the three samples (first three rows) and by Madgraph directly (last row). On top they are shown in the total phase space and on the bottom in the VBS phase space.

the one with polarized on-shell bosons. The other majors observation is that the reweighting of the WZDecay samples now also gives fractions that significantly deviate from the values obtained directly from Madgraph. This is because not all of the dependencies of the helicity fractions on other variables can reproduced correctly. Thus, some phase space cuts effect the two samples differently.

These differences between the on-shell samples and the reweighting of the other two can be made plausible by the different diagrams, off-shell and interference effects that still play a significant role in the total phase space that the fit is done in.

5.2.3.2 Study of Reweighted Samples

Since the fits already show significant issues it is questionable that the reweighted samples will give good results either. The first thing, however, is to make sure that the reweighting does what it is supposed to do in the first place. That is to reproduce the distributions of the decay angles in the total phase space. This is shown in Figure 5.17. On the left it is visible that the total cross section differences seen in Section 5.2.1 are propagated through to the polarized samples. Additionally the different overall values of the helicity fraction discussed above also effect the normalization of the different samples. The right picture, however, shows that the distribution itself is reproduced properly for the transversal W boson in WTZL events.

However, this is not always the case. Figure 5.18 shows the decay angle distribution of the Z in WTZL events and both decay angles in the WLZT case. The decay angles for the other two helicity combinations are shown in Appendix **??**. It can be seen that the distributions of longitudinal Z bosons shows significant deviations. Figure 5.19a shows that WZdecay models this angle correctly. This means that the reweighted samples reproduce this observable incorrectly. The cause of this deviation was not studied further in this thesis. The decay angle distribution of the W boson in WLZT events also shows differences between the reweighting method and the approach using WZDecay. This time, however, the problem lies with the WZdecay sample. This can be seen in Figure 5.19b. There it has deviations from the analytical distribution in the left most bins. As WZdecay produced the correct distributions for both bosons in the parton level studies the issue most likely lies either in the showering, the small cuts that are already applied in the total phase space or in the analysis itself. Additionally the reweighted Full and Chain samples show deviations in the bin closest to $\cos\theta_V^* = -1$ for transversally polarized bosons.

Figure 5.20 shows both decay angles for WLZT and WTZL events in the VBS phase space. While the transversal distributions are correctly described like in the total phase space the longitudinal ones show significant deviations. The longitudinal Z shows deviations similar to the ones in the total phase space but with larger differences. The distributions of the longitudinal W also do not match exactly. The differences do not, however, align with those seen in the total phase space and are fairly similar to the ones for the longitudinal Z boson.

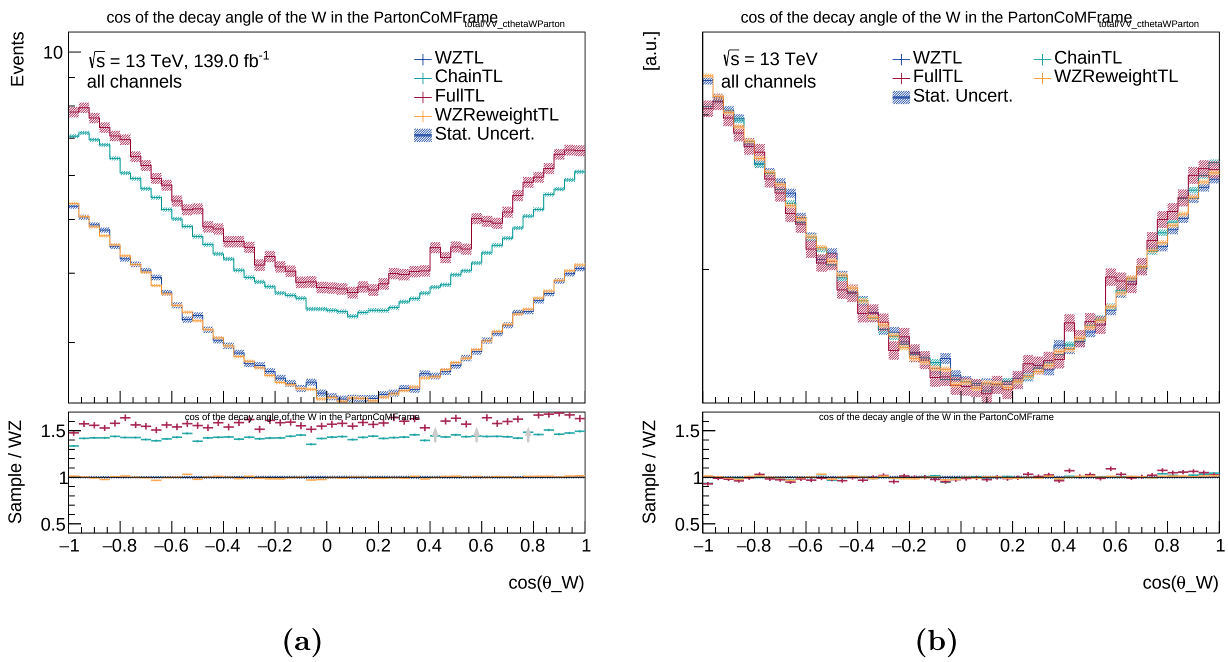

Figure 5.17: Comparison of the decay angle distributions of the W boson in the total phase space for events with a longitudinal Z and transversal W boson. ShShown are the reweighted samples of the full (red), decay chain (green) and WZdecay (orange) processes as well as the events produced with WZDecay (blue). On the left the distributions are shown as they are and on the right they are normalized to one.

The strong deviations of the decay angles from the analytical functions and those produced with Madgraph and WZDecay are already a strong argument against the reweighting method. Other distributions are still studied as a proper modelling of those could make the reweighting approach useful in some cases.

All actual studies of polarization in vector boson scattering are done in the VBS phase space. This means that the validity of the reweighting methode has to be proven there. Figure 5.21 shows some jet distributions. More observables can be found in Appendix A.4. The left side depicts both the Chain sample as well as all the samples produced by reweighting it to a specific helicity combination. Figure 5.21a and 5.21e show that the reweighting clearly has an effect even on distributions that the fit was not binned in. The important question is this is the effect that is expected for samples of that helicity. For that one helicity combination is picked out and the distributions of the reweighted Chain and Full samples are compared with the ones produced by WZDecay. Additionally the full WZDecay sample is also reweighted to the same helicity combination. This is done as a test to differentiate between inherent problems of the reweighting and those caused by using approximations. The latter not only causes problems for the variables that are directly affected by them in the VBS phase space but also for those that differ in the total phase space as the determination of the polarization fractions is done there.

Some variables that were affected by the use of the approximations even in the VBS phase

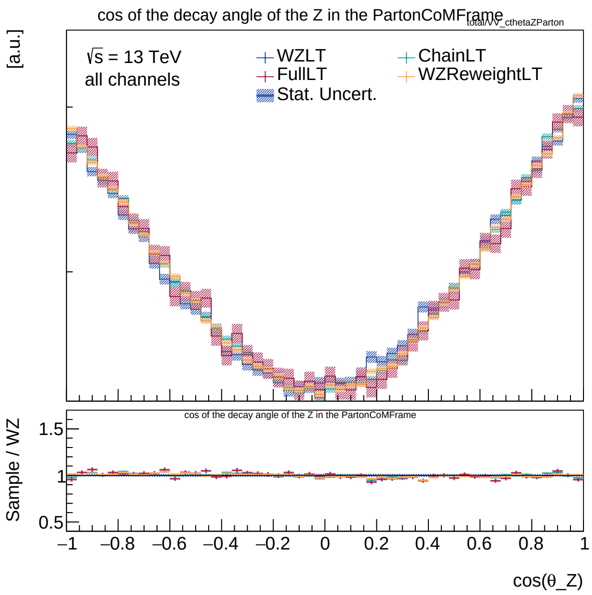

(a)

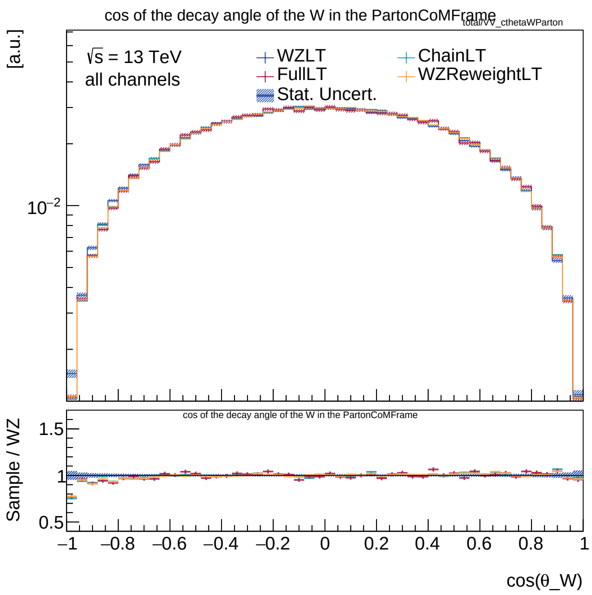

(b)

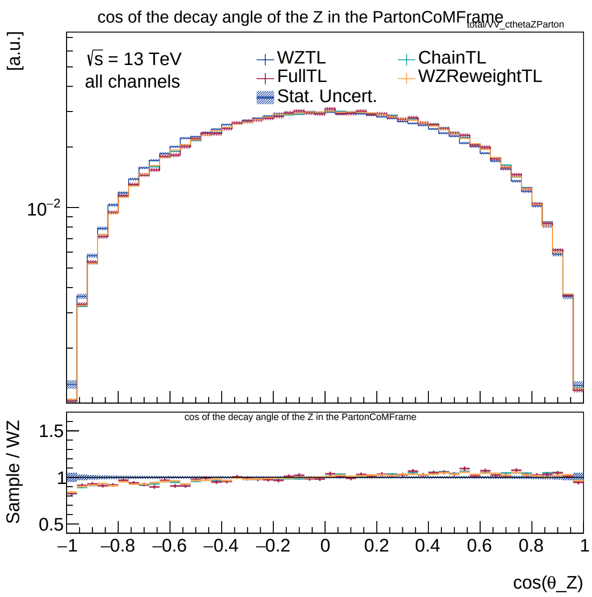

(c)

Figure 5.18: Comparison of normalized decay angle distributions in the total phase space. On top they are shown for WLZT event. On the left the angle of the Z and on the right the angle of the W is depicted. The figure on the bottom is of the Z boson in WTZL events. Shown are the reweighted samples of the full (red), decay chain (green) and WZdecay (orange) processes as well as the events produced with WZDecay (blue).

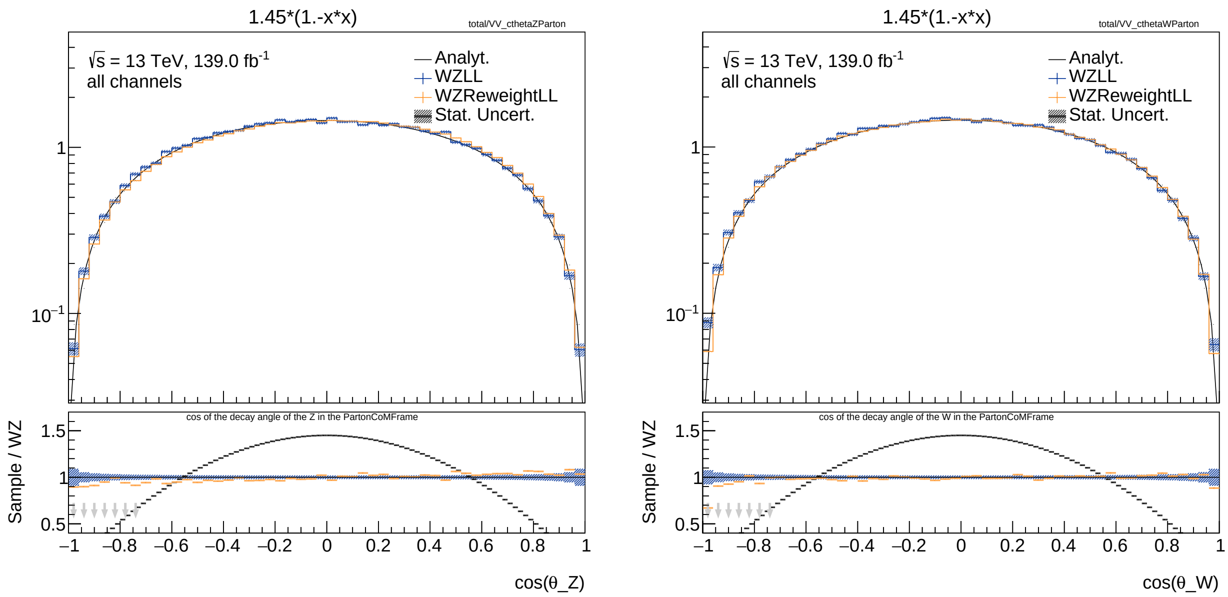

(a) **(b)**

Figure 5.19: Comparison of the longitudinal decay angle distributions. Shown are the sample produced with WZDecay (blue) as well as it reweighted (orange). Also depicted is the analytically expected distribution (black).

space where the transverse momentum of the leading jet, the pseudo-rapidity of the subleading jet and the rapidity difference between those two shown in Figures 5.9b, 5.9d and 5.9f. If the reweighting reproduces these variables correctly except for the direct effects of the restriction to resonant diagrams and the narrow-width-approximation the reweighted shapes should show the same deviations.

The the comparison of one polarization as produced by the different methods are shown in Figures 5.21b, 5.21d and 5.21f. It can be seen that the deviations are no the same as the ones for the full samples. In the case of the subleading jet's pseudo-rapidity the effect is even the reverse one. Interestingly enough the transverse momentum of the leading jet and the rapidity difference show fewer differences. This could either be because the reweighting corrects these mistakes or because it it reproduces them incorrectly with the effect of the wrong reweighting and the approximations cancelling each other. The strong deviation in Figure 5.21d suggests it might be latter.

No significant effect of the approximations was observed for the decay angle of the bosons, their transverse momenta and their pseudo-rapidities. As the first one is the distribution that the samples are reweighted to match and the latter two are the ones that the fit was binned in these are the observables that should definitely be modelled correctly. Figure 5.22 shows these distributions. Again the left side shows them for all the helicitys as produced by the reweighting of the Chain sample while the right side compares the reweighted samples with the WZDecay one for one specific helicity combination. Figures 5.22a and 5.22c clearly show the steps cause by the reweighting procedure. They are most visible in the distributions of

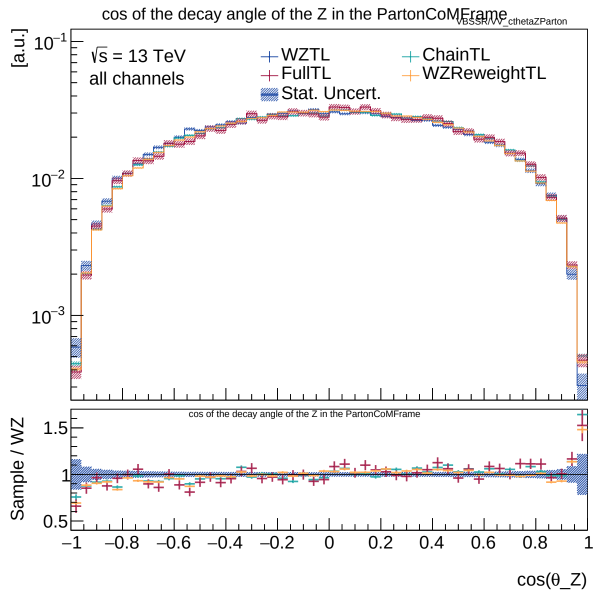

(a)

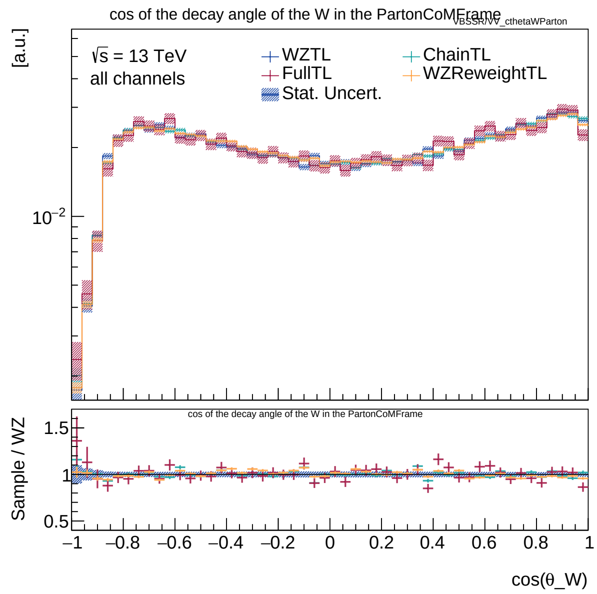

(b)

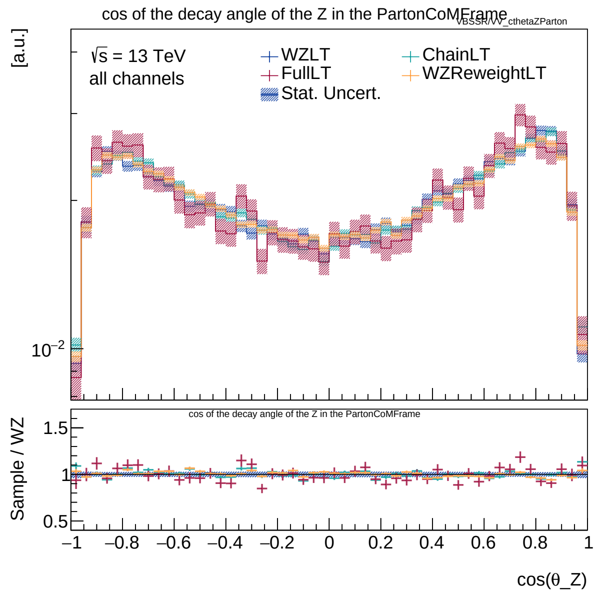

(c)

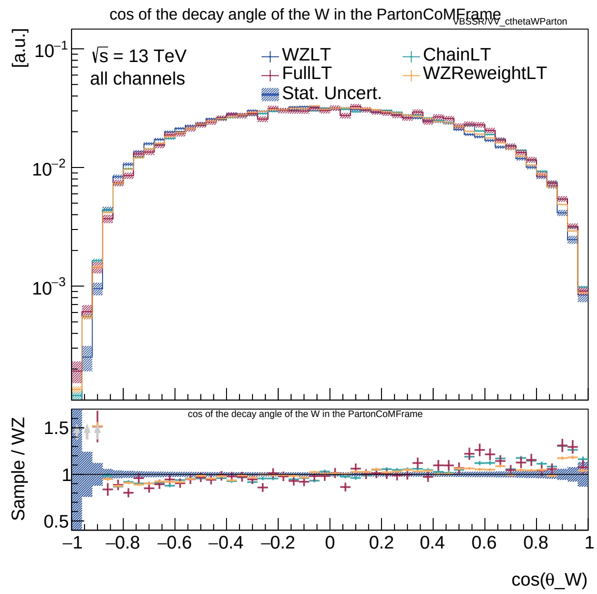

(d)

Figure 5.20: Comparison of normalized decay angle distributions in the VBS phase space.On top they are shown for WTZL events while the left depicts WLZT event. The left side shows the decay angle of the Z while the right side shows the one of the W.Shown are the reweighted samples of the full (red), decay chain (green) and WZdecay (orange) processes as well as the events produced with WZDecay (blue).

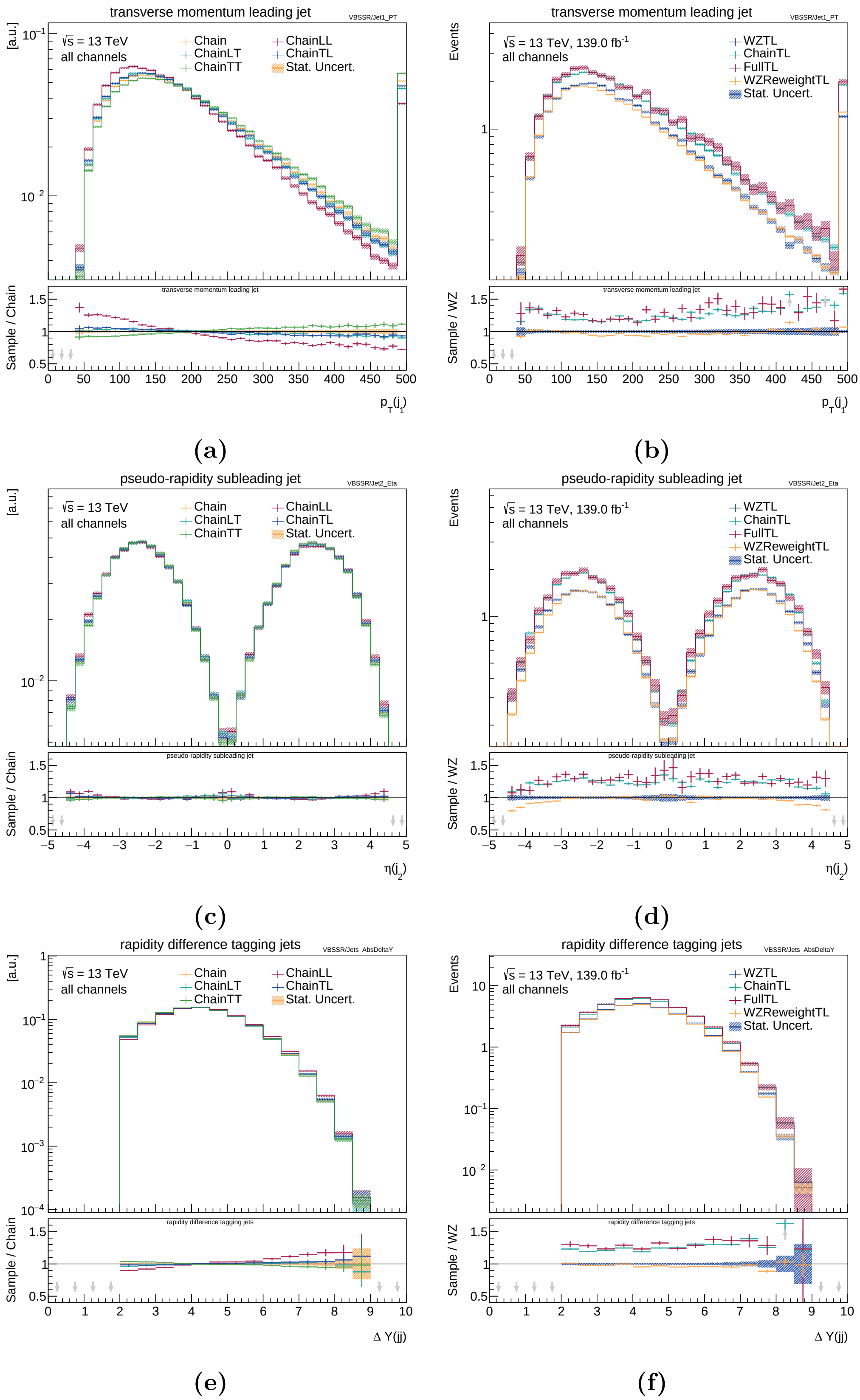

Figure 5.21: Comparisons of distributions for samples representing polarized bosons. On the left side the normalized distributions are shown for the reweighted samples produced with the decay chain syntax. The letters 'T' and 'L' represent the polarization of the W and Z bosons in that order. The right side compares the TL samples produced by reweighting the full (red) , chain decay (cyan) and WZDecay (organge) samples with the one produced by WZDecay (blue). All distributions are shown in the VBS phase space. From top to bottom the p_T of the leading jet, η of the subleading jet and the rapidity differences between those two are shown.

the transverse momentum but can also be seen for the pseudo-rapidity. There they are most visible at $|\eta| = 1$.

It can be seen that the ratios of polarizations in each bin is changed according to what one would expect from the fractions listed in Table 5.11. This expectation is that the distribution of the transverse momentum gets lowered at every bin edge for longitudinal Z's as the calculated fractions decreased with increasing p_T. For the pseudo-rapidity it is not immediately clear what the expectation for the shape of the distribution is. This is because the polarization fractions and their dependency on η differ widely depending on the transverse momentum. As can be seen in Figure 5.23 for η's close to zero most events have a Z with a p_T of 60 GeV or more which corresponds to an f_0 of around 3 %. For larger values of the absolute pseudo-rapidity lower transverse momenta dominate causing the fraction of longitudinal bosons to increase. This is exactly what can be seen in 5.22c.

The right side however shows that they still do not match all of the distributions produced by Madgrapgh and WZDecay. The transverse momentum distribution is fairly well described in the range of $30 - 90$ GeV. For higher and lower values the difference in determined polarization fractions and the binning cause significant deviations. The latter can be seen by the fact that also the reweighting of the WZDecay sample does not match the distribution for high p_T while the former can be seen in the fact that the reweighted distributions of the Full and Chain sample lie so much higher than the one of the reweighted WZDecay sample.

For the pseudo-rapidity the most obvious difference is visible for values smaller than between -1.5 and 1.5. There the reweighted samples with less approximations have significantly more events. This is mainly due to the fact that in this range the bin with higher transverse momentum contribute more and in those the fit to these samples produced significantly higher longitudinal fractions. For example for a transverse momentum between 60 and 90 GeV and $|\eta| < 1$ the fit to the Chain sample produced $f_0 = 30.9\,\%$ while the one to the WZDecay sample resulted in $f_0 = 23.0\,\%$. The deviations between the nominal and reweighted WZDecay samples are again because of the limited number of bins.

Overall the reweighting method showed significant problems in determining helicity fractions as well as reproducing correct distributions for most observables. Only the decay angle distributions of the W boson in the total phase space could be confirmed to have been modelled accurately. Meanwhile the samples generated via WZDecay showed some deviations for the decay angle distribution of the W boson. However, as this deviation was not present in the parton level studies the problem most does not lie with the approach itself. Due to this the approach utilizing the narrow-width-approximation should be used in the future.

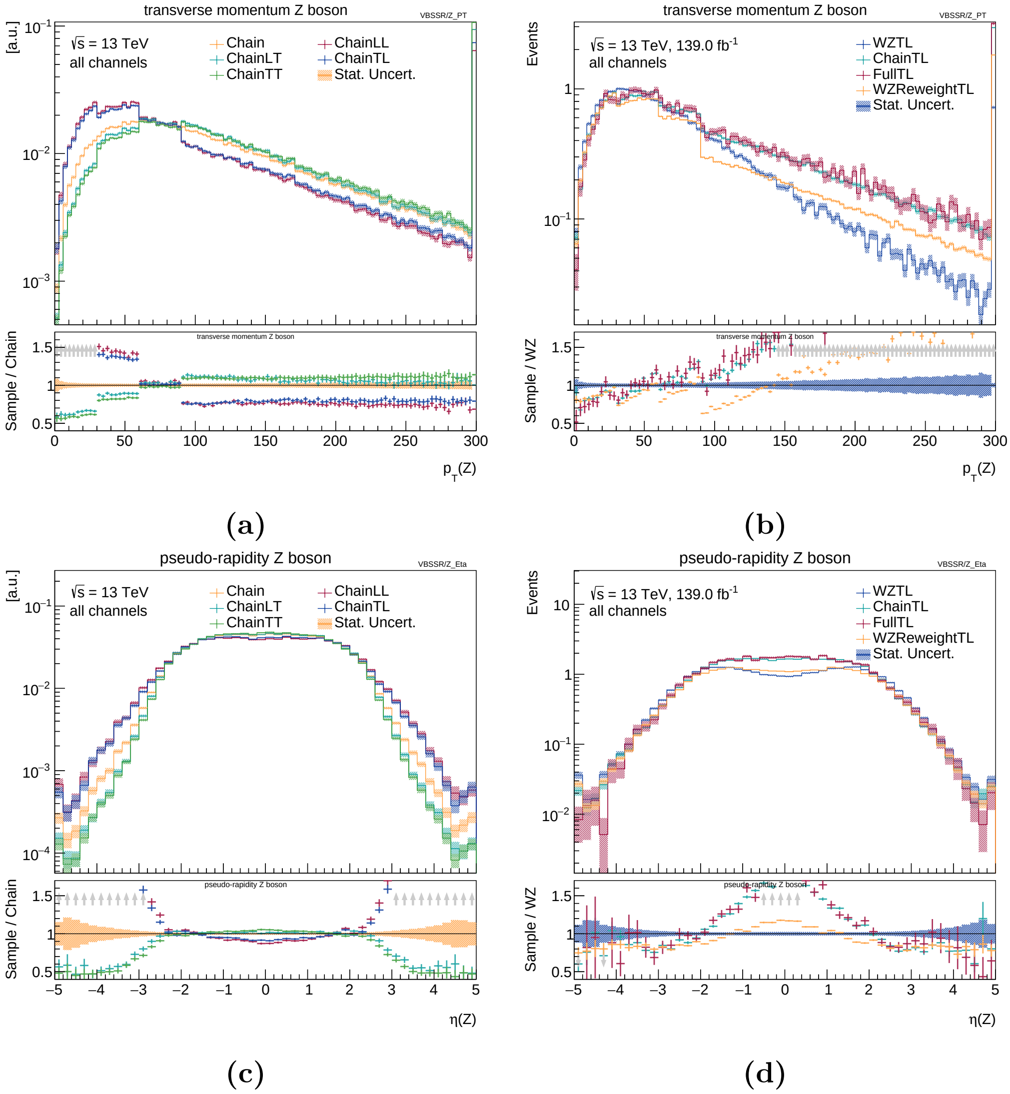

Figure 5.22: Comparisons of distributions for samples representing polarized bosons. On the left side the normalized distributions are shown for the reweighted samples produced with the decay chain syntax. The letters 'T' and 'L' represent the polarization of the W and Z bosons in that order. The right side compares the TL samples produced by reweighting the full (red) , chain decay (cyan) and WZDecay (organge) samples with the one produced by WZDecay (blue). All distributions are shown in the VBS phase space. From top to bottom the decay angle of the W, and the p_T and η of the Z are shown.

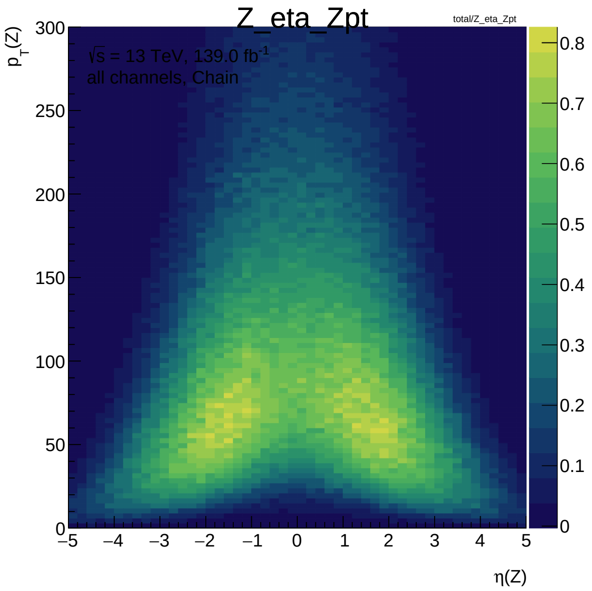

Figure 5.23: Visualization of the dependency of the Z's transverse momentum on its pseudo-rapidity. The distributions is shown for the Chain sample in the total phase space.

5.2.4 Determination of Sensitive Observables

The final thing to do at particle level is to do a study of which observables are good candidates for the eventual fit. This means to find out which variables are most effected by the polarization of one or both bosons. For this the samples produced with WZDecay were looked at. A table of scaled event numbers and ratios of the different samples can be found in Table 5.13.

Naively the variables that are expected to be sensitive to a bosons polarization are the corresponding decay angle as well as all kinematic variables of the reconstructed boson as well as those of the individual leptons and for the W the missing momentum. To first get a sense if these assumptions hold and what other observables might be sensitive the distributions of some of them are shown for the different polarizations in Figures 5.24,5.25 and 5.26. Even more distributions can be found in Appendix A.5.

The first figure, Figure 5.24, shows the distributions for the decay angle of the Z boson and the transverse momentum of the W boson. Both of which are expected to be sensitive from theoretical considerations as well as based on the parton level distributions shown in Section 5.1.2. The same is true here with strong shape deviations with differences over 50 % in some bins. Also shown is the p_T balance of the tagging jets. It is defined as $p^T_{bal}(jj) = \frac{\sqrt{(p_x(j_1)+p_x(j_2))^2+(p_y(j_1)+p_y(j_2))^2}}{\sqrt{p_x(j_1)^2+p_y(j_1)^2}+\sqrt{p_x(j_2)^2+p_y(j_2)^2}}$. While this variable shows differences for the cases with one longitudinal boson they get significantly bigger for the LL case. Figure 5.25 shows the distributions for some variables related to the jets. Like in the parton level case the jet distributions only show fairly small deviations of up to around 20 % for the case where a single boson is longitudinal but larger differences of up to 50 % for the double longitudinal case. Lastly Figure 5.26 shows shows variables that are not expected to be sensitive. That this is

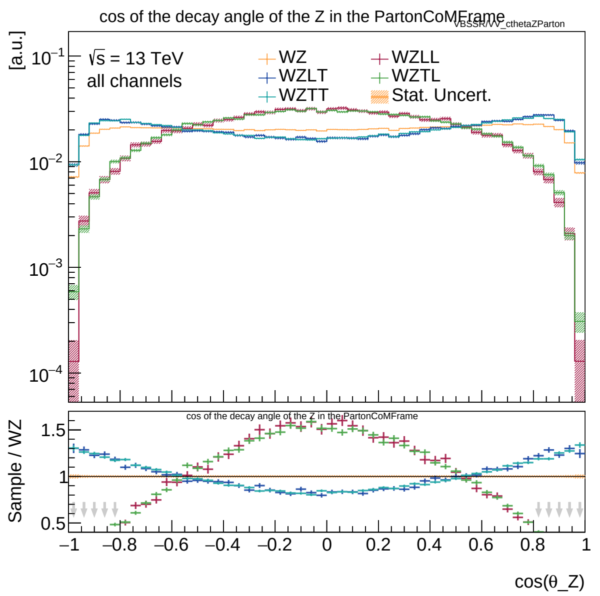

(a)

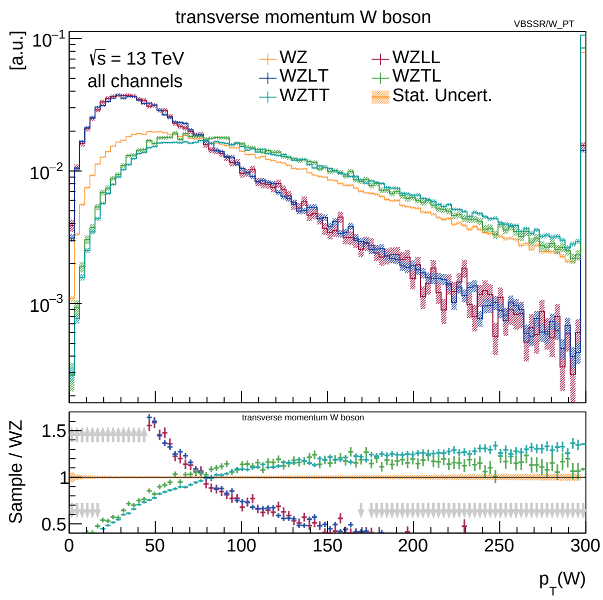

(b)

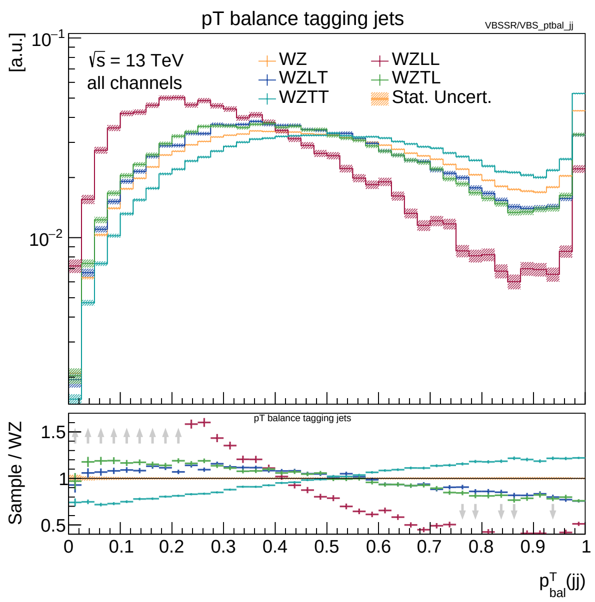

(c)

Figure 5.24: Comparison of normalized distributions between the different polarized samples produced with WZDecay for the partonic center-of-mass frame. The letters 'T' and 'L' refer to the polarization of the W and Z bosons in that order. The distributions are shown for the VBS phase space. From left to right and top to bottom the decay angle of the Z boson, the transverse momentum of the W boson and the balance of transverse momenta of the leading jets are depicted.

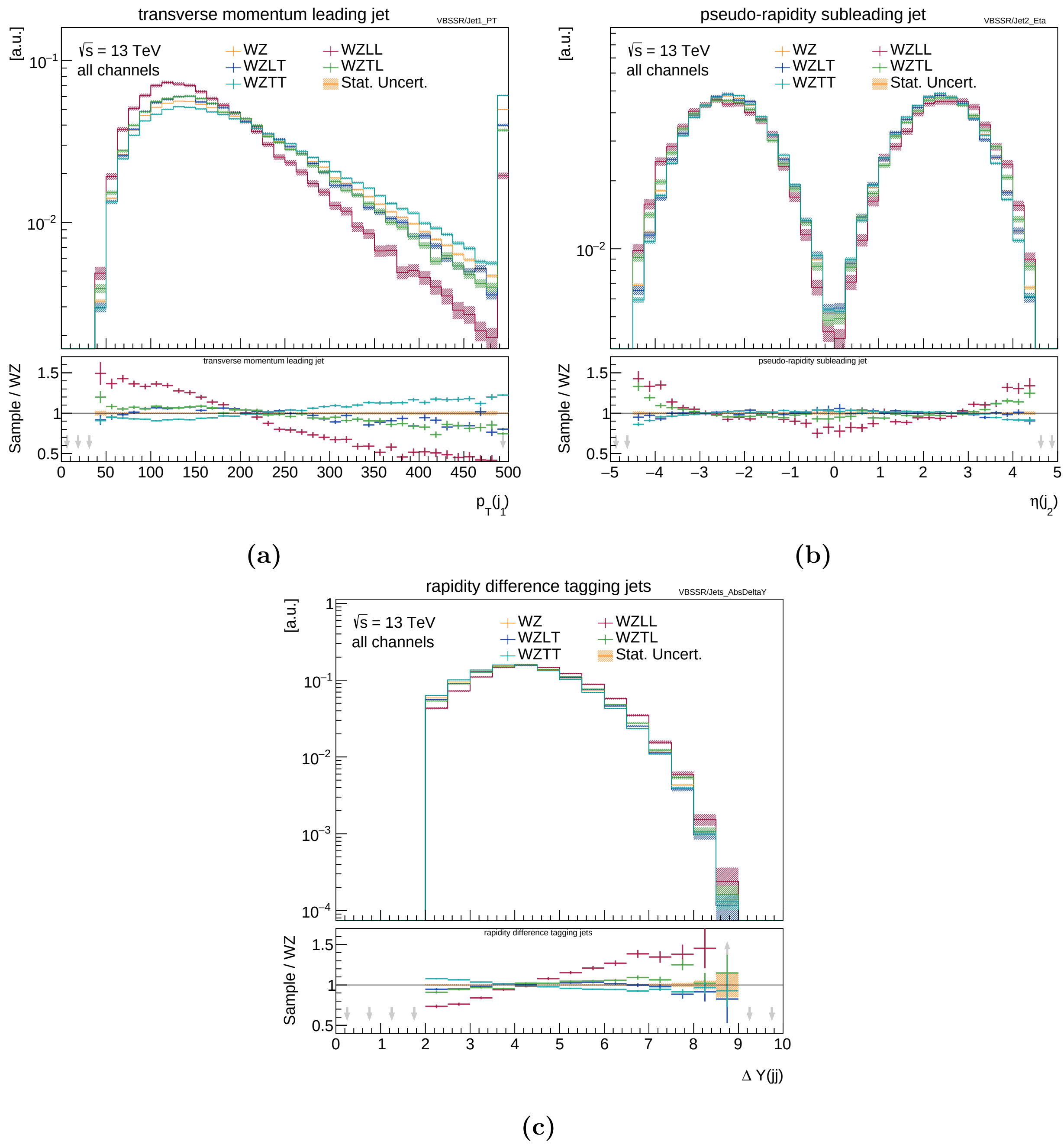

Figure 5.25: Comparison of normalized distributions between the different polarized samples produced with WZDecay for the partonic center-of-mass frame. The letters 'T' and 'L' refer to the polarization of the W and Z bosons in that order. The distributions are shown for the VBS phase space. From left to right and top to bottom the transverse momentum of the leading jet, the pseudo-rapidity of the subleading jet and the rapidity difference between those two are depicted.

WZ	180.43	± 0.30
WZLL	12.06	± 0.08
WZLT	35.33	± 0.13
WZTL	32.16	± 0.13
WZTT	100.89	± 0.23
Ratio:LL	0.0668 ± 0.0017	
Ratio:LT	0.1958 ± 0.0018	
Ratio:TL	0.1782 ± 0.0018	
Ratio:TT	0.5592 ± 0.0021	

Table 5.13: Event numbers of the polarized samples produced by Madgraph and WZDecay scaled a luminosity of 139 fb^{-1} in the VBS phase space. Also depicted are the ratios to the sum of all of them.

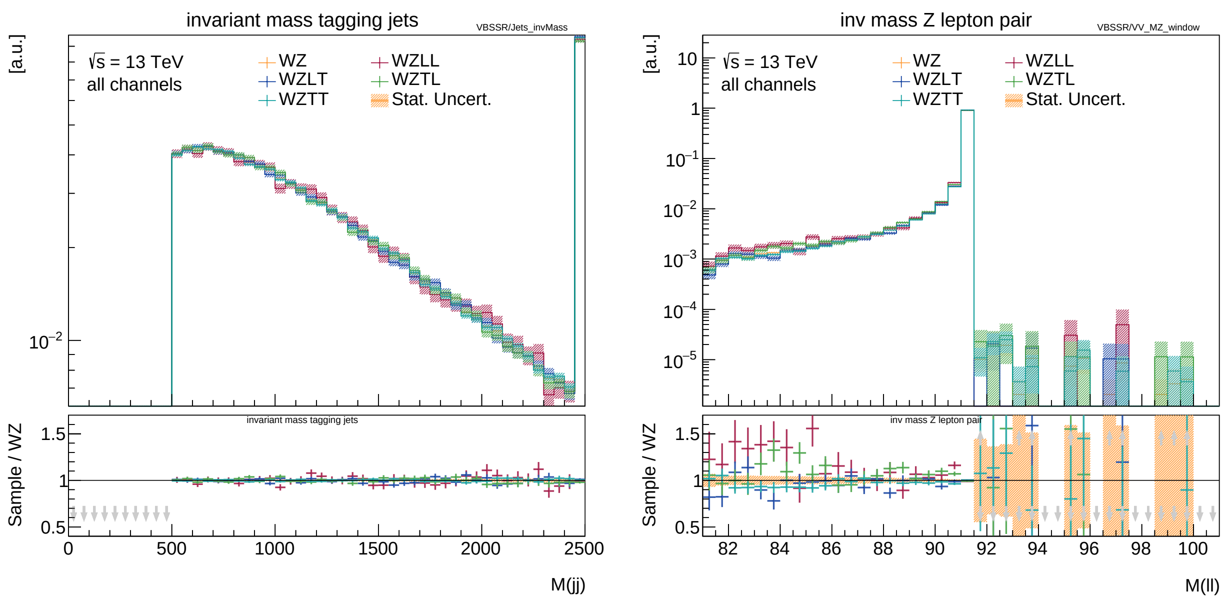

(a) **(b)**

Figure 5.26: Comparison of normalized distributions between the different polarized samples produced with WZDecay for the partonic center-of-mass frame. The letters ’T’ and ’L’ refer to the polarization of the W and Z bosons in that order. The distributions are shown for the VBS phase space. On the left the invariant mass of the tagging jets and on the right the mass of the reconstructed Z boson are shown.

in fact the case can be clearly seen by the fact that in the normalized plots no significant differences are visible. All of these results align with those of parton level study. Observables that showed differences for single boson polarization like the boson's transverse momentum at parton level do also show deviations at particle level. The same goes for observables showing difference for LL events like jet observables and those seeming unaffected by the polarization like the invariant mass of the Z leptons.

These visualizations are very helpful to get some rough idea of which variables could lead to good fit results. While such qualitative discussions are nice quantitative results are still needed, For this a template fit was done with the distributions of the individual polarized samples to the sum of them as well as the two samples with less approximations using the ROOT TFractionFitter [51] which employs a likelihood method. The results of this fit are the fractions of the scaled integrals of the polarized samples over the integral of the mixed sample. The used fitting method does not constrain the sum of the individual integrals to be exactly equal to the integral of the mixed sample. This results in the sum of fractions not being exactly equal to one. The fit considers both the statistical uncertainties of the mixed sample and the polarized templates. However, the uncertainties of the templates are not introduced as formal fit parameters. The minimisation with respect to those is done analytically. If the determined fraction is the same as the one that polarization was produced with by Madgraph then that observable is sensitive to the helicity of the studied bosons. The fractions of longitudinal W bosons was $f_0(W) = (26.26 \pm 0.35)\,\%$. For the Z boson it is $f_0(Z) = (24.50 \pm 0.35)\,\%$. The amount of events where both bosons were longitudinally polarized is $f_0(WZ) = (6.68 \pm 0.17)\,\%$ of the total. For each observable four separate fits were done . The first one fitted all four individual helicity (LL/LT/TL/TT) templates to the provided reference. This fit will be called the four-template fit. The second and third one each combined two of the templates so only the helicity of one boson was the same in the two remaining templates (WL/WT and ZL/ZT). The last fit also looked at just two templates. The first one included only events where both bosons were longitudinally polarized while the second one included the three other combinations. These will be referred to as two-template fits. The fraction of longitudinal W bosons is then either the direct fraction of the WL sample in the fit of WL and WT or the sum of the LL and LT fractions in the fit of all four templates. The latter is called the ALL-Fit while the former is referred to as the W-Fit. First a closure test was done to make sure the fit does what it is supposed to do. For this the individual polarization samples were fitted to their own sum. This means that theoretically all distributions should reproduce the actual values exactly. Since the fit takes the statistical uncertainties into account it is not expected that every variable gives the perfect result. Especially those that are extremely insensitive to the bosons polarization can still show significant deviations. The results of this fit can be seen in Table 5.14.

Here S_Z is the scalar sum of the transverse momenta of the Z leptons and S_W the scalar sum of

Table 5.14: List of longitudinal helicity fractions as determined by template fits based on different observables in %. Here the polarized samples were fitted directly to their sum. Fractions as produced by madgraph:
$f_0(W) = 26.26\,\%$ | $f_0(Z) = 24.50\,\%$ | $f_0(WZ) = 6.68\,\%$.

	WL		ZL		LL	
Observable	W-Fit	ALL-Fit	Z-Fit	ALL-Fit	LL-Fit	ALL-Fit
$p_T(Z)$	26.2 ± 1.4	26.0 ± 3.7	26.3 ± 0.3	26.3 ± 4.0	7.1 ± 0.3	7.0 ± 2.0
$p_T(W)$	27.9 ± 0.3	27.9 ± 4.5	24.4 ± 1.4	23.7 ± 3.9	7.0 ± 0.3	6.6 ± 2.2
S_Z	26.2 ± 1.5	25.9 ± 4.3	26.4 ± 0.3	26.4 ± 5.3	7.1 ± 0.4	7.1 ± 2.6
S_W	28.0 ± 0.3	28.0 ± 28.3	24.5 ± 1.4	23.4 ± 35.1	7.1 ± 0.3	6.4 ± 13.6
$\eta(Z)$	25.5 ± 1.4	22.9 ± 7.6	24.3 ± 0.3	24.4 ± 11.7	6.5 ± 0.4	5.5 ± 5.8
$\eta(W)$	26.0 ± 0.3	26.1 ± 2.9	23.9 ± 1.7	23.9 ± 5.7	6.6 ± 0.4	9.0 ± 1.3
$cos(\theta_Z^*)$	24.6 ± 1.5	25.0 ± 34.6	24.3 ± 0.4	24.3 ± 28.0	6.6 ± 0.5	6.6 ± 13.7
$cos(\theta_W^*)$	26.0 ± 0.4	26.0 ± 3.7	22.3 ± 1.5	24.6 ± 8.0	6.6 ± 0.4	7.6 ± 1.8
$p_T(\ell_1^Z)$	26.3 ± 1.5	26.4 ± 8.6	27.2 ± 0.3	27.2 ± 4.2	7.4 ± 0.4	7.4 ± 2.3
$p_T(\ell_2^Z)$	25.7 ± 1.7	24.5 ± 5.5	24.5 ± 0.4	24.6 ± 7.0	6.6 ± 0.5	5.8 ± 3.6
$p_T(\ell^W)$	27.7 ± 0.4	27.8 ± 9.7	24.2 ± 1.5	24.9 ± 10.2	7.0 ± 0.5	10.0 ± 4.7
$p_T(\nu)$	27.3 ± 0.4	27.3 ± 7.8	24.2 ± 1.5	23.8 ± 6.4	6.9 ± 0.5	6.6 ± 3.9
$\eta(\ell_1^Z)$	24.0 ± 1.6	24.6 ± 34.4	24.0 ± 20.5	24.1 ± 28.7	0.2 ± 9.9	6.5 ± 13.5
$\eta(\ell_2^Z)$	24.3 ± 1.6	24.9 ± 7.3	23.1 ± 0.9	23.1 ± 1.8	6.2 ± 11.6	5.2 ± 0.6
$\eta(\ell^W)$	25.0 ± 20.8	25.2 ± 5.3	24.2 ± 20.5	22.7 ± 4.6	6.2 ± 11.5	5.7 ± 3.0
$\eta(\nu)$	24.1 ± 1.0	23.8 ± 4.4	19.6 ± 1.7	29.6 ± 13.6	6.0 ± 11.2	12.2 ± 1.4
$p_T(J)1$	26.5 ± 1.1	24.5 ± 4.9	24.8 ± 1.0	26.8 ± 3.6	6.8 ± 0.6	6.4 ± 1.9
$p_T(J)2$	25.9 ± 1.4	25.5 ± 4.6	24.1 ± 1.4	25.8 ± 4.6	6.4 ± 11.6	3.7 ± 3.1
$\eta(J)1$	26.0 ± 1.3	21.5 ± 1.9	24.0 ± 1.4	35.3 ± 1.5	6.5 ± 11.7	3.5 ± 1.2
$\eta(J)2$	25.6 ± 1.7	24.6 ± 4.5	24.3 ± 1.2	24.5 ± 5.2	6.6 ± 1.2	6.1 ± 2.8
M_{JJ}	21.5 ± 1.6	36.7 ± 7.7	19.9 ± 1.6	37.2 ± 7.8	5.9 ± 11.3	8.3 ± 7.0
p_T^{miss}	27.3 ± 0.4	27.3 ± 28.9	24.0 ± 1.5	24.2 ± 16.0	6.9 ± 0.5	7.0 ± 14.2
M_Z	22.6 ± 1.4	28.4 ± 4.6	23.7 ± 1.3	23.1 ± 4.9	5.7 ± 1.1	5.7 ± 3.1
$M_T(W)$	26.0 ± 0.7	25.9 ± 24.7	22.2 ± 1.4	25.6 ± 34.1	6.6 ± 11.6	4.6 ± 12.4
$M(WZ)$	26.8 ± 1.1	25.9 ± 7.6	25.0 ± 0.9	25.9 ± 6.7	6.8 ± 9.9	6.9 ± 3.5
$M_T(WZ)$	26.2 ± 0.5	26.3 ± 6.6	24.5 ± 21.0	24.4 ± 6.2	6.6 ± 0.4	6.6 ± 1.0
$p_{bal}^T(jj)$	26.0 ± 0.6	26.0 ± 3.2	24.3 ± 0.6	24.3 ± 3.5	6.6 ± 0.3	6.6 ± 0.7
$p_{bal}^T(\ell\ell\ell\nu)$	26.0 ± 1.0	26.1 ± 2.9	24.3 ± 0.9	24.3 ± 3.2	6.6 ± 0.5	6.6 ± 0.7
$p_{bal}^T(\ell\ell\ell\nu jj)$	26.0 ± 1.2	25.8 ± 33.9	24.1 ± 1.3	24.5 ± 34.3	0.1 ± 12.0	6.3 ± 12.8
$\Delta Y(jj)$	26.2 ± 1.3	30.9 ± 1.4	24.5 ± 20.6	24.1 ± 1.6	6.6 ± 0.9	2.5 ± 1.1
n_{Jets}	25.9 ± 21.0	27.8 ± 1.7	23.8 ± 1.3	21.9 ± 2.0	4.9 ± 1.3	4.3 ± 1.2

the p_T of the W lepton and p_T^{miss}. Almost all observables reproduced the expected values fairly well. Only M_Z and M_{JJ} give consistently poor results. Which are exactly those observables that should be the least sensitive. Otherwise observables related to the other boson give worse results. Additionally both fit options give roughly the same result for the longitudinal fractions for most observables.

The second test was to split each of the polarization samples and fit one half of them to the sum of the other half. With this one get two separate samples while the one the fraction are fitted to still has the same expected fractions of longitudinal and transverse bosons. The results of that are shown in Table 5.15.

Here one can see that the observables that are naively expected to be sensitive produce better results. This include the decay angle of each boson, the rapidity and transverse momentum of the bosons and their decay products. While $\eta(W)$ gives fractions of 25.9 % and 25.4 % for longitudinal W bosons,which is still not perfect, $\eta(Z)$ gives 30.9 % and 24.2 % which is worse. The simple jet observables, however, give fairly poor results even though they should reflect the kinematics of the bosons which are sensitive to the helicities. As discussed in Section 2.3.2 this correlation is suppressed by helicity changes during the scattering. An important thing to note is that doing the two template fits one necessarily loses sensitivity to some variables. For example in doing the two-template W-Fit one presumes the ratio of longitudinal and transversal Z bosons in both of the templates to be the one produced by Madgraph. This means that any fits to observables sensitive to this fraction will be biased. Additionally the fractions of longitudinal Z bosons is slightly different for transversal and longitudinal W's. This means that the W templates still have some sensitivity to Z observables. Especially when the templates can add up exactly to the shapes of the total sample. A visualisation of this is shown in Figure 5.27. Slight shape differences can be seen for the transverse momenta of both the Z boson as well as its leading lepton. This is not the case for the decay angle or the leptons rapidity. This fact is reflected in the table. The two-template fit for the longitudinal fractions of the W boson still gives decent results of 25.9 % and 18.9 % for the fit of the momenta relating to the Z boson. However, the fits to the other two mentioned variables give 0 %.

As this is not the case for the four-template fits the results of these two methods are expected to differ in those variables. Which is exactly what can be seen in the tables. For example the four-template fit of the Z bosons transverse momentum gives a longitudinal fraction of W's of 38.6 %. Curious are the fit results for the balance of the transverse momenta of the tagging jets. While the two-template fits give consistently decent results for all three investigated fractions the four-template one gives an acceptable value for fraction of events where both bosons are longitudinal. This can be explained by the fact that the distributions of this variables are extremely similar for the case where the W is transversal and the Z longitudinal and the reverse one. These distributions are shown in Figure 5.28.

Table 5.15: List of longitudinal helicity fractions as determined by template fits based on different observables in %. In this fit each polarized sample was split in half. Then the one half was summed up and the remaining polarized samples were fitted to that sum. Fractions as produced by madgraph:
$f_0(W) = 26.26\,\%$ | $f_0(Z) = 24.50\,\%$ | $f_0(WZ) = 6.68\,\%$.

	WL		ZL		LL	
Observable	W-Fit	ALL-Fit	Z-Fit	ALL-Fit	LL-Fit	ALL-Fit
$p_T(Z)$	25.9 ± 2.1	38.6 ± 4.7	26.0 ± 0.4	25.4 ± 4.8	6.8 ± 0.4	14.2 ± 2.3
$p_T(W)$	27.9 ± 0.4	27.7 ± 24.6	27.0 ± 2.1	26.0 ± 26.0	7.0 ± 0.4	0.3 ± 0.9
S_Z	24.6 ± 2.1	27.0 ± 22.2	26.0 ± 0.4	25.6 ± 3.1	6.6 ± 0.5	0.0 ± 0.0
S_W	28.0 ± 0.4	29.1 ± 3.6	16.3 ± 2.2	13.6 ± 2.2	7.1 ± 0.5	10.7 ± 1.7
$\eta(Z)$	30.9 ± 2.0	24.2 ± 5.3	24.1 ± 0.5	24.2 ± 9.5	6.6 ± 0.6	24.2 ± 1.2
$\eta(W)$	25.9 ± 0.5	25.4 ± 0.9	26.1 ± 2.0	41.2 ± 9.1	6.6 ± 0.6	25.4 ± 0.8
$cos(\theta^*_Z)$	0.0 ± 0.5	8.8 ± 21.3	23.5 ± 0.5	23.3 ± 2.0	5.6 ± 13.1	8.6 ± 1.0
$cos(\theta^*_W)$	25.7 ± 0.5	25.5 ± 3.2	58.6 ± 2.5	64.6 ± 4.0	6.2 ± 0.6	25.5 ± 0.8
$p_T(\ell^Z_1)$	18.9 ± 3.1	48.7 ± 4.3	26.5 ± 0.4	25.6 ± 2.5	6.6 ± 0.5	25.6 ± 0.9
$p_T(\ell^Z_2)$	17.4 ± 2.2	13.7 ± 4.4	23.9 ± 0.6	24.4 ± 2.3	5.9 ± 0.7	0.0 ± 1.1
$p_T(\ell^W)$	27.5 ± 0.5	25.5 ± 68.1	29.5 ± 2.1	62.7 ± 76.7	6.7 ± 0.7	0.5 ± 58.6
$p_T(\nu)$	27.3 ± 0.5	26.1 ± 7.4	31.9 ± 2.1	49.5 ± 6.3	6.9 ± 0.7	9.9 ± 3.8
$\eta(\ell^Z_1)$	0.0 ± 0.1	0.0 ± 3.4	26.5 ± 21.2	28.3 ± 3.1	4.2 ± 3.7	0.0 ± 1.2
$\eta(\ell^Z_2)$	0.0 ± 2.5	100.0 ± 3.6	22.3 ± 1.3	19.4 ± 70.7	4.5 ± 2.9	19.4 ± 2.3
$\eta(\ell^W)$	22.6 ± 20.1	22.8 ± 2.9	31.7 ± 2.2	41.3 ± 7.4	4.1 ± 2.1	22.8 ± 1.7
$\eta(\nu)$	23.9 ± 20.4	26.9 ± 3.8	51.2 ± 26.1	27.7 ± 12.7	6.7 ± 1.6	26.9 ± 2.4
$p_T(J)1$	23.5 ± 19.8	1.6 ± 1.8	22.7 ± 1.5	49.3 ± 6.7	5.9 ± 1.2	1.6 ± 1.7
$p_T(J)2$	23.3 ± 2.1	24.0 ± 6.2	23.1 ± 2.0	25.6 ± 6.2	4.6 ± 2.9	1.1 ± 4.3
$\eta(J)1$	25.9 ± 1.9	21.8 ± 0.8	27.4 ± 2.5	21.9 ± 0.6	8.6 ± 1.5	21.8 ± 0.4
$\eta(J)2$	21.0 ± 2.1	19.7 ± 8.6	22.7 ± 1.8	18.7 ± 4.9	6.5 ± 11.8	17.3 ± 3.2
M_{JJ}	9.8 ± 13.0	16.9 ± 1.2	77.9 ± 19.7	64.0 ± 1.2	0.0 ± 1.4	0.2 ± 0.6
p_T^{miss}	27.2 ± 0.5	25.1 ± 5.8	37.0 ± 2.1	74.2 ± 11.0	6.8 ± 0.7	0.6 ± 2.3
M_Z	85.4 ± 3.0	98.1 ± 19.5	34.2 ± 1.9	4.0 ± 18.9	21.0 ± 1.6	2.2 ± 9.1
$M_T(W)$	27.4 ± 1.0	26.8 ± 24.9	18.2 ± 2.1	40.4 ± 26.2	7.3 ± 12.6	0.0 ± 0.0
$M(WZ)$	26.0 ± 1.2	49.0 ± 32.5	24.1 ± 1.2	0.0 ± 13.2	6.3 ± 9.7	0.0 ± 0.0
$M_T(WZ)$	26.1 ± 0.7	41.5 ± 34.9	24.1 ± 20.9	6.5 ± 17.5	6.5 ± 0.5	4.6 ± 11.3
$p^T_{bal}(jj)$	26.9 ± 0.9	39.3 ± 2.7	25.0 ± 0.9	10.1 ± 3.2	7.2 ± 0.5	10.1 ± 0.8
$p^T_{bal}(\ell\ell\ell\nu)$	25.3 ± 20.4	42.5 ± 17.9	23.5 ± 1.3	9.5 ± 4.6	6.6 ± 0.7	9.3 ± 3.9
$p^T_{bal}(\ell\ell\ell\nu jj)$	26.2 ± 1.8	31.0 ± 33.9	24.1 ± 1.8	30.1 ± 34.5	0.0 ± 0.0	30.1 ± 22.4
$\Delta Y(jj)$	25.3 ± 1.9	58.1 ± 36.4	22.9 ± 20.1	1.2 ± 15.1	5.3 ± 10.4	0.0 ± 12.6
n_{Jets}	29.0 ± 1.9	29.4 ± 3.3	27.1 ± 1.9	24.6 ± 3.9	0.1 ± 0.2	6.5 ± 2.4

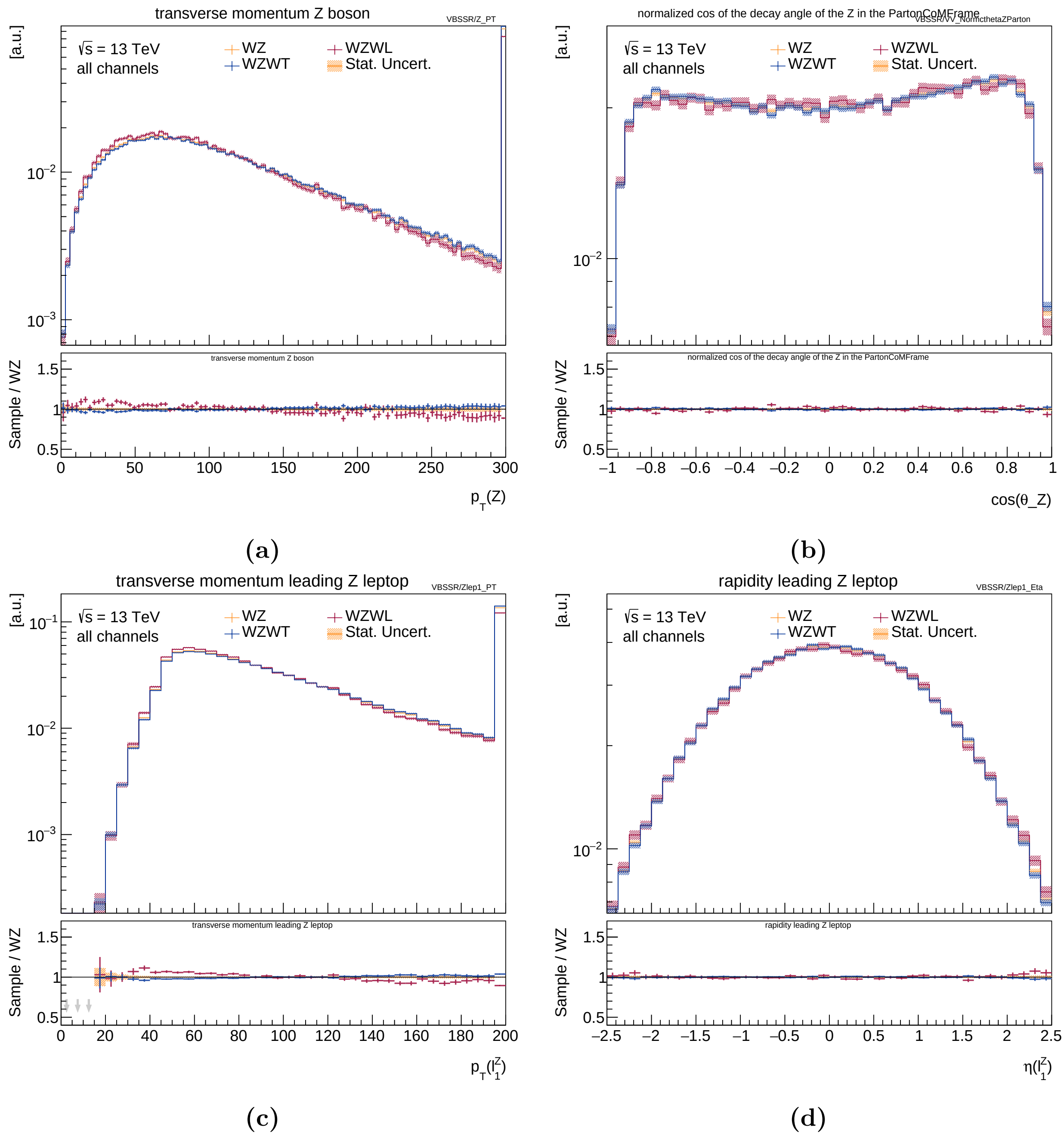

(a) **(b)** **(c)** **(d)**

Figure 5.27: Comparison of normalized distributions between the samples with longitudinal and transversal W bosons. These were produced using WZDecay with respect to the partonic center-of-mass frame. The distributions are shown for the VBS phase space. From top left to bottom right the transverse momentum of the Z boson, its decay angle and the p_T and η of the Z's leading lepton are shown.

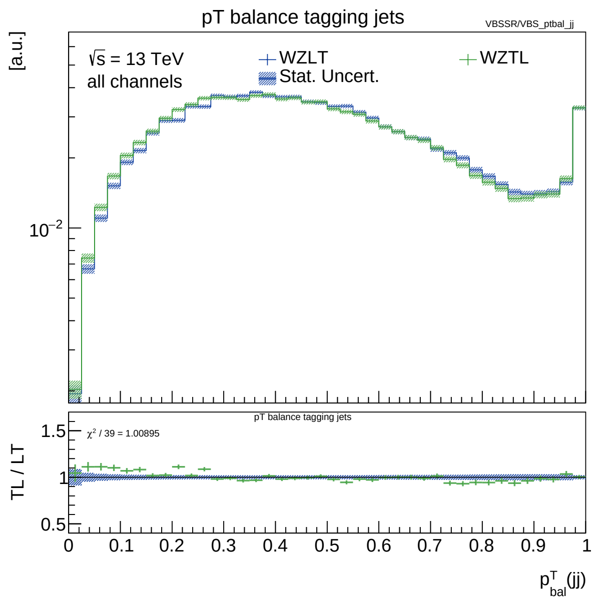

Figure 5.28: Comparison of the normalized distribution of $p^T_{bal}(jj)$ between the samples where the W is longitudinal and the Z is transversal (blue) and the reverse case (green). These were produced with WZDecay for the partonic center-of-mass frame. The distributions are shown for the VBS phase space.

This means that the four-template fit can only accurately determine the sum of these two fractions. It then has to distribute it to the two fractions which it can no do properly. The result is that either the LT or the TL fraction is too high. This then propagates to the fractions of longitudinal W and Z bosons. The two-template fits circumvent this problem again by fixing the fractions LT/LL and TT/TL for the W fit. This however means that the result is good because of the knowledge put into the fit and not because the variable is inherently sensitive to the polarization of single bosons. Similarly it behaves with the two-template fits to determine the LL fraction. Most observables even those not expected to be sensitive to the combination of both bosons give very good results. Meanwhile no variable gives a decent result in the four-template fit. This is again because one fixes the fraction of TT/TL and TT/LT in the two-template fit. For actually sensitive observables like the bosons transverse momenta and lepton observables the deviations to the actual values should be purely due to statistical fluctuations.

These same fits are done with the Chain and Full samples. There the individual helicity templates produced with WZDecay are fitted to the samples produced purely with Madgraph. For those fits the fractions are not expected to reproduce the values given above exactly as there are still some small deviations between the on-shell samples and these two as was shown in Section 5.2.1. This is especially the case for those variables most affected by these approximation effects. The results of these fits are shown in Tables 5.16 and 5.17 for the decay chain sample and the full sample respectively.

Again the observables that were naively expected to be sensitive and showed different distri-

Table 5.16: Longitudinal helicity fractions as determined by template fits based on different observables in %. Here the polarized samples produced with the help of WZDecay were fitted to the sample produced by madgraph via the decay chain syntax. Fractions as produced by madgraph:
$f_0(W) = 26.26\,\%$ | $f_0(Z) = 24.50\,\%$ | $f_0(WZ) = 6.68\,\%$.

	WL		ZL		LL	
Observable	W-Fit	ALL-Fit	Z-Fit	ALL-Fit	LL-Fit	ALL-Fit
$p_T(Z)$	67.3 ± 2.2	75.2 ± 4.8	28.6 ± 0.4	26.4 ± 68.4	10.0 ± 0.4	26.4 ± 3.7
$p_T(W)$	28.4 ± 0.3	25.8 ± 0.6	56.9 ± 2.1	88.6 ± 7.0	7.7 ± 0.4	25.7 ± 0.5
S_Z	100.0 ± 0.3	100.0 ± 1.1	24.2 ± 0.4	19.5 ± 0.6	4.0 ± 0.5	19.5 ± 0.5
S_W	24.7 ± 0.4	20.3 ± 1.7	100.0 ± 0.9	100.0 ± 1.6	2.6 ± 0.5	20.3 ± 0.9
$\eta(Z)$	100.0 ± 2.7	99.8 ± 44.6	28.8 ± 0.5	25.7 ± 33.6	12.0 ± 0.5	25.6 ± 20.9
$\eta(W)$	26.9 ± 0.5	27.7 ± 1.0	40.9 ± 1.9	29.6 ± 5.3	7.7 ± 0.5	27.7 ± 0.8
$cos(\theta^*_Z)$	100.0 ± 3.1	100.0 ± 4.5	27.9 ± 0.5	27.5 ± 3.5	11.0 ± 0.6	27.5 ± 1.0
$cos(\theta^*_W)$	28.6 ± 0.5	28.4 ± 13.5	100.0 ± 4.4	89.8 ± 6.4	9.8 ± 0.7	28.4 ± 2.1
$p_T(\ell^Z_1)$	0.0 ± 0.3	100.0 ± 1.4	23.7 ± 0.4	19.1 ± 1.6	2.7 ± 0.5	19.1 ± 0.7
$p_T(\ell^Z_2)$	70.1 ± 2.1	58.6 ± 13.2	27.4 ± 0.6	25.2 ± 11.9	10.1 ± 0.7	5.7 ± 6.2
$p_T(\ell^W)$	26.8 ± 0.5	23.3 ± 24.0	42.6 ± 2.0	95.1 ± 17.3	5.9 ± 0.5	19.5 ± 13.0
$p_T(\nu)$	27.5 ± 0.5	24.9 ± 27.2	0.0 ± 15.9	75.1 ± 30.1	7.0 ± 0.6	0.0 ± 2.7
$\eta(\ell^Z_1)$	100.0 ± 12.2	37.7 ± 65.4	38.6 ± 2.7	38.7 ± 3.8	25.2 ± 1.6	37.7 ± 1.3
$\eta(\ell^Z_2)$	0.0 ± 11.9	39.1 ± 16.4	18.7 ± 17.0	18.0 ± 0.9	0.1 ± 0.2	18.0 ± 0.9
$\eta(\ell^W)$	26.9 ± 1.3	29.2 ± 2.3	20.6 ± 18.9	28.8 ± 1.4	8.6 ± 1.4	28.4 ± 0.7
$\eta(\nu)$	24.8 ± 20.8	26.3 ± 1.7	49.2 ± 2.5	27.2 ± 4.8	6.9 ± 1.7	26.3 ± 1.6
$p_T(J)1$	38.5 ± 23.3	26.8 ± 15.9	36.8 ± 1.8	27.3 ± 15.5	14.0 ± 0.7	26.8 ± 3.7
$p_T(J)2$	56.4 ± 8.0	20.5 ± 2.3	70.3 ± 2.2	67.8 ± 3.2	36.9 ± 1.7	20.0 ± 2.0
$\eta(J)1$	67.1 ± 1.9	46.0 ± 7.0	99.9 ± 12.0	39.2 ± 2.8	32.8 ± 1.5	39.2 ± 2.8
$\eta(J)2$	77.3 ± 2.4	66.7 ± 28.5	38.5 ± 1.6	23.5 ± 4.0	18.7 ± 1.2	23.4 ± 4.0
M_{JJ}	100.0 ± 3.3	99.8 ± 3.8	100.0 ± 4.6	93.3 ± 2.1	100.0 ± 17.0	93.2 ± 1.9
p_T^{miss}	27.4 ± 0.5	24.8 ± 11.2	0.0 ± 3.0	75.1 ± 12.6	6.9 ± 0.6	0.0 ± 10.2
M_Z	100.0 ± 0.2	100.0 ± 0.3	100.0 ± 0.2	100.0 ± 0.3	100.0 ± 0.6	100.0 ± 0.3
$M_T(W)$	67.4 ± 1.3	96.9 ± 1.5	100.0 ± 0.8	99.9 ± 2.4	100.0 ± 0.7	96.9 ± 1.4
$M(WZ)$	25.2 ± 1.1	0.8 ± 2.6	23.6 ± 1.1	47.2 ± 3.6	5.4 ± 0.8	0.0 ± 0.3
$M_T(WZ)$	23.1 ± 0.6	0.0 ± 0.1	23.3 ± 0.7	51.9 ± 0.7	3.9 ± 0.5	0.0 ± 0.1
$p^T_{bal}(jj)$	27.2 ± 21.5	18.7 ± 5.3	25.4 ± 0.8	32.1 ± 6.8	7.1 ± 0.4	5.7 ± 1.2
$p^T_{bal}(\ell\ell\ell\nu)$	54.1 ± 1.3	56.9 ± 44.1	44.7 ± 1.0	18.8 ± 22.3	16.6 ± 0.6	18.4 ± 18.1
$p^T_{bal}(\ell\ell\ell\nu jj)$	100.0 ± 0.2	100.0 ± 0.4	100.0 ± 0.3	100.0 ± 0.4	100.0 ± 4.5	100.0 ± 0.2
$\Delta Y(jj)$	70.1 ± 2.0	41.6 ± 3.3	58.8 ± 23.6	44.5 ± 2.6	26.7 ± 1.3	24.1 ± 1.2
n_{Jets}	100.0 ± 0.2	100.0 ± 0.4	0.0 ± 0.0	100.0 ± 0.4	100.0 ± 0.5	100.0 ± 0.3

Table 5.17: List of longitudinal helicity fractions as determined by template fits based on different observables in %. Here the polarized samples produced with the help of WZDecay were fitted to the sample of the full process produced by madgraph. Fractions as produced by madgraph:
$f_0(W) = 26.26\,\%$ | $f_0(Z) = 24.50\,\%$ | $f_0(WZ) = 6.68\,\%$.

	WL		ZL		LL	
Observable	W-Fit	ALL-Fit	Z-Fit	ALL-Fit	LL-Fit	ALL-Fit
$p_T(Z)$	51.8 ± 11.8	44.5 ± 35.0	27.6 ± 0.8	26.3 ± 2.8	8.7 ± 0.9	0.1 ± 0.3
$p_T(W)$	28.8 ± 0.8	26.7 ± 14.1	56.1 ± 9.9	80.8 ± 9.6	8.3 ± 0.8	24.8 ± 7.1
S_Z	0.0 ± 1.9	79.9 ± 2.9	22.7 ± 0.9	18.6 ± 1.2	2.2 ± 1.0	0.0 ± 0.2
S_W	25.4 ± 0.8	21.7 ± 3.7	7.5 ± 3.6	78.3 ± 4.2	3.6 ± 1.0	0.0 ± 2.2
$\eta(Z)$	100.0 ± 1.4	98.5 ± 44.0	28.5 ± 1.0	25.5 ± 22.1	11.7 ± 1.2	25.5 ± 21.4
$\eta(W)$	27.4 ± 1.0	26.0 ± 3.0	48.4 ± 3.6	52.9 ± 4.5	8.1 ± 1.1	4.8 ± 1.4
$cos(\theta^*_Z)$	100.0 ± 10.7	26.8 ± 0.8	26.7 ± 1.1	26.4 ± 0.8	9.7 ± 1.2	26.4 ± 0.7
$cos(\theta^*_W)$	28.2 ± 1.1	28.1 ± 45.2	0.0 ± 76.2	12.8 ± 23.6	9.3 ± 1.3	12.8 ± 21.7
$p_T(\ell^Z_1)$	0.0 ± 1.3	82.4 ± 5.6	22.0 ± 0.9	18.1 ± 7.9	0.7 ± 1.0	0.4 ± 4.5
$p_T(\ell^Z_2)$	46.1 ± 3.4	41.3 ± 11.2	26.3 ± 1.2	25.9 ± 14.2	8.9 ± 2.1	14.9 ± 7.1
$p_T(\ell^W)$	26.7 ± 1.1	25.3 ± 10.1	25.1 ± 3.6	65.0 ± 13.3	5.6 ± 1.6	25.2 ± 8.9
$p_T(\nu)$	27.3 ± 1.1	27.8 ± 4.5	10.4 ± 3.3	10.2 ± 7.7	6.8 ± 1.3	2.6 ± 2.2
$\eta(\ell^Z_1)$	100.0 ± 20.1	48.2 ± 7.9	35.7 ± 3.2	29.4 ± 6.8	22.4 ± 3.2	22.0 ± 3.4
$\eta(\ell^Z_2)$	0.0 ± 65.8	62.6 ± 14.1	17.2 ± 2.2	15.4 ± 17.2	0.0 ± 55.4	1.6 ± 11.5
$\eta(\ell^W)$	26.4 ± 2.6	20.9 ± 3.3	31.1 ± 65.3	63.6 ± 12.7	5.5 ± 2.8	0.0 ± 0.1
$\eta(\nu)$	21.3 ± 2.7	24.5 ± 3.8	0.0 ± 67.9	27.9 ± 11.3	3.6 ± 2.2	24.4 ± 3.3
$p_T(J)1$	40.1 ± 2.8	25.5 ± 22.6	38.7 ± 2.7	31.5 ± 38.0	15.1 ± 1.8	25.3 ± 22.6
$p_T(J)2$	69.7 ± 3.5	61.5 ± 54.2	53.0 ± 11.3	34.9 ± 31.3	32.3 ± 22.3	34.1 ± 25.0
$\eta(J)1$	61.3 ± 3.3	84.3 ± 90.6	79.1 ± 3.6	3.8 ± 9.9	28.0 ± 2.7	0.0 ± 0.3
$\eta(J)2$	55.5 ± 3.5	59.0 ± 76.9	34.6 ± 3.6	32.3 ± 77.2	13.2 ± 2.8	0.1 ± 73.8
M_{JJ}	100.0 ± 61.7	100.0 ± 77.4	0.0 ± 18.4	0.0 ± 12.8	0.0 ± 6.5	0.0 ± 5.4
p_T^{miss}	27.3 ± 1.1	28.1 ± 12.8	13.9 ± 16.2	9.5 ± 11.3	6.9 ± 1.3	5.9 ± 6.2
M_Z	100.0 ± 0.3	100.0 ± 0.7	100.0 ± 0.7	100.0 ± 0.7	100.0 ± 3.0	100.0 ± 0.7
$M_T(W)$	55.5 ± 23.8	61.2 ± 3.1	100.0 ± 0.5	61.2 ± 4.9	51.6 ± 2.8	61.2 ± 2.6
$M(WZ)$	28.2 ± 21.7	11.1 ± 12.8	26.7 ± 2.4	43.3 ± 36.0	8.1 ± 3.1	11.0 ± 12.8
$M_T(WZ)$	22.9 ± 1.4	0.0 ± 0.4	22.9 ± 1.5	50.7 ± 1.7	3.7 ± 0.9	0.0 ± 0.2
$p^T_{bal}(jj)$	28.0 ± 1.9	3.3 ± 3.1	26.1 ± 1.8	49.3 ± 9.6	7.4 ± 1.0	3.3 ± 2.8
$p^T_{bal}(\ell\ell\ell\nu)$	52.7 ± 2.6	56.2 ± 42.7	43.6 ± 2.2	18.4 ± 22.2	16.2 ± 1.2	18.2 ± 16.7
$p^T_{bal}(\ell\ell\ell\nu jj)$	100.0 ± 1.4	100.0 ± 9.9	100.0 ± 0.6	100.0 ± 9.9	100.0 ± 6.9	100.0 ± 8.8
$\Delta Y(jj)$	63.0 ± 3.3	31.3 ± 5.6	54.8 ± 3.1	41.2 ± 14.6	24.2 ± 2.5	31.3 ± 5.0
n_{Jets}	0.0 ± 0.4	0.0 ± 0.7	0.0 ± 0.3	0.0 ± 0.6	0.0 ± 0.2	0.0 ± 0.2

butions for the different polarizations of each boson give results close to the expected value. In contrast to the fit to the split sum of the templates, insensitive variables now give results that are significantly different from the expected values for both two- and four-template fits. Only the jet p_T balance gives good results for the LL fraction in both of the fits. Some variables again give decent results in the two-template fit but are nowhere close in the four-template one. The variables that give somewhat sensible results in both fits for both samples are summarized in Table 5.18.

For the single boson fits these are the observables directly related to that boson or its leptons.

One thing to note is that the four-template fits has significantly higher uncertainties. For one this is because it has to fit four templates with less statistics each and also because the shown uncertainties are the sum of the individual contributions. As these two contributions have almost the same exact shapes the fit can push them from one value to the other increasing the uncertainties. Additionally the values tend to be higher then the direct Madgraph ones for most observables. Some are even extremely far away. This are mostly the rapidities of the leptons. These differences can be explained by the fact that the approximations have a fairly significant effect on these variables. This is demonstrated in Figure 5.29. In Figure 5.29a it can be seen that the deviation between the stack and the decay chain sample is at high values of lepton pseudo-rapidity. Incidentally longitudinal Z bosons produce leptons with higher absolute rapidity. The opposite can be seen in Figure 5.29c. Figure 5.29e shows that the W decay angle distribution has the biggest deviation around a cosine of 0. That the values provided by the fit do indeed lead to a better agreement between the distributions can be seen in Figure 5.30. The left side corresponds to the fractions as they were produced by Madgraph in the on-shell sample while the right side depicts the values of the fit.

If the sample that the templates are fit to are scaled to the Run-2 luminosity of $139\,\mathrm{fb}^{-1}$ and the errors for each bin are set to the poissonian errors the uncertainties of the fit increase considerably. The results of this fit are shown in Table 5.19. For the single boson fits uncertainties remain small enough so that the longitudinal fractions are still incompatible with zero. The scaled distributions of this can be found in Figure 5.31. The same is not true for the fraction of both bosons being longitudinal. There the fraction is underestimated significantly and the uncertainties of the fit are extremely large. Based in the results of Table 5.18 this was also not expected, atleast not for the full sample. The distributions used for this fit are shown in Figure 5.32. The increased number of fit parameters, the generally small fraction of doubly longitudinal events and the fact that the used approximations have a not insignificant effect on the distributions of the jets p_T balance cause the poor agreement with the value generated by Madgraph. The last part is shown in For the sample of the full process which was used for these last fits the poor statistics also play a role. Increasing the Luminosity even further to the roughly $3000\,\mathrm{fb}^{-1}$ of the High-Luminosity LHC and increasing the number of bins used for the fitting from 10 to 20 the fraction of doubly longitudinal events gets estimated to $(3.4 \pm 12.1)\,\%$. This is not a

Table 5.18: List of longitudinal helicity fractions as determined by template fits based on selected observables in %. Here the polarized samples produced with the help of WZDecay were fitted to the samples produced by Madgraph either via the decay chain syntax or as the full process. Fractions as produced by Madgraph:
$f_0(W) = 26.26\,\%$ | $f_0(Z) = 24.50\,\%$ | $f_0(WZ) = 6.68\,\%$.

	Chain		**Full**	
WL	W-Fit	ALL-Fit	W-Fit	ALL-Fit
$p_T(W)$	28.4 ± 0.3	25.8 ± 0.6	28.8 ± 0.8	26.7 ± 14.1
S_W	24.7 ± 0.4	20.3 ± 1.7	25.4 ± 0.8	21.7 ± 3.7
$\eta(W)$	26.9 ± 0.5	27.7 ± 1.0	27.4 ± 1.0	26.0 ± 3.0
$\cos\theta^*_W$	28.6 ± 0.5	28.4 ± 13.5	28.2 ± 1.1	28.1 ± 45.2
$p_T(\ell^W)$	26.8 ± 0.5	23.3 ± 24.0	26.7 ± 1.1	25.3 ± 10.1
$\eta(\ell^W)$	26.9 ± 1.3	29.2 ± 2.3	26.4 ± 2.6	20.9 ± 3.3
p_T^{miss}	27.4 ± 0.5	24.8 ± 11.2	27.3 ± 1.1	28.1 ± 12.8
ZL	Z-Fit	ALL-Fit	Z-Fit	ALL-Fit
$p_T(Z)$	28.6 ± 0.4	26.4 ± 68.4	27.6 ± 0.8	26.3 ± 2.8
$\eta(Z)$	28.8 ± 0.5	25.7 ± 33.6	28.5 ± 1.0	25.5 ± 22.1
$\cos\theta^*_Z$	27.9 ± 0.5	27.5 ± 3.5	26.7 ± 1.1	26.4 ± 0.8
$p_T(\ell^Z_1)$	23.7 ± 0.4	19.1 ± 1.6	22.0 ± 0.9	18.1 ± 7.9
$p_T(\ell^Z_2)$	27.4 ± 0.6	25.2 ± 11.9	26.3 ± 1.2	25.9 ± 14.2
$\eta(\ell^Z_1)$	38.6 ± 2.7	38.7 ± 3.8	35.7 ± 3.2	29.4 ± 6.8
$\eta(\ell^Z_2)$	18.7 ± 17.0	18.0 ± 0.9	17.2 ± 2.2	15.4 ± 17.2
LL	LL-Fit	ALL-Fit	LL-Fit	ALL-Fit
$p^T_{bal}(jj)$	7.1 ± 0.4	5.7 ± 1.2	7.4 ± 1.0	3.3 ± 2.8

Table 5.19: List of longitudinal helicity fractions as determined by template fits based on selected observables in %. Here the polarized samples produced with the help of WZDecay were fitted to the samples produced by Madgraph either via the decay chain syntax or as the full process. For this fit the errors of the 'data' samples was set as the poisson errors of the events numbers corresponding to a luminosity of $139\,\mathrm{fb}^{-1}$. Fractions as produced by Madgraph: $f_0(W) = 26.26\,\%$ | $f_0(Z) = 24.50\,\%$ | $f_0(WZ) = 6.68\,\%$.

	Chain	**Full**
WL	**W-Fit**	
$p_T(W)$	28.4 ± 7.7	28.8 ± 7.6
S_W	24.8 ± 8.2	25.0 ± 8.1
$p_T(\ell^W)$	27.2 ± 9.6	27.1 ± 11.0
ZL	**Z-Fit**	
$\cos\theta^*_Z$	27.8 ± 9.3	26.9 ± 10.6
LL	**ALL-Fit**	
$p^T_{bal}(jj)$	1.7 ± 5.4	2.3 ± 11.4

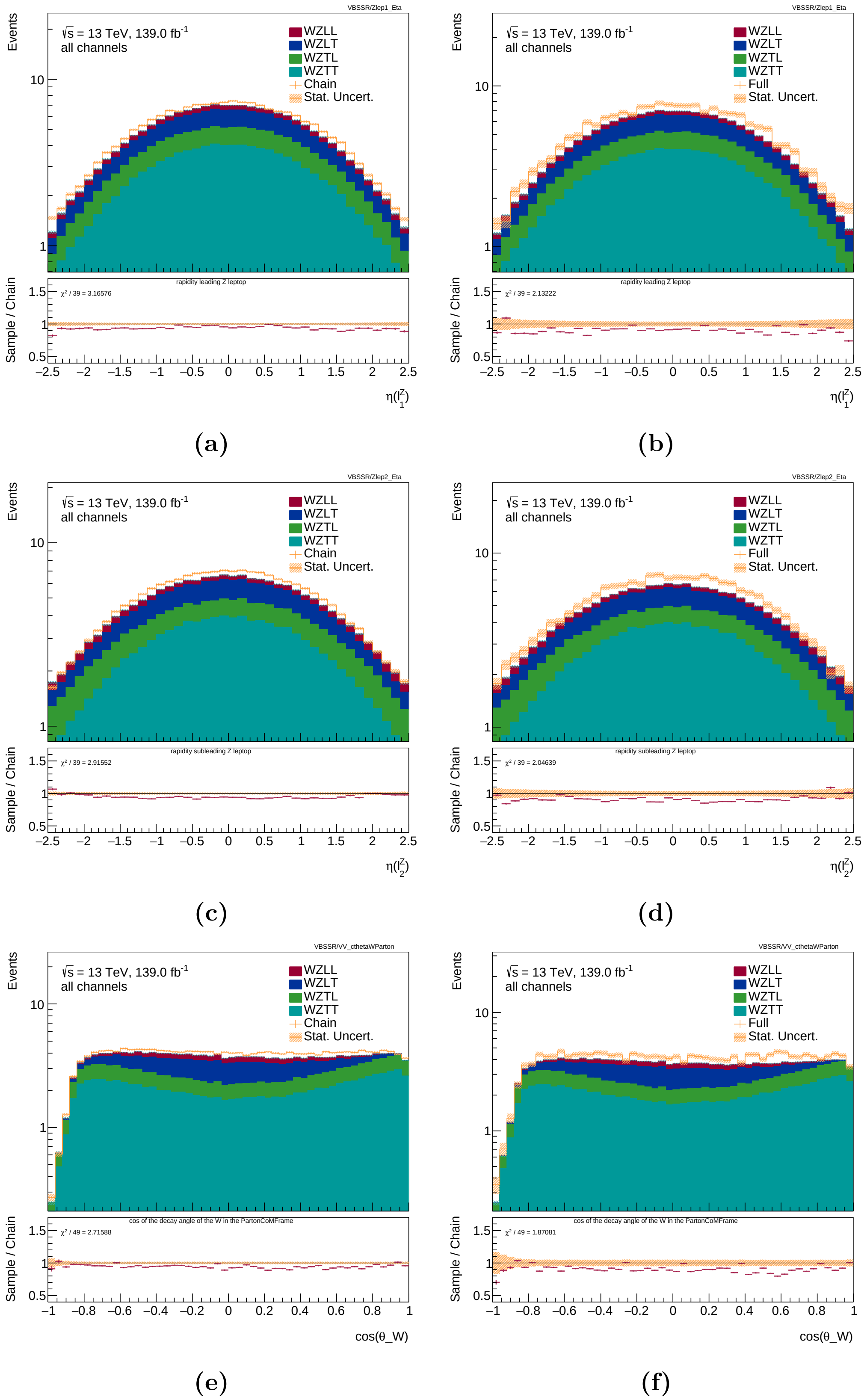

Figure 5.29: Comparison of distributions between the pure Madgraph samples and the stacked polarized samples. The left side shows the comparison to the sample with the decay chain syntax while the right side shows it to the full process. The distributions are shown for the VBS phase space. On top the pseudo-rapidity of the leading Z lepton, in the middle of the subleading one and on the bottom the decay angle of the W is shown.

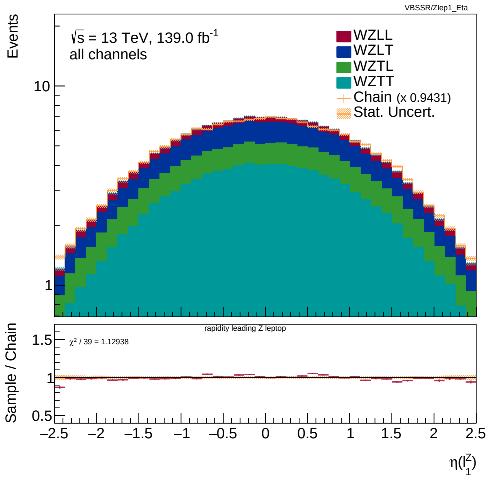

(a)

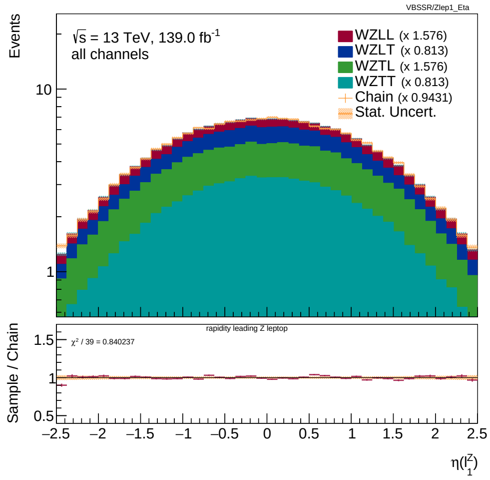

(b)

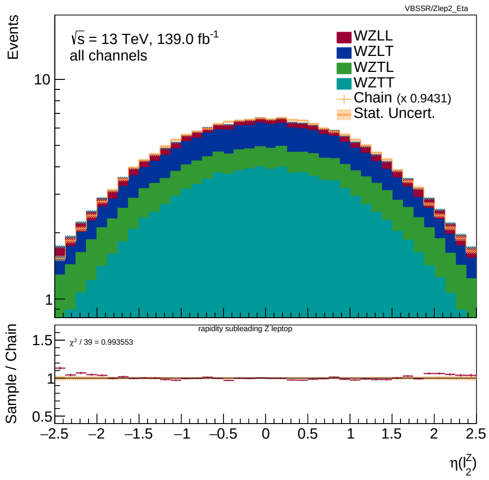

(c)

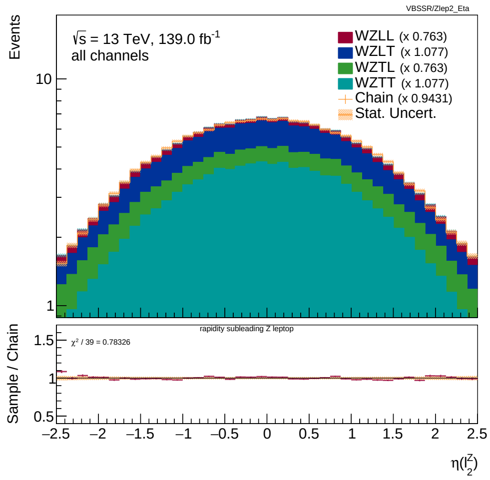

(d)

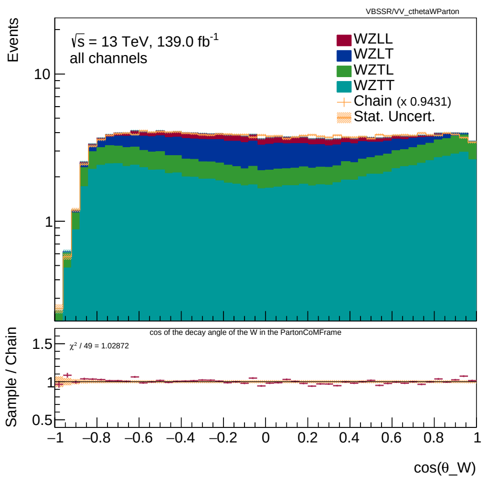

(e)

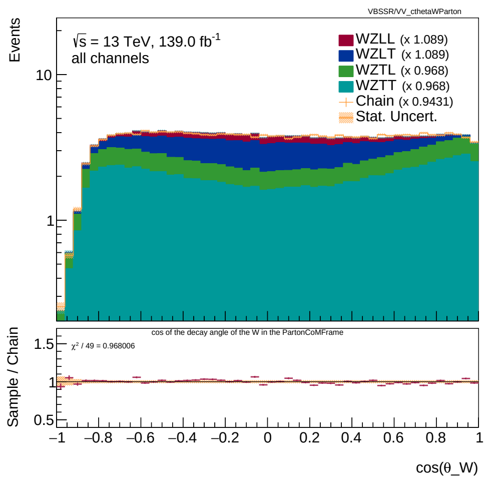

(f)

Figure 5.30: Comparison of distributions between the decay chain sample and the stacked polarized samples. On the left side the decay chain sample is scaled to the cross section of the stack. On the right the stack templates are additionally scaled to represent the polarization fractions determined based on this variable as shown in Table 5.18. On top the pseudo-rapidity of the leading Z lepton, in the middle of the subleading one and on the bottom the decay angle of the W are shown. The distributions are depicted in the VBS phase space.

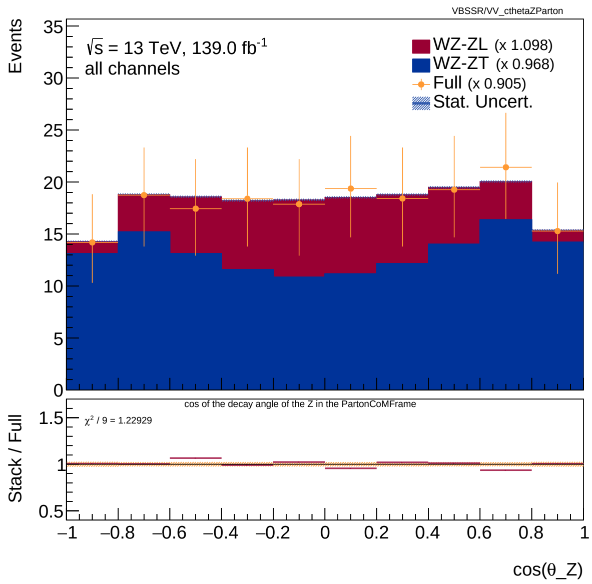

(a)

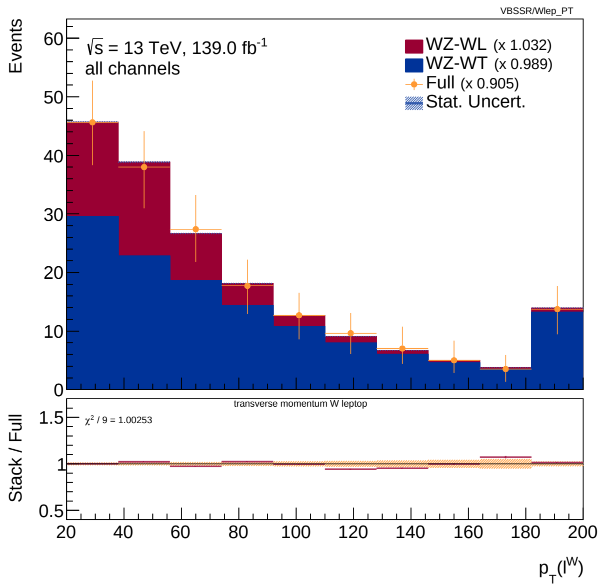

(b)

Figure 5.31: Comparison of distributions between the full sample and the stacked polarized samples. The full sample is scaled to the cross section of the stack templates. Additionally the templates are scaled according to the helicity fractions determined by the fit and shown in Table 5.19. The distributions are shown in the VBS phase space and the uncertainties are set to the poissonian error of the events scaled to a luminosity of 139 fb^{-1}. The left side shows the distributions of the decay angle of the Z and the right side shows it for the transverse momentum of the W lepton.

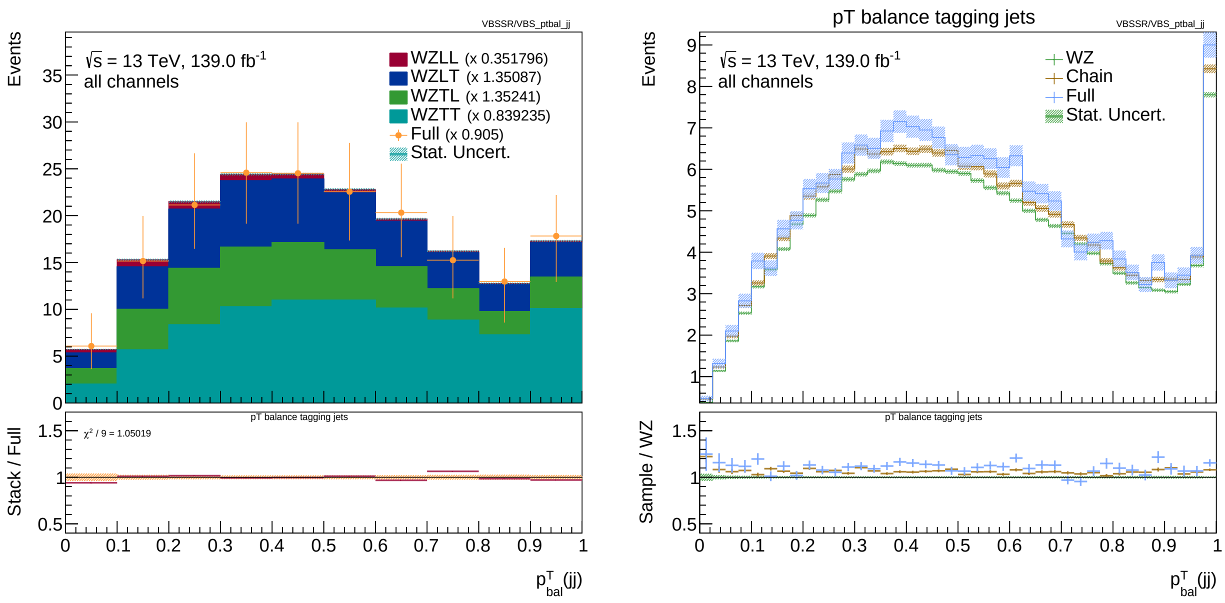

(a) **(b)**

Figure 5.32: Comparison of distributions between the full sample and the stacked polarized samples. The full sample is scaled to the cross section of the stack templates. Additionally the templates are scaled according to the helicity fractions determined by the fit and shown in Table 5.19. The distributions are shown in the VBS phase space and the uncertainties are set to the poissonian error of the events scaled to a luminosity of $SI139$fb. Depicted are the distributions of $p^T_{bal}(jj)$.

strong improvement neither in value nor in accuracy. Doing the same procedure for the decay chain sample the fraction changes from the (1.7 ± 5.4) % listed in Table 5.19 to (5.8 ± 6.6) %. This makes it likely tat the poor result for the full sample is due to its poor statistics. All of these values were generated using purely samples simulating $WZjj - EW$ or approximations thereof. Adding detector effects and backgrounds can reduce the accuracy of these fits considerably. This is especially the case when they mimic the distributions of interest, which for this study are those of events with one or two longitudinal bosons. For this reason the samples produced with WZDecay are compared with ones simulating $WZjj - QCD$. For this the sample *mc15_13TeV.364253.Sherpa_222_NNPDF30NNLO_lllv.merge.DAOD_STDM5.e5916_s2726_r7772_r7676_p3317* was used [52]. It contains Diboson processes with three charged leptons and one neutrino simulated with the Sherpa 2.2.2 event generator [31]. Matrix elements contain all diagrams with four electroweak vertices. They are calculated for up to one parton at NLO and up to 3 partons at LO using Comix [53] and OpenLoops [54], and merged with the Sherpa parton shower [55] according to the ME+PS@NLO prescription [56]. The NNPDF3.0nnlo PDF set is used in conjunction with dedicated parton shower tuning developed by the Sherpa authors. The event generator cross sections are used in this case (already at NLO).

Table 5.20 shows the expected event numbers of the samples at a luminosity of $139\,\text{fb}^{-1}$. It can be seen that even with all of the cuts listed in Table 5.6 the QCD background still has a significantly higher cross section than the electroweak signal process. The distributions of $p_{bal}^{T}(jj)$, $\cos\theta_Z^*$ and $p_T(\ell^W)$ are compared in Figure 5.33. It can be seen that the QCD sample and the total electroweak one produced with Madgraph and WZDecay show no significant differences for the decay angle of the Z boson or the transverse momentum of the W lepton. For a fit this means that the background will have no effect on the determined helicity fractions besides increasing the general uncertainties. However, it will not be possible to determine the overall fraction of WZ/QCD or WLZL/QCD with such a fit. For $p_{bal}^{T}(jj)$ differences can be seen between the QCD samples and all helicity combinations as well as the sum of them. Crucially the distribution of the QCD samples does not have a shape similar to the one with two longitudinally polarized bosons. This means that using a fit it is in principle possible to not only determine the individual helicity fractions within the electroweak sample but also to determine the ratio of WZ/QCD and WLZL/QCD.

All	931	± 5
WZ	180.43	± 0.30
QCD	750	± 5
Ratio:WZ/All	0.1938	± 0.0027
Ratio:QCD/All	0.806	± 0.008

Table 5.20: Comparison of the event numbers between the electroweak sample generated with WZDecay and the QCD sample generated with Sherpa scaled to a luminosity of $139\,\mathrm{fb}^{-1}$ in the VBS phase space. 'All' is the sum of the two samples.

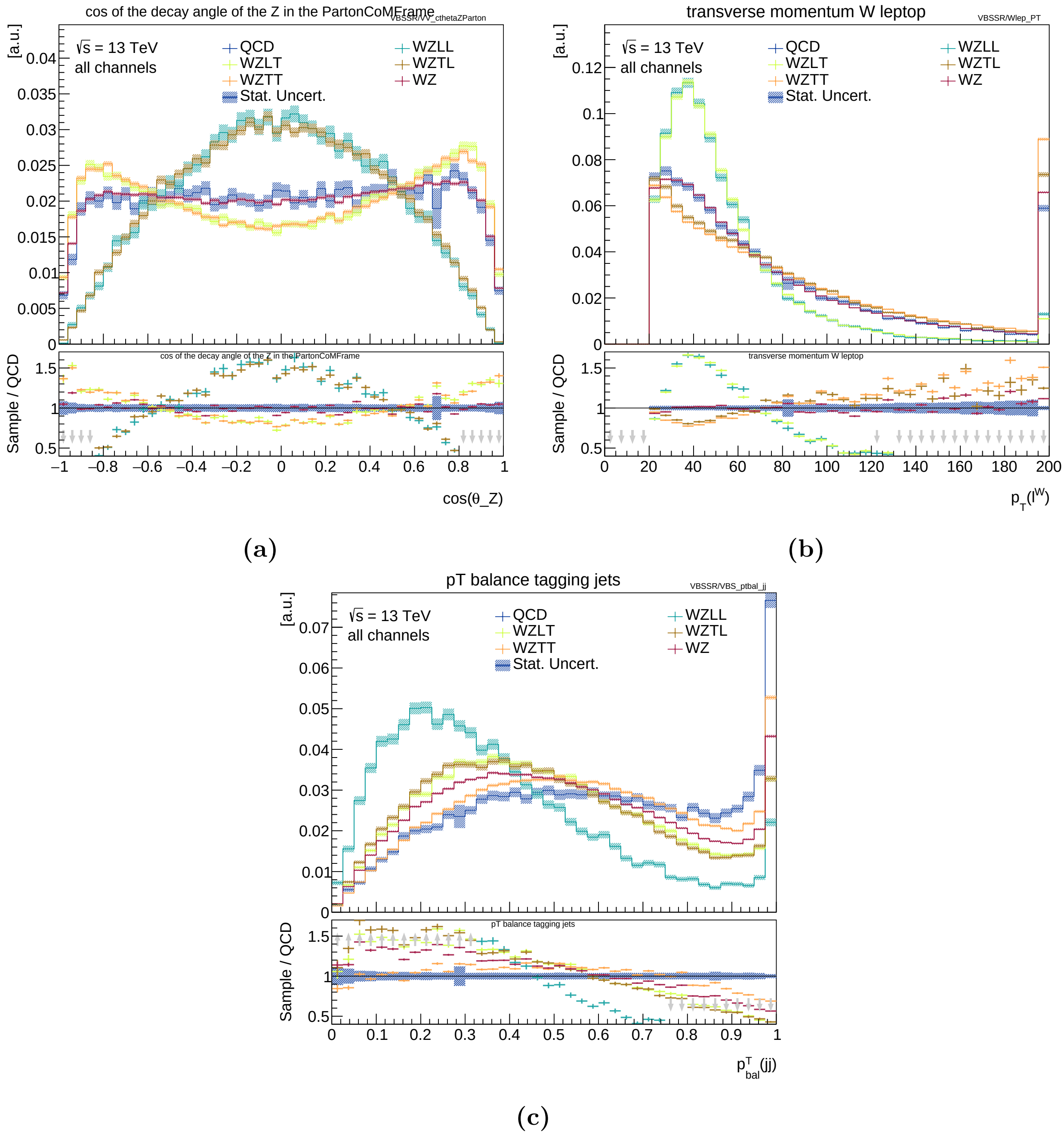

Figure 5.33: Comparison of normalized distributions between the WZDecay and $WZjj-QCD$ samples in the VBS phase space. On the top left the decay angle of the Z, on the top right the transverse momentum of the W's lepton and on the bottom the balance of transverse jet momenta are shown.

6 Summary and Outlook

This thesis expanded on previously done work regarding polarization in the scattering of $W^{\pm}$ and Z bosons at the LHC. Especially the scattering of longitudinally polarized bosons is interesting to study because without a Standard Model Higgs it violates unitarity at high energies. A precise measurement of WZ scattering might thus lead to a better understanding of the exact mechanism of EWSB or give hints for physics beyond the Standard Model. Using the full data set of the Run-2 of the LHC with its integrated luminosity of $\mathscr{L} = 139\,\mathrm{fb}^{-1}$ it might be possible to extract useful limits on the polarizations fraction in the scattering of a W and a Z boson.

In this thesis two methods to produce polarized samples were studied. The one employing the narrow-width-approximation was investigated in detail while the older one using reweighting did not need in depth studying and was simply compared to the new approach. First the validity of all approximations needed for the new method were examined at parton level. Additionally a rough qualitative study was done of which observables are sensitive to boson polarization. Next the approximation study was redone at particle level. The result was that while the approximation has measurable effects in the VBS phase space they remain small especially for observables of interest. It was also shown that while it is beneficial to know the frame in which the bosons helicity was defined in useful studies can still be done even if it is not exactly known. This only holds if the frame is not too different from the laboratory frame or if the used observables are restricted to one related to the jets and bosons. In the future Madgraph will allow the frame in which the helicity is defined in to be chosen by the user. This will make it possible to verify that the choice of frame has no effect on the final distributions as long as the same frame is used for production and decay. A comparison between the new approach and the older one that reweighted inclusive samples was performed. It was found that the reweighting approach gives bad results in almost all variables as well as for the total helicity fractions. This is because the fit is done in the total phase but utilized in a completely different one. This means that in the future it should not be employed when observables other than the decay angle are studied. Instead approaches like the narrow-width-approximation should be utilized.

Lastly a qualitative and quantitative investigation of observables sensitive to the bosons polarization was done. It was found that variables related to the kinematics of the full reconstructed bosons were generally the most sensitive. Observables relating to single leptons still showed a considerable sensitivity. However, especially for the Z bosons these produced helicity fractions that could deviate significantly from the values produced by Madgraph if fitted to the inclusive samples. This is at least partially due to the necessary approximations having a large effects on these variables. For the W boson these seem to be smaller. As for this particle the full reconstruction is not possible due to the neutrino not interacting with the detector observables of the W boson's lepton should be used.

One observable even proved to be sensitive to the combination of both bosons being polarized longitudinally. This is the balance of transverse momenta of the tagging jets.

A simple visual investigation of the $WZjj-QCD$ background showed that the distributions of the Z boson's decay angle and the transverse momentum of the W lepton are identical between the electroweak and QCD processes. The balance of the jets transverse momenta shows a different behaviour for the QCD process compared to the electroweak one. However, it does not mimic the shape of any of the individual helicity combinations.

The next steps are to investigate the sensitivity after detector simulations and including all other backgrounds and systematic uncertainties. While an observation of longitudinal polarizations is unlikely with the data produced during Run-2 of the LHC the availability of a multitude of sensitive observables might allow it with the help of the High-Luminosity LHC.

A Appendix

A.1 Mathematical Definitions

$$\sigma_1 = \begin{pmatrix} 0 & 1 \\ 1 & 0 \end{pmatrix}, \qquad \sigma_2 = \begin{pmatrix} 0 & -i \\ i & 0 \end{pmatrix}, \qquad \sigma_3 = \begin{pmatrix} 1 & 0 \\ 0 & -1 \end{pmatrix}. \tag{A.1}$$

$$\gamma^0 = \begin{pmatrix} 1 & 0 & 0 & 0 \\ 0 & 1 & 0 & 0 \\ 0 & 0 & -1 & 0 \\ 0 & 0 & 0 & -1 \end{pmatrix}, \qquad \gamma^1 = \begin{pmatrix} 0 & 0 & 0 & 1 \\ 0 & 0 & 1 & 0 \\ 0 & -1 & 0 & 0 \\ -1 & 0 & 0 & 0 \end{pmatrix}, \tag{A.2}$$

$$\gamma^2 = \begin{pmatrix} 0 & 0 & 0 & -i \\ 0 & 0 & i & 0 \\ 0 & i & 0 & 0 \\ -i & 0 & 0 & 0 \end{pmatrix}, \qquad \gamma^3 = \begin{pmatrix} 0 & 0 & 1 & 0 \\ 0 & 0 & 0 & -1 \\ -1 & 0 & 0 & 0 \\ 0 & 1 & 0 & 0 \end{pmatrix}. \tag{A.3}$$

$$(\gamma^0)^2 = \mathbb{1}, \qquad (\gamma^k)^2 = -\mathbb{1}, \qquad \gamma^{0\dagger} = \gamma^0, \qquad \gamma^{k\dagger} = -\gamma^k, \qquad \gamma^\mu\gamma^\nu + \gamma^\nu\gamma^\mu = 2g^{\mu\nu}. \tag{A.4}$$

$$\gamma^5 = i\gamma^0\gamma^1\gamma^2\gamma^3 = \begin{pmatrix} 0 & 0 & 1 & 0 \\ 0 & 0 & 0 & 1 \\ 1 & 0 & 0 & 0 \\ 0 & 1 & 0 & 0 \end{pmatrix} \tag{A.5}$$

$$(\gamma^5)^2 = \mathbb{1}, \qquad \gamma^{5\dagger} = \gamma^5, \qquad \gamma^5\gamma^\mu = \gamma^\mu\gamma^5 \tag{A.6}$$

A.2 Comparison of Different Approximations

The following figures show kinematic distributions for samples containing different approximations. Sample Full contains the full process without approximations and is shown in blue, Chain employs Madgraphs decay chain syntax and is depicted in brown and WZ was produced using Madgraph and WZDecay and is shown in green. They are depicted in the VBS phase space.

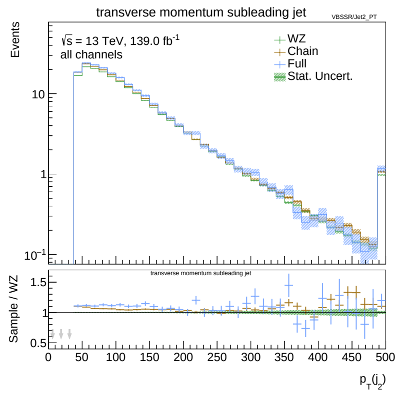

(a) $p_T(j_2)$

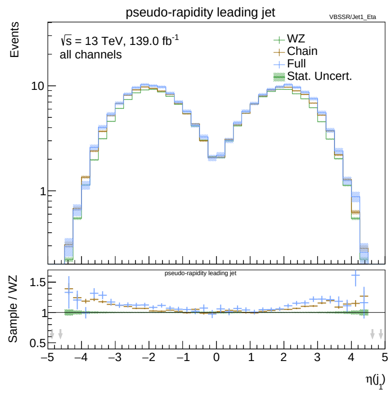

(b) $\eta(j_1)$

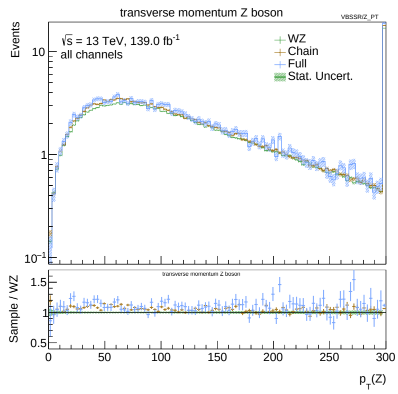

(c) $p_T(Z)$

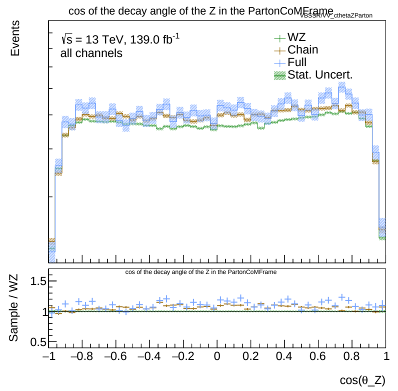

(d) $\cos\theta^*_Z$

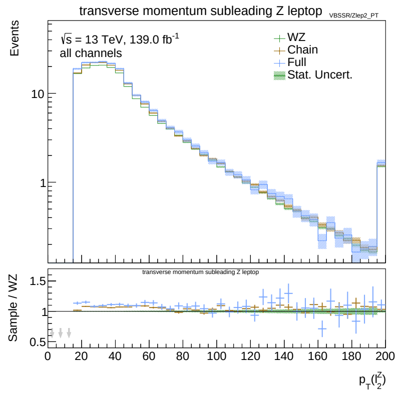

(e) $p_T(\ell_2^Z)$

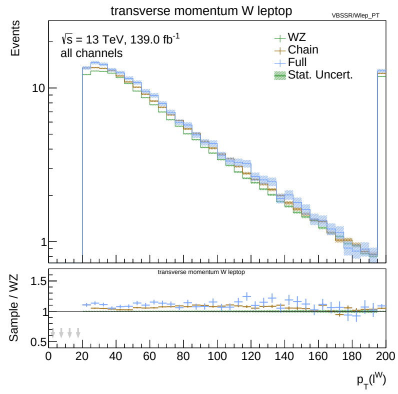

(f) $p_T(\ell^W)$

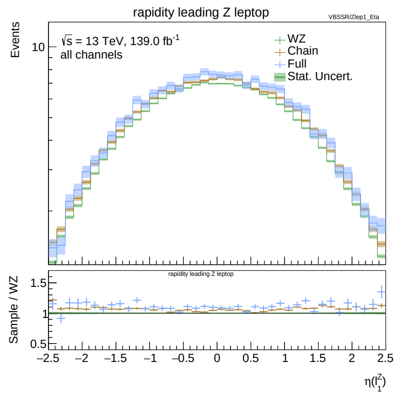

(g) $\eta(\ell_1^Z)$

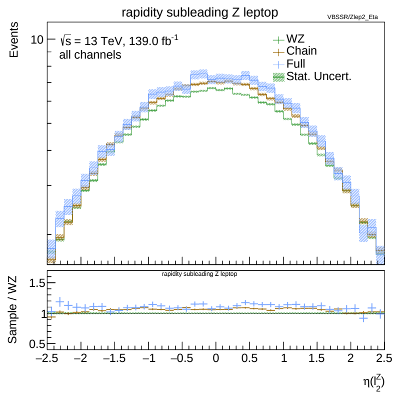

(h) $\eta(\ell_2^Z)$

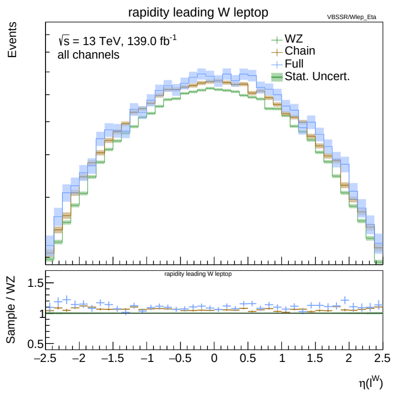

(i) $\eta(\ell^W)$

A.3 Comparison of Decay in LabFrame and PCoMFrame

The following figures show kinematic distributions for the samples produced by Madgraph and WZDecay either using the LabFrame (red) or the PCoMFrame (blue). Shown are events where the W is polarized longitudinally and the Z transversally. They are depicted in the VBS phase space.

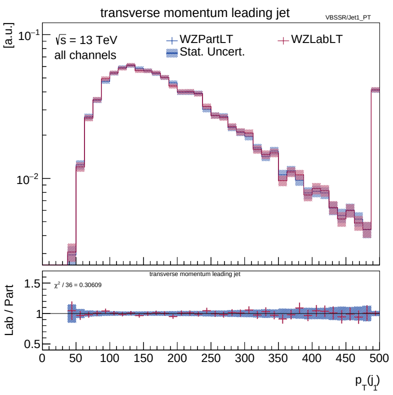

(a) $p_T(j_1)$

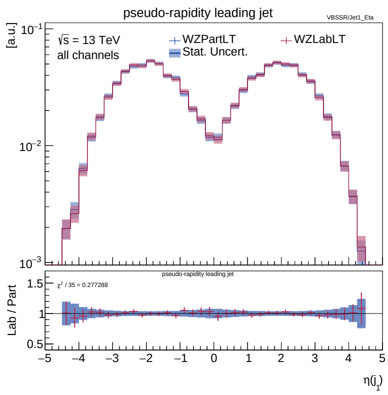

(b) $\eta(j_1)$

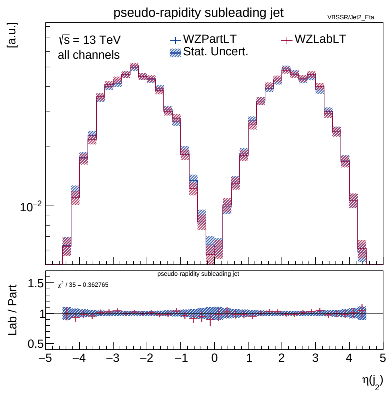

(c) $\eta(j_2)$

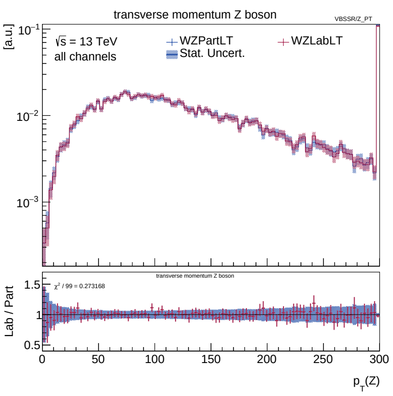

(d) $p_T(Z)$

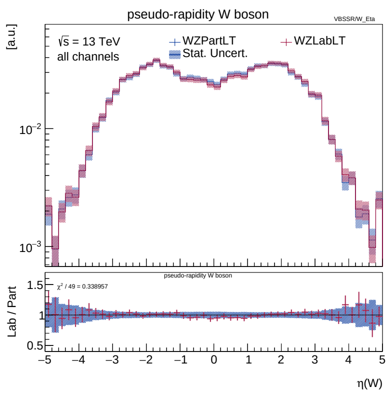

(e) $\eta(W)$

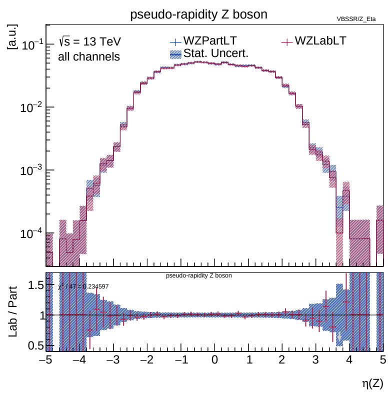

(f) $\eta(Z)$

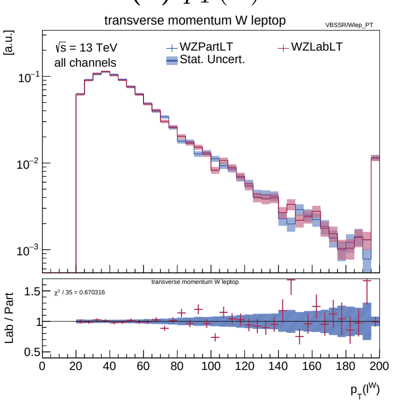

(g) $p_T(\ell^W)$

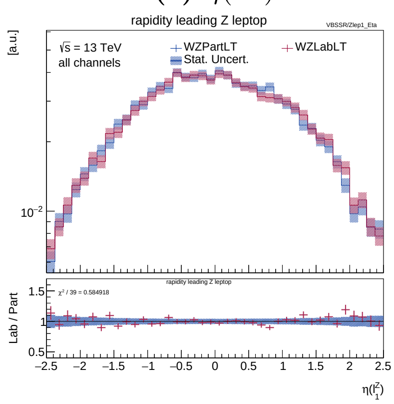

(h) $\eta(\ell_1^Z)$

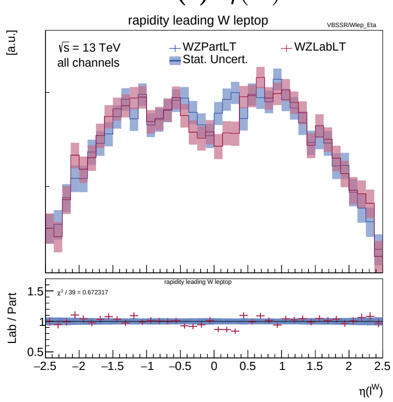

(i) $\eta(\ell^W)$

A.4 Comparison of WZDecay and Reweighting Method

The following figures show kinematic distributions for samples with longitudinal Z and transversal W bosons. These were produced either by reweighting the Full, Chain or WZ sample or by using the WZ sample directly. They are depicted in the VBS phase space.

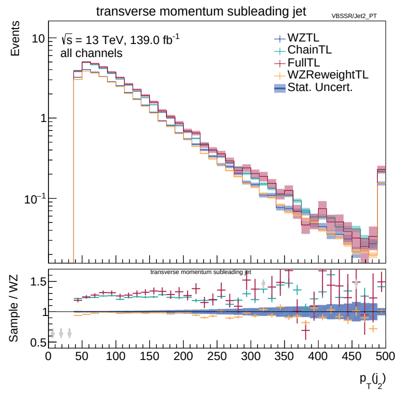

(a) $p_T(j_2)$

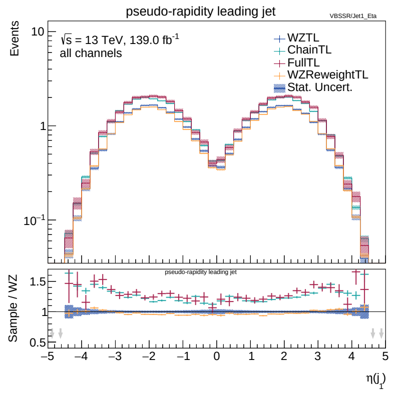

(b) $\eta(j_1)$

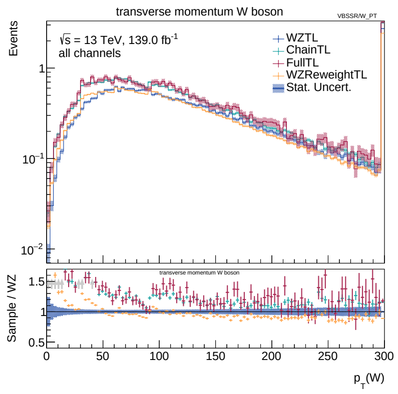

(c) $p_T(W)$

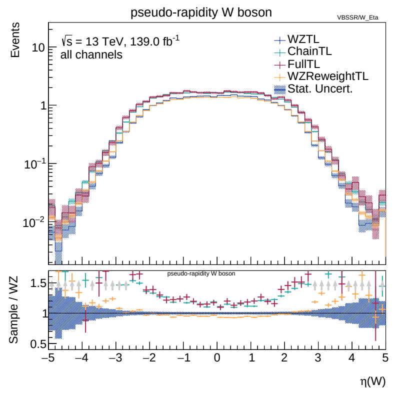

(d) $\eta(W)$

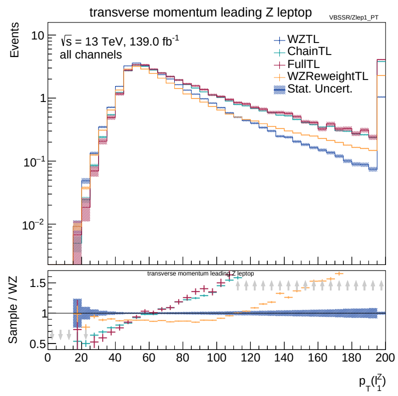

(e) $p_T(\ell_1^Z)$

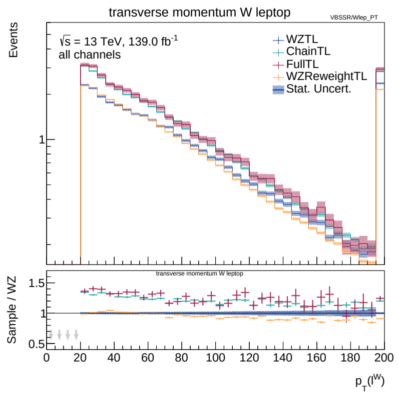

(f) $p_T(\ell^W)$

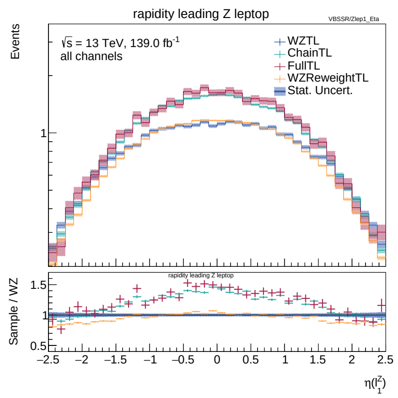

(g) $\eta(\ell_1^Z)$

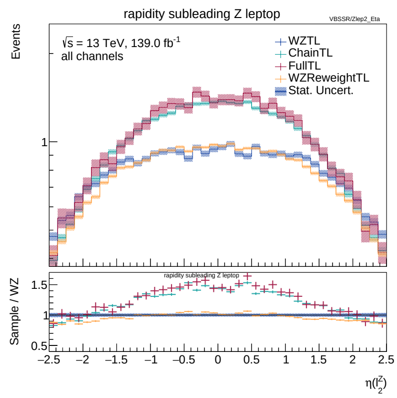

(h) $\eta(\ell_2^Z)$

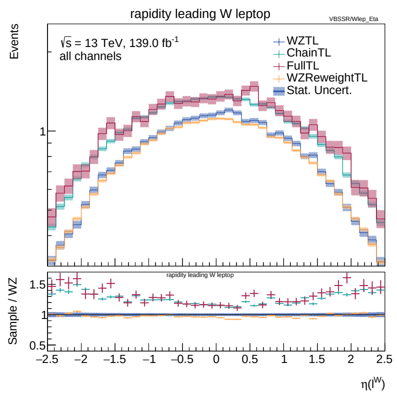

(i) $\eta(\ell^W)$

The following figures show the decay angle distributions for samples with two longitudinal bosons. These were produced either by reweighting the Full, Chain or WZ sample or by using the WZ sample directly. On top they are depicted in the total phase space and on the bottom in the VBS phase space. The left side shows the decay angle for the Z while the right side shows it for the W.

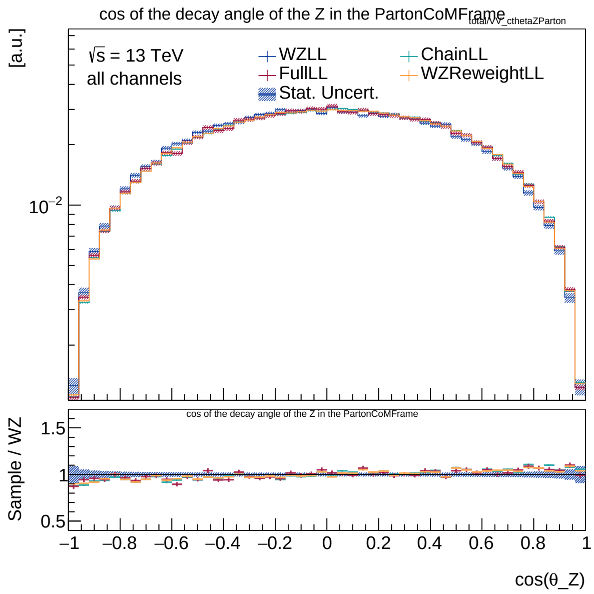

(a)

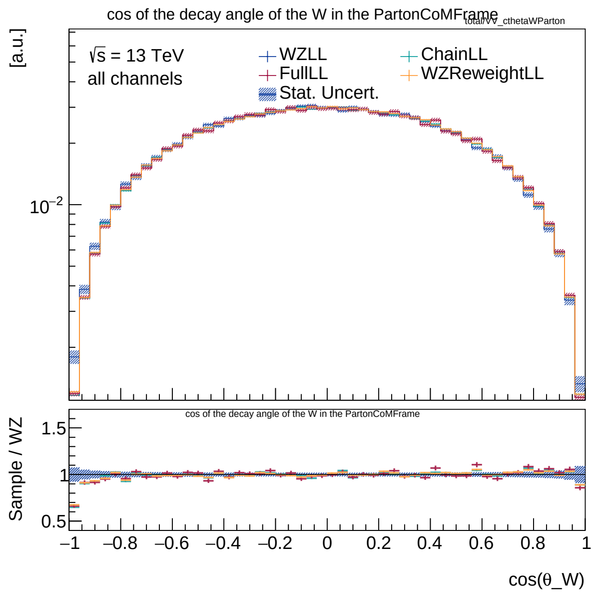

(b)

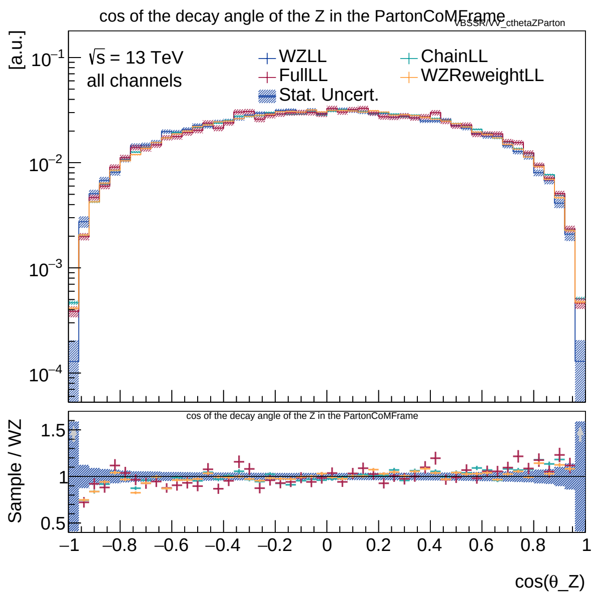

(c)

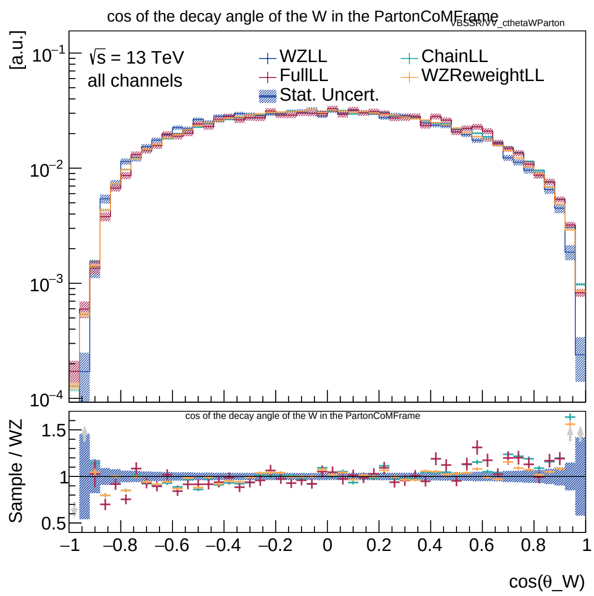

(d)

The following figures show the decay angle distributions for samples with two transversal bosons. These were produced either by reweighting the Full, Chain or WZ sample or by using the WZ sample directly. On top they are depicted in the total phase space and on the bottom in the VBS phase space. The left side shows the decay angle for the Z while the right side shows it for the W.

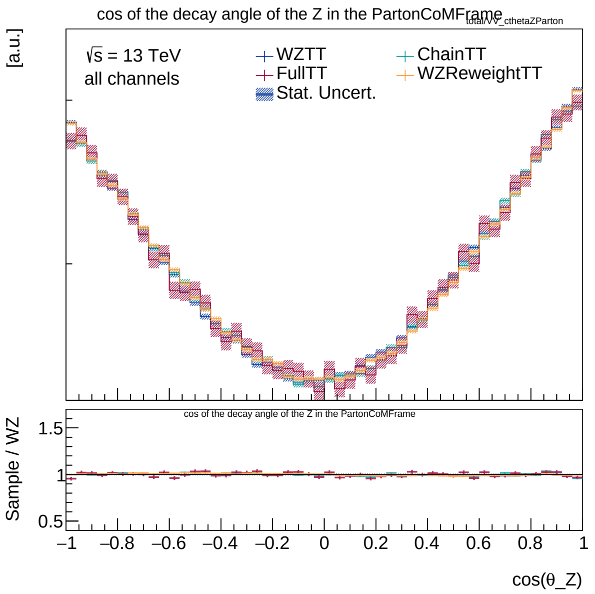

(a)

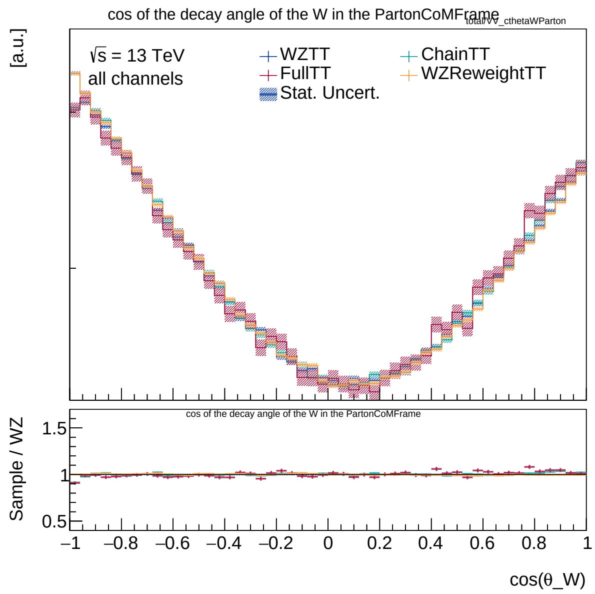

(b)

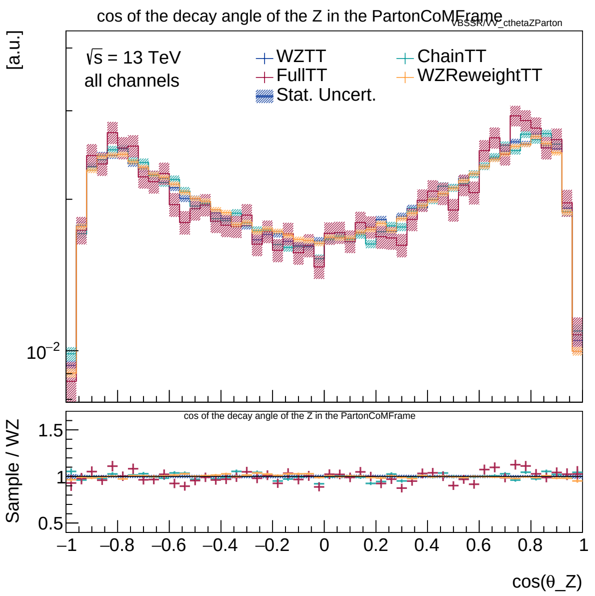

(c)

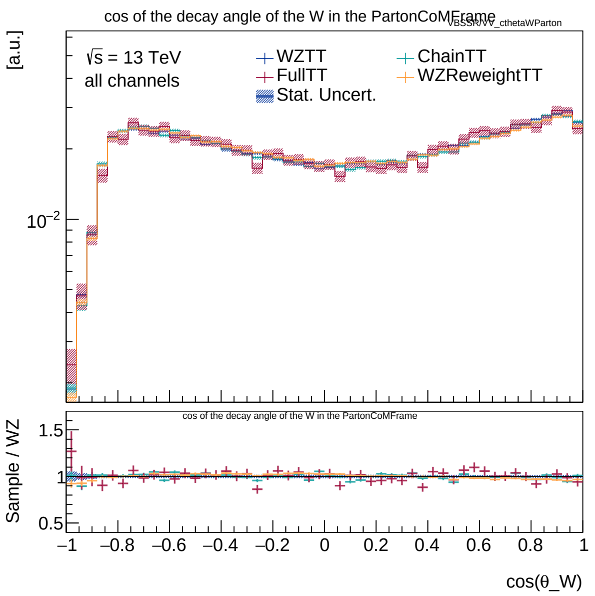

(d)

A.5 Comparison of Different Polarizations

The following figures show kinematic distributions for samples produced with Madgraph and WZDecay. They are depicted in the VBS phase space.

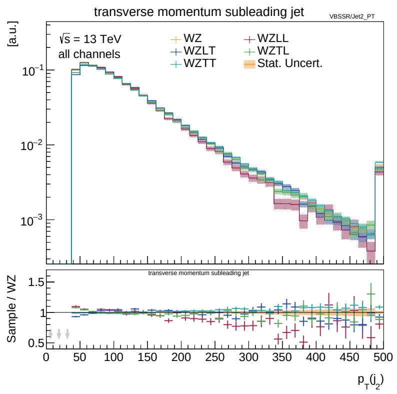

(a) $p_T(j_2)$

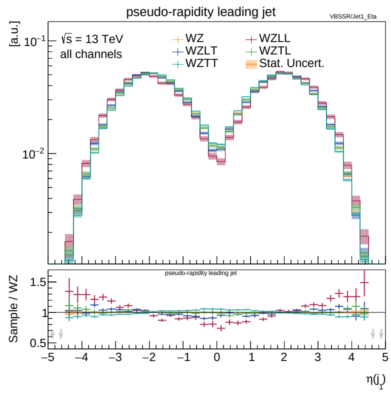

(b) $\eta(j_1)$

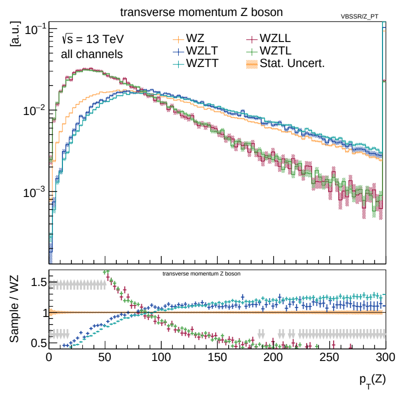

(c) $p_T(Z)$

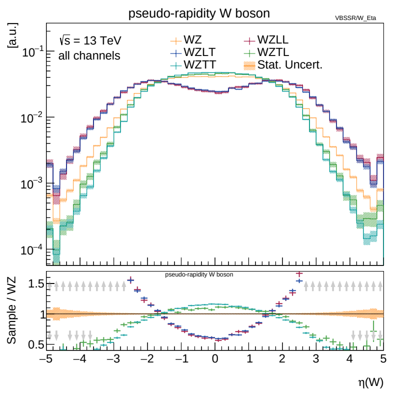

(d) $\eta(W)$

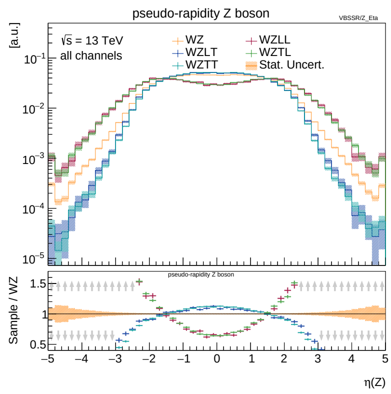

(e) $\eta(Z)$

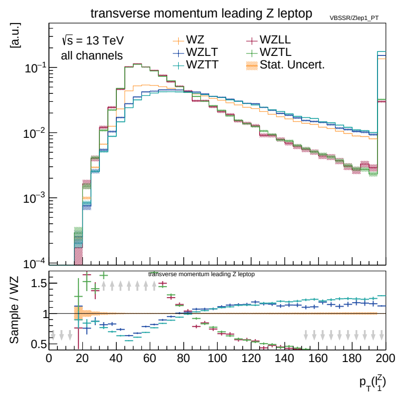

(f) $p_T(\ell_1^Z)$

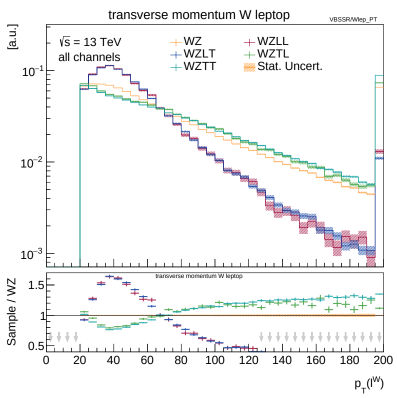

(g) $p_T(\ell^W)$

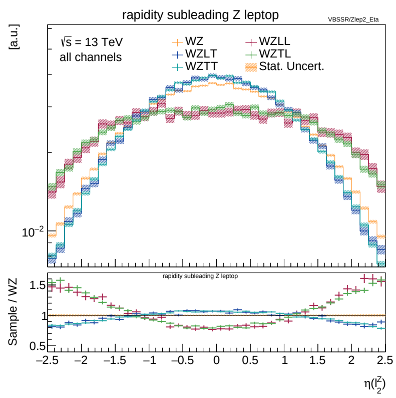

(h) $\eta(\ell_2^Z)$

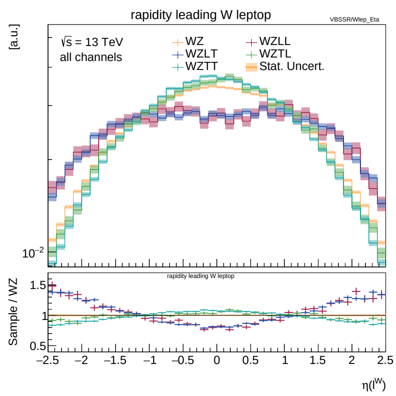

(i) $\eta(\ell^W)$

A.6 Tables of Helicity Fractions

Table A.1: List of $f_0(W^+)$ helicity fractions for the W^+Z WZDecay sample in different $(p_T/|\eta|)$-bins of the vector boson in %. The left column represent the root fits in the first step of the reweighting and the right one the actual fractions as produced by madgraph.

		W^+			
		Fit	MG	Fit	MG
$p_T(V)$ \ $\|\eta\|(V)$		$0-1$		$1-2$	
$0-30$	[GeV]	48.1 ± 1.7	49.7 ± 0.5	54.4 ± 1.3	52.2 ± 0.4
$30-60$	[GeV]	31.3 ± 0.8	31.7 ± 0.2	34.7 ± 0.7	35.2 ± 0.2
$60-90$	[GeV]	20.4 ± 0.7	20.8 ± 0.2	23.4 ± 0.7	23.4 ± 0.2
$90-\infty$	[GeV]	10.1 ± 0.3	10.7 ± 0.1	11.1 ± 0.4	11.4 ± 0.1
		$2-3$		$3-\infty$	
$0-30$	[GeV]	56.3 ± 1.1	56.0 ± 0.3	57.6 ± 0.8	57.3 ± 0.3
$30-60$	[GeV]	38.4 ± 0.8	38.8 ± 0.2	34.6 ± 0.9	33.8 ± 0.3
$60-90$	[GeV]	23.9 ± 0.8	23.9 ± 0.2	15.6 ± 1.2	17.4 ± 0.3
$90-\infty$	[GeV]	10.8 ± 0.6	10.9 ± 0.1	5.1 ± 1.1	7.2 ± 0.2

Table A.2: List of $f_0(W^+)$ helicity fractions for the three samples in different $(p_T/|\eta|)$-bins of the vector boson in %. The values are as produced by the root fit. This is true even for the WZDecay sample.

		W^+					
		Chain	Full	WZ	Chain	Full	WZ
$p_T(V)$ \ $\lvert\eta\rvert(V)$			$0-1$			$1-2$	
$0-30$	[GeV]	50.8 ± 2.8	54.5 ± 5.8	48.1 ± 1.7	51.2 ± 2.1	52.0 ± 4.8	54.4 ± 1.3
$30-60$	[GeV]	37.6 ± 1.4	42.2 ± 3.6	31.3 ± 0.8	38.3 ± 1.2	36.6 ± 3.2	34.7 ± 0.7
$60-90$	[GeV]	30.6 ± 1.2	35.7 ± 3.3	20.4 ± 0.7	27.2 ± 1.2	27.4 ± 3.3	23.4 ± 0.7
$90-\infty$	[GeV]	20.1 ± 0.6	17.8 ± 1.7	10.1 ± 0.3	19.1 ± 0.7	17.9 ± 2.0	11.1 ± 0.4
			$2-3$			$3-\infty$	
$0-30$	[GeV]	51.6 ± 1.8	44.6 ± 4.5	56.3 ± 1.1	53.6 ± 1.4	51.5 ± 3.6	57.6 ± 0.8
$30-60$	[GeV]	35.5 ± 1.3	31.0 ± 3.3	38.4 ± 0.8	26.8 ± 1.4	25.5 ± 3.9	34.6 ± 0.9
$60-90$	[GeV]	22.7 ± 1.4	22.0 ± 3.8	23.9 ± 0.8	14.3 ± 1.8	15.7 ± 5.1	15.6 ± 1.2
$90-\infty$	[GeV]	14.7 ± 1.0	12.3 ± 2.6	10.8 ± 0.6	10.3 ± 2.0	9.4 ± 5.5	5.1 ± 1.1

Table A.3: List of $f_0(W^-)$ helicity fractions for the three samples in different $(p_T/|\eta|)$-bins of the vector boson in %. The values are as produced by the root fit. This is true even for the WZDecay sample.

		W^-					
		Chain	Full	WZ	Chain	Full	WZ
$p_T(V)$ \ $\lvert\eta\rvert(V)$			$0-1$			$1-2$	
$0-30$	[GeV]	46.9 ± 2.6	39.4 ± 5.2	47.1 ± 1.6	48.9 ± 2.0	52.0 ± 4.2	49.4 ± 1.2
$30-60$	[GeV]	37.0 ± 1.3	39.6 ± 3.2	30.2 ± 0.8	34.3 ± 1.2	35.0 ± 2.9	32.8 ± 0.7
$60-90$	[GeV]	28.7 ± 1.2	30.8 ± 3.1	21.2 ± 0.7	27.3 ± 1.2	28.7 ± 3.0	23.6 ± 0.7
$90-\infty$	[GeV]	20.3 ± 0.6	19.8 ± 1.6	11.4 ± 0.3	18.6 ± 0.7	18.1 ± 1.8	13.1 ± 0.4
			$2-3$			$3-\infty$	
$0-30$	[GeV]	50.3 ± 1.7	49.2 ± 3.7	55.3 ± 1.0	53.1 ± 1.4	54.1 ± 3.4	60.1 ± 0.9
$30-60$	[GeV]	33.6 ± 1.2	34.2 ± 3.1	37.8 ± 0.7	31.1 ± 1.6	33.4 ± 4.1	38.7 ± 1.0
$60-90$	[GeV]	21.8 ± 1.4	21.1 ± 3.6	26.8 ± 0.8	17.9 ± 2.3	11.1 ± 5.6	23.2 ± 1.4
$90-\infty$	[GeV]	16.9 ± 1.0	19.5 ± 2.8	14.5 ± 0.6	15.1 ± 2.5	23.5 ± 6.4	17.0 ± 1.6

A.7 Plots of Reweighting Fit

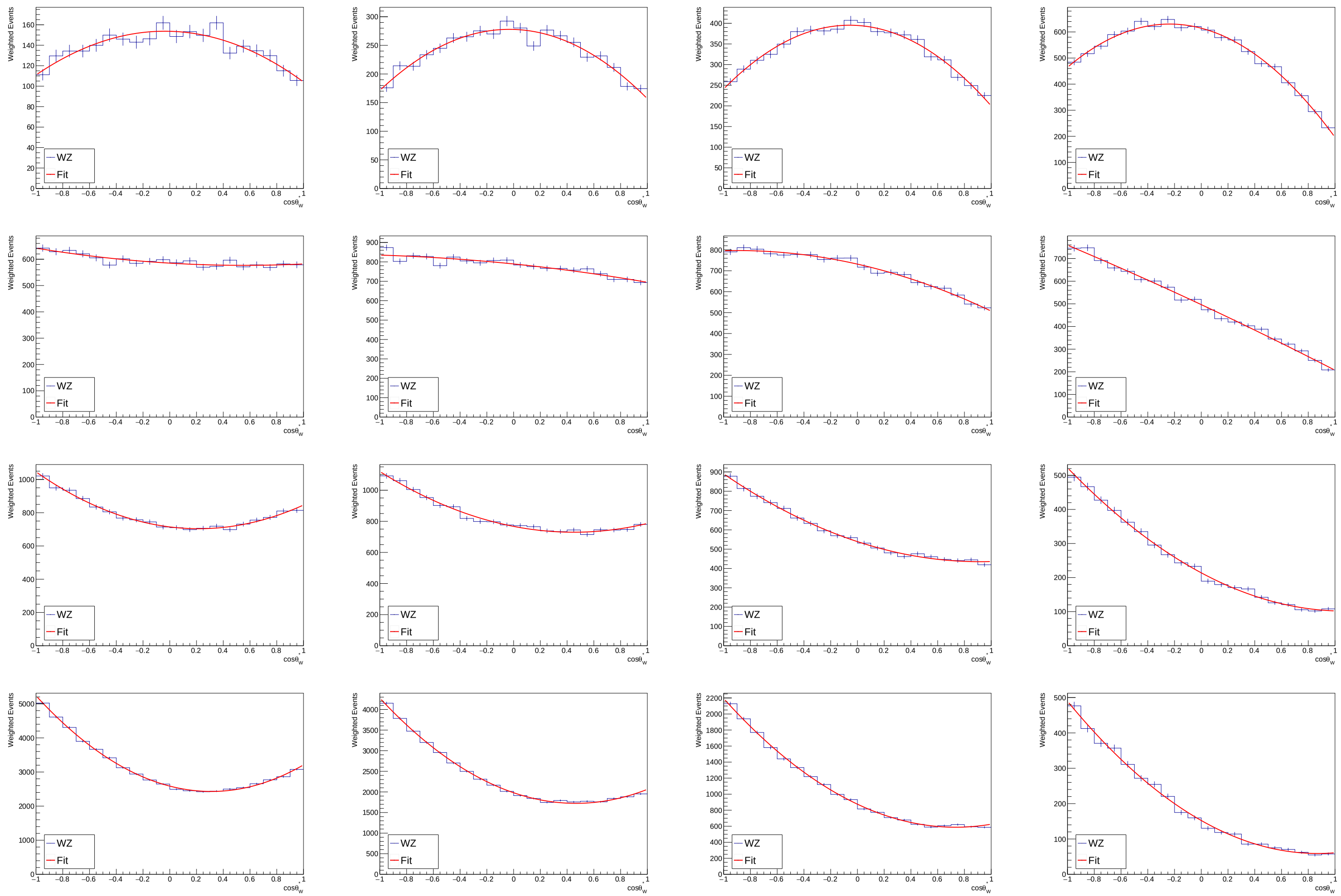

Figure A.7: Decay angle distributions of the W alongside the fit to it for the sample with on-shell bosons. Shown are only events with positively charged W bosons. From top to bottom the transverse momentum of the boson is between $0-30\,\mathrm{GeV}$, $30-60\,\mathrm{GeV}$, $60-90\,\mathrm{GeV}$, $90-\infty\mathrm{GeV}$. From left to right the absolute value of the pseudo-rapidity is between $0-1$, $1-2$, $2-3$, $3-\infty$.

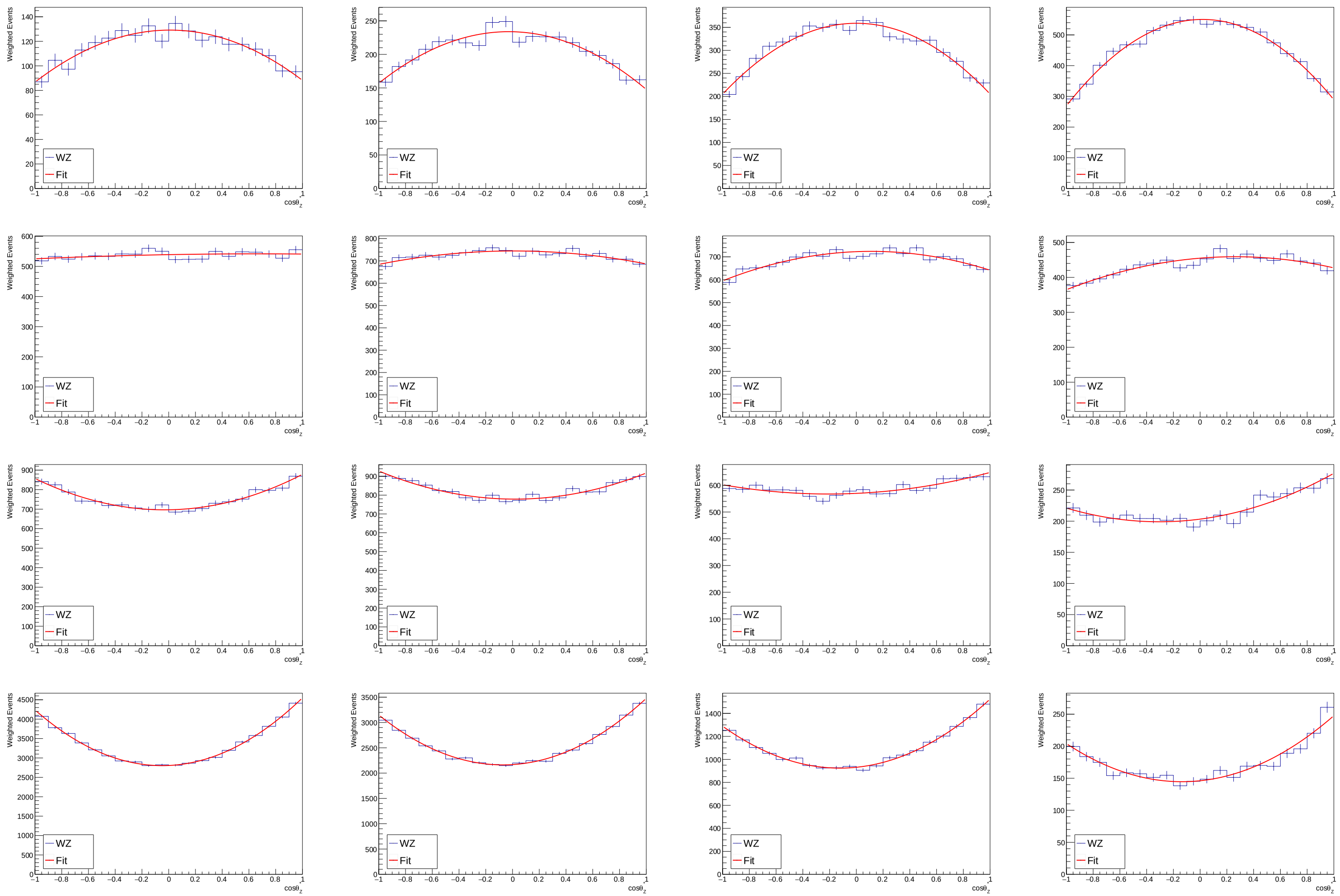

Figure A.8: Decay angle distributions of the Z alongside the fit to it for the sample with on-shell bosons. Shown are only events with positively charged W bosons. From top to bottom the transverse momentum of the boson is between $0-30\,\mathrm{GeV}$, $30-60\,\mathrm{GeV}$, $60-90\,\mathrm{GeV}$, $90-\infty\mathrm{GeV}$. From left to right the absolute value of the pseudo-rapidity is between $0-1$, $1-2$, $2-3$, $3-\infty$.

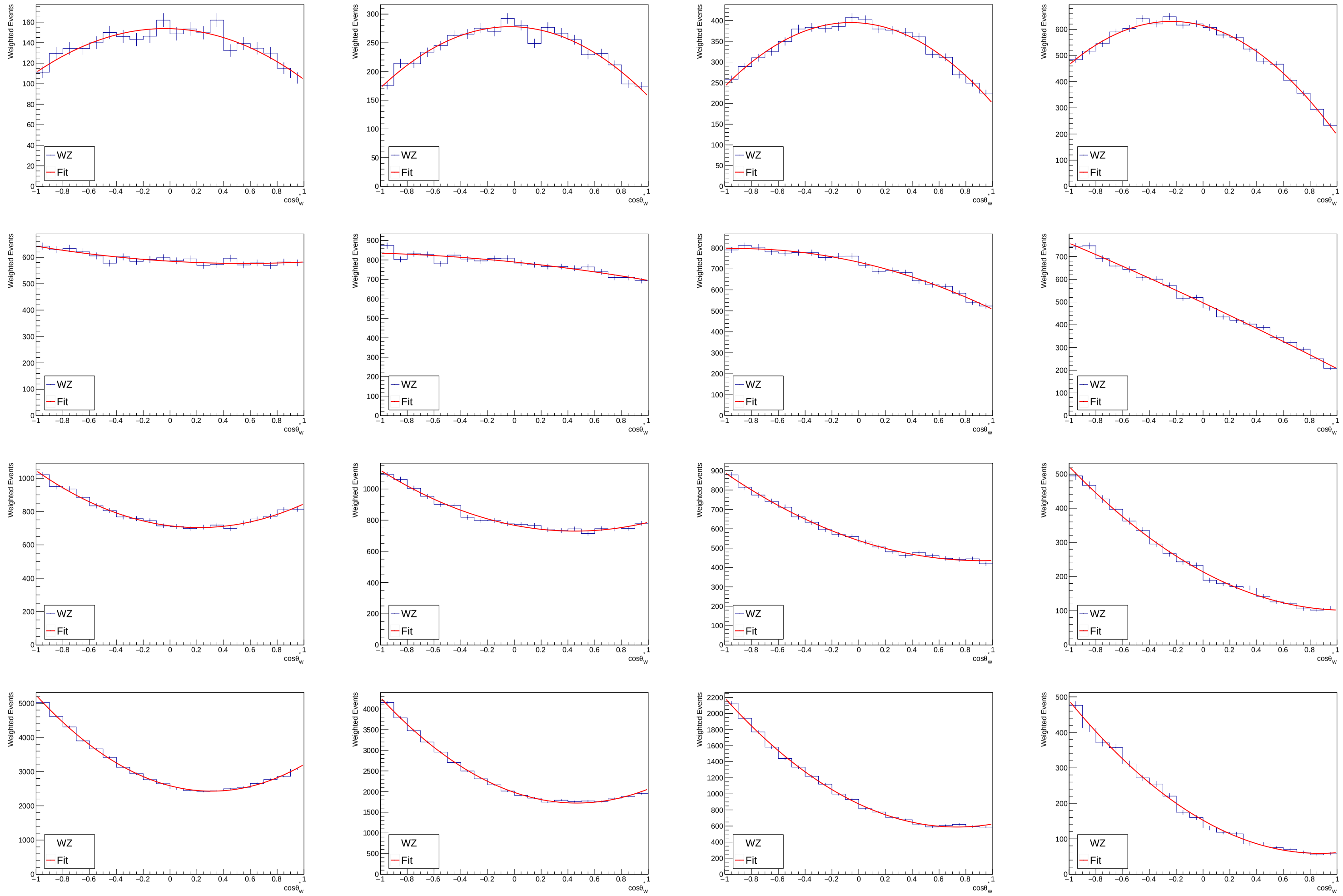

Figure A.9: Decay angle distributions of the W^+ alongside the fit to it for the sample with on-shell bosons. From top to bottom the transverse momentum of the boson is between $0-30\,\text{GeV}$, $30-60\,\text{GeV}$, $60-90\,\text{GeV}$, $90-\infty\text{GeV}$. From left to right the absolute value of the pseudo-rapidity is between $0-1$, $1-2$, $2-3$, $3-\infty$.

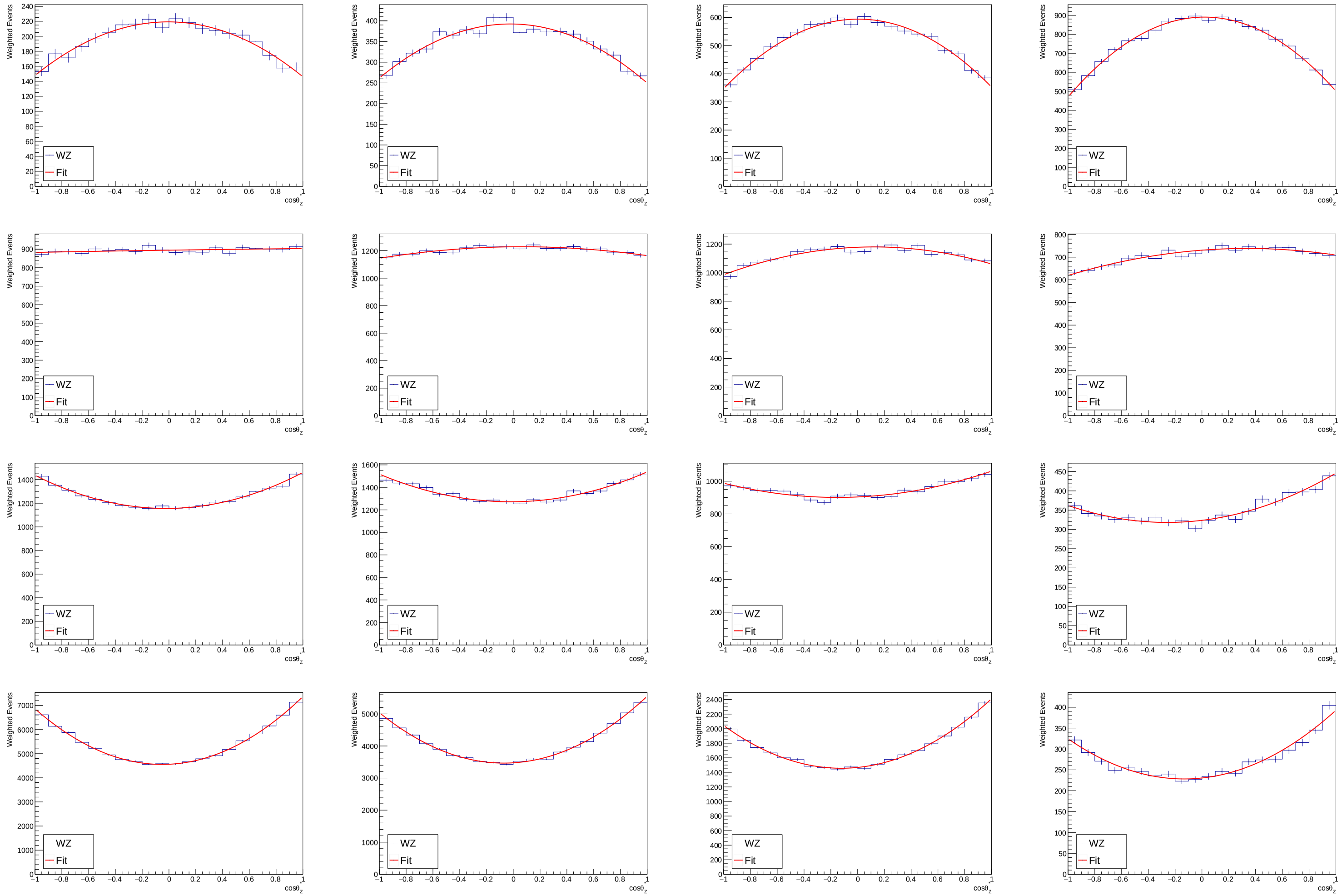

Figure A.10: Decay angle distributions of the Z alongside the fit to it for the sample with on-shell bosons. From top to bottom the transverse momentum of the boson is between $0-30$ GeV, $30-60$ GeV, $60-90$ GeV, $90-\infty$GeV. From left to right the absolute value of the pseudo-rapidity is between $0-1$, $1-2$, $2-3$, $3-\infty$.

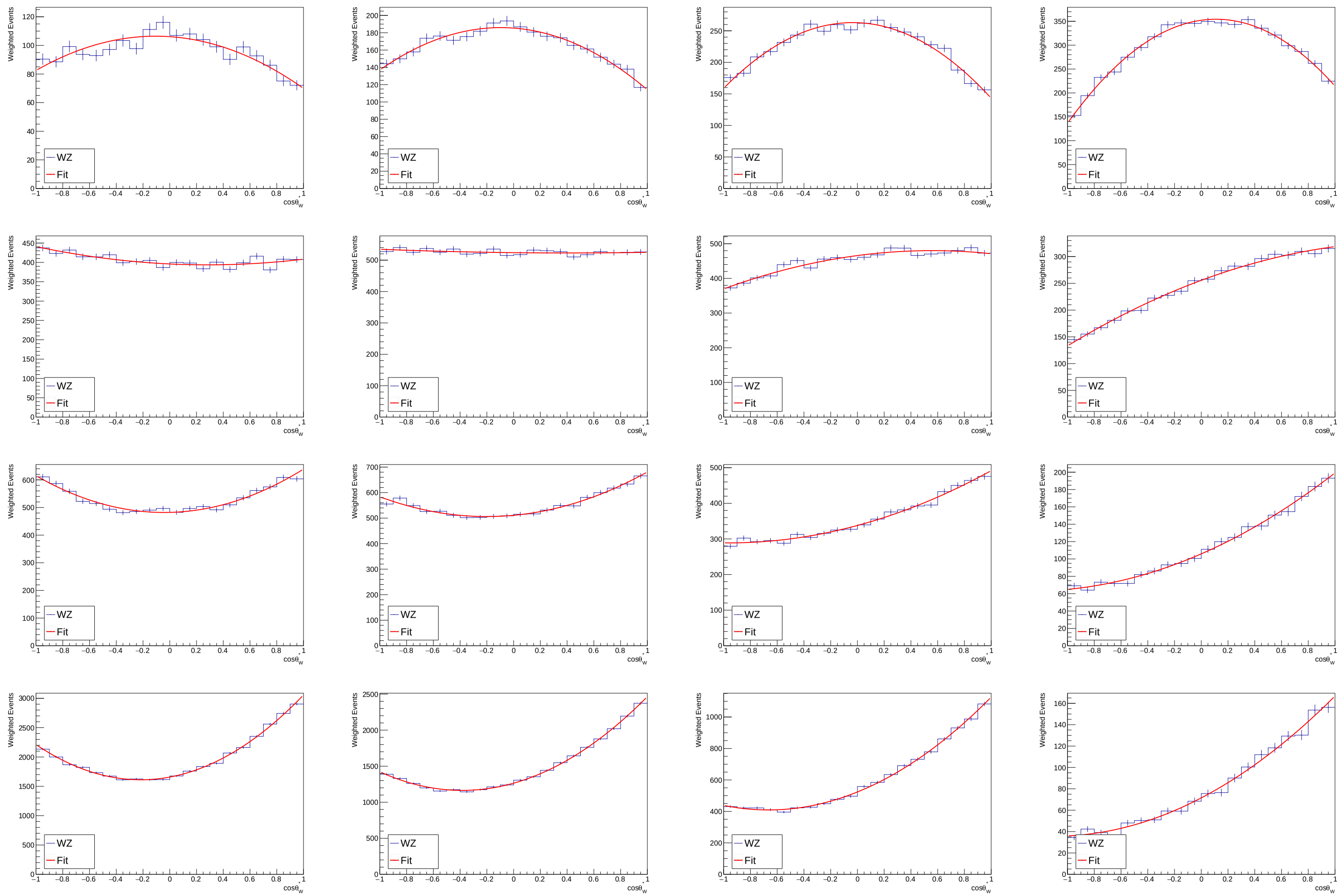

Figure A.11: Decay angle distributions of the W^- alongside the fit to it for the sample with on-shell bosons. From top to bottom the transverse momentum of the boson is between $0-30\,\mathrm{GeV}$, $30-60\,\mathrm{GeV}$, $60-90\,\mathrm{GeV}$, $90-\infty\mathrm{GeV}$. From left to right the absolute value of the pseudo-rapidity is between $0-1$, $1-2$, $2-3$, $3-\infty$.

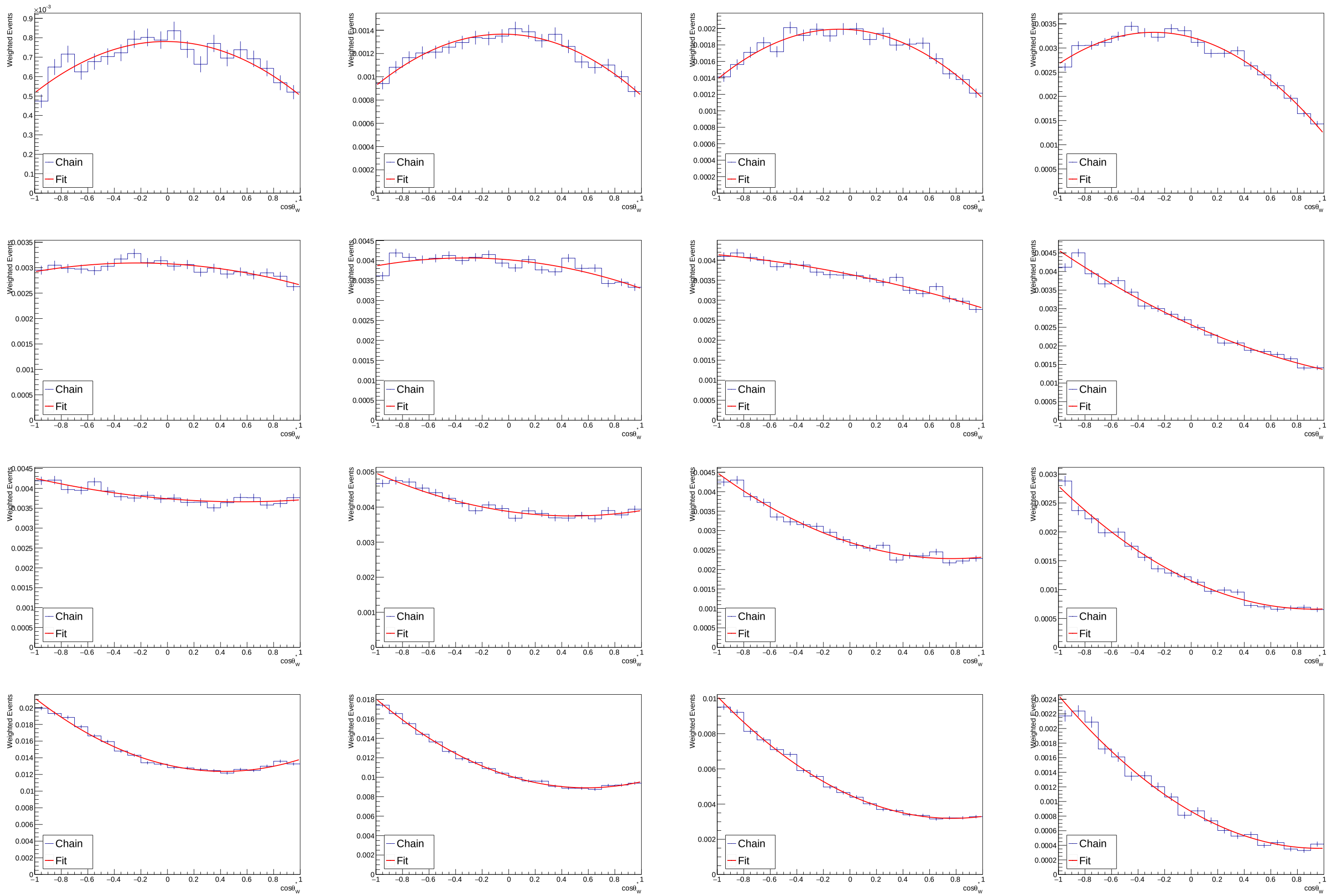

Figure A.12: Decay angle distributions of the W^+ alongside the fit to it for the sample using the decay chain syntax. From top to bottom the transverse momentum of the boson is between $0-30\,\mathrm{GeV}$, $30-60\,\mathrm{GeV}$, $60-90\,\mathrm{GeV}$, $90-\infty\mathrm{GeV}$. From left to right the absolute value of the pseudo-rapidity is between $0-1$, $1-2$, $2-3$, $3-\infty$.

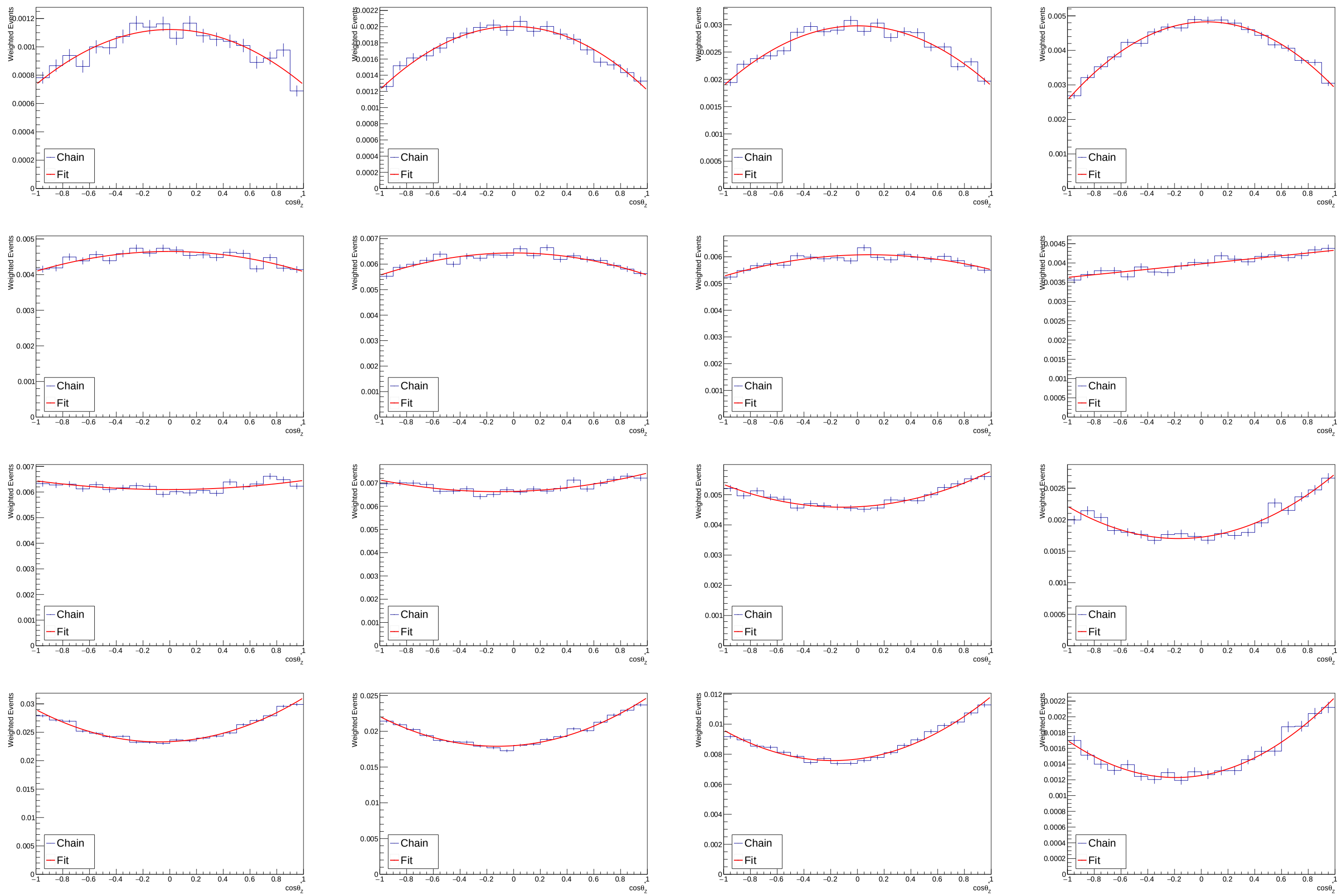

Figure A.13: Decay angle distributions of the Z alongside the fit to it for the sample using the decay chain syntax. From top to bottom the transverse momentum of the boson is between $0-30\,\mathrm{GeV}$, $30-60\,\mathrm{GeV}$, $60-90\,\mathrm{GeV}$, $90-\infty\mathrm{GeV}$. From left to right the absolute value of the pseudo-rapidity is between $0-1$, $1-2$, $2-3$, $3-\infty$.

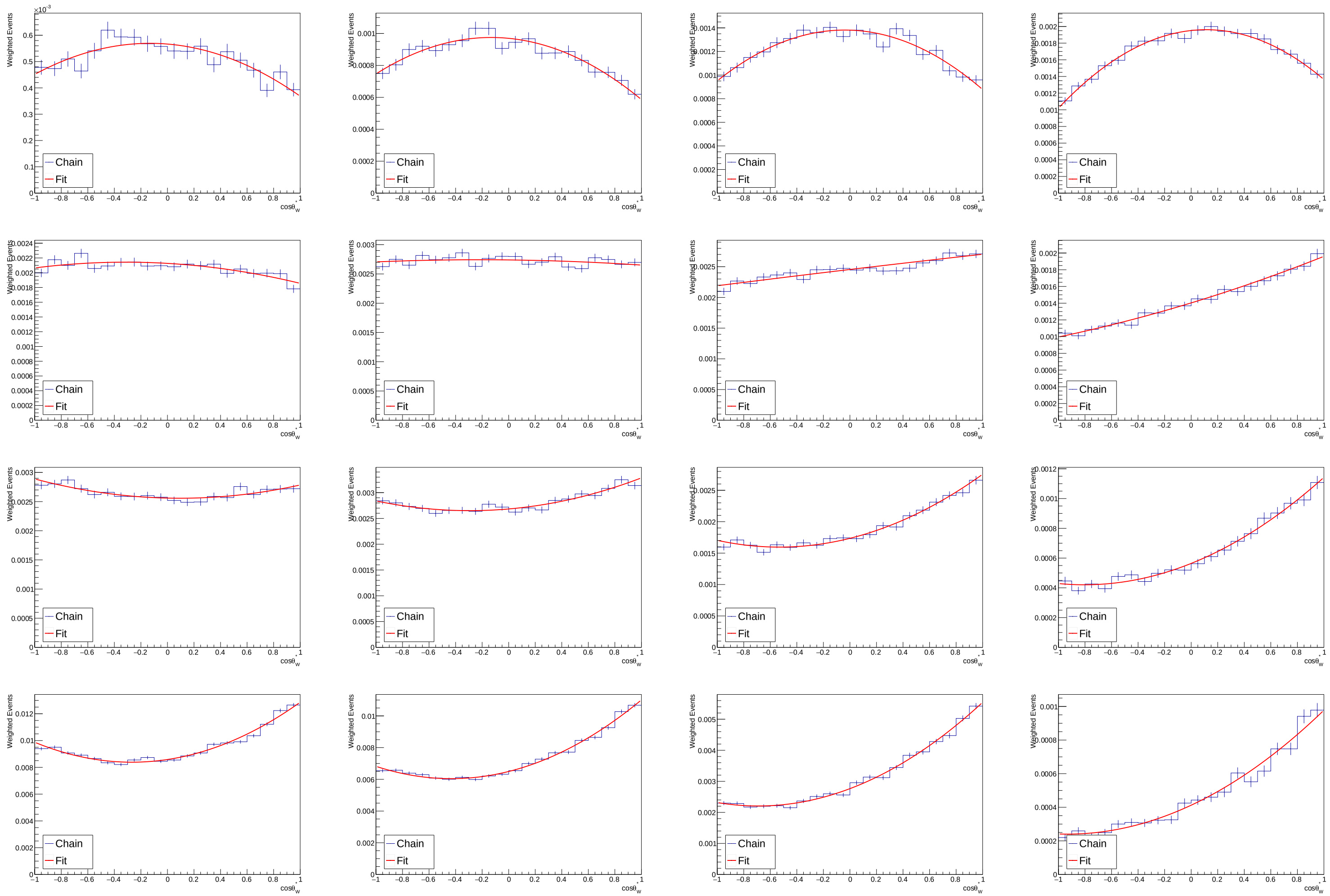

Figure A.14: Decay angle distributions of the W^- alongside the fit to it for the sample using the decay chain syntax. From top to bottom the transverse momentum of the boson is between $0-30$ GeV, $30-60$ GeV, $60-90$ GeV, $90-\infty$GeV. From left to right the absolute value of the pseudo-rapidity is between $0-1$, $1-2$, $2-3$, $3-\infty$.

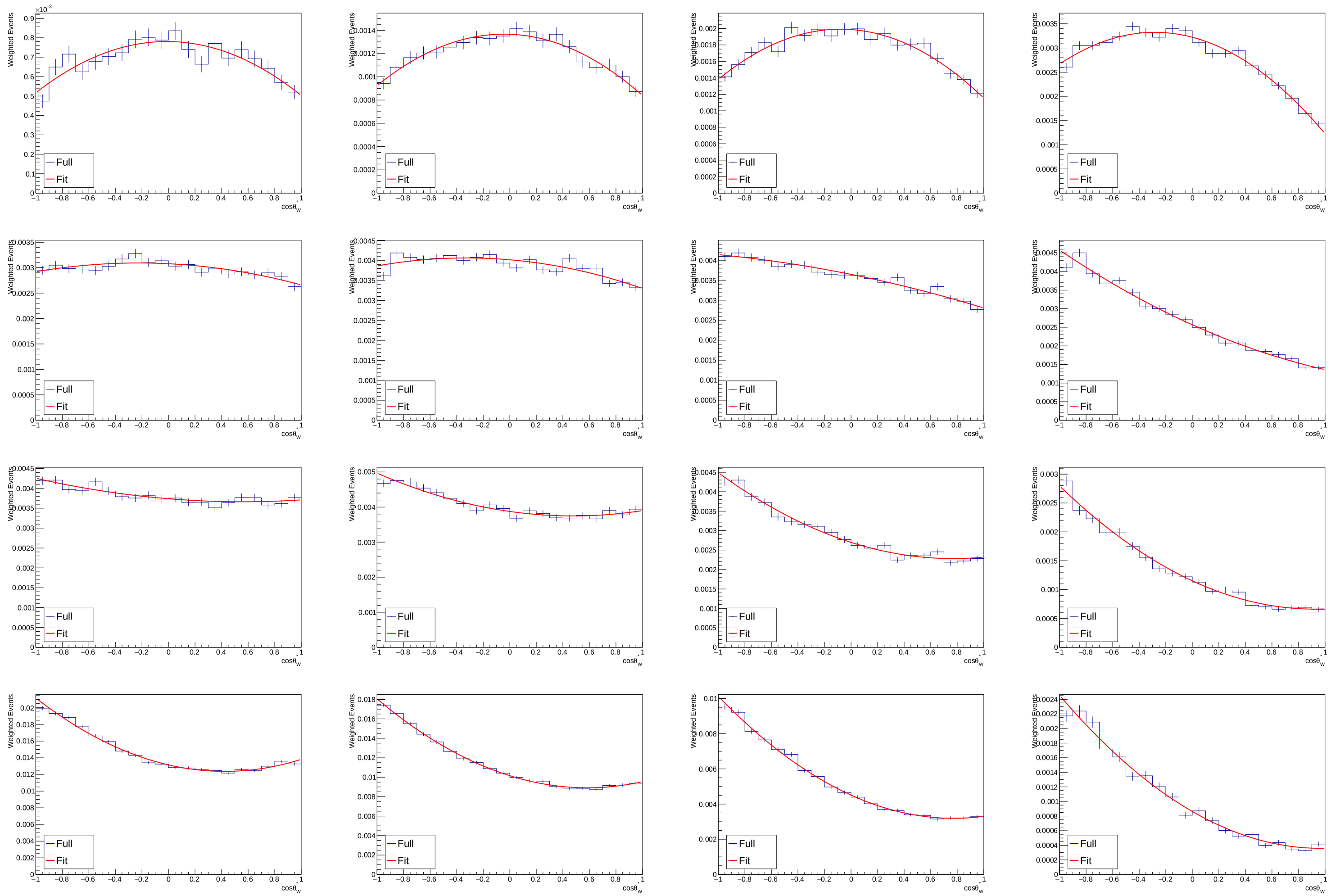

Figure A.15: Decay angle distributions of the W^+ alongside the fit to it for the sample of the full process. From top to bottom the transverse momentum of the boson is between $0-30\,\text{GeV}$, $30-60\,\text{GeV}$, $60-90\,\text{GeV}$, $90-\infty\,\text{GeV}$. From left to right the absolute value of the pseudo-rapidity is between $0-1$, $1-2$, $2-3$, $3-\infty$.

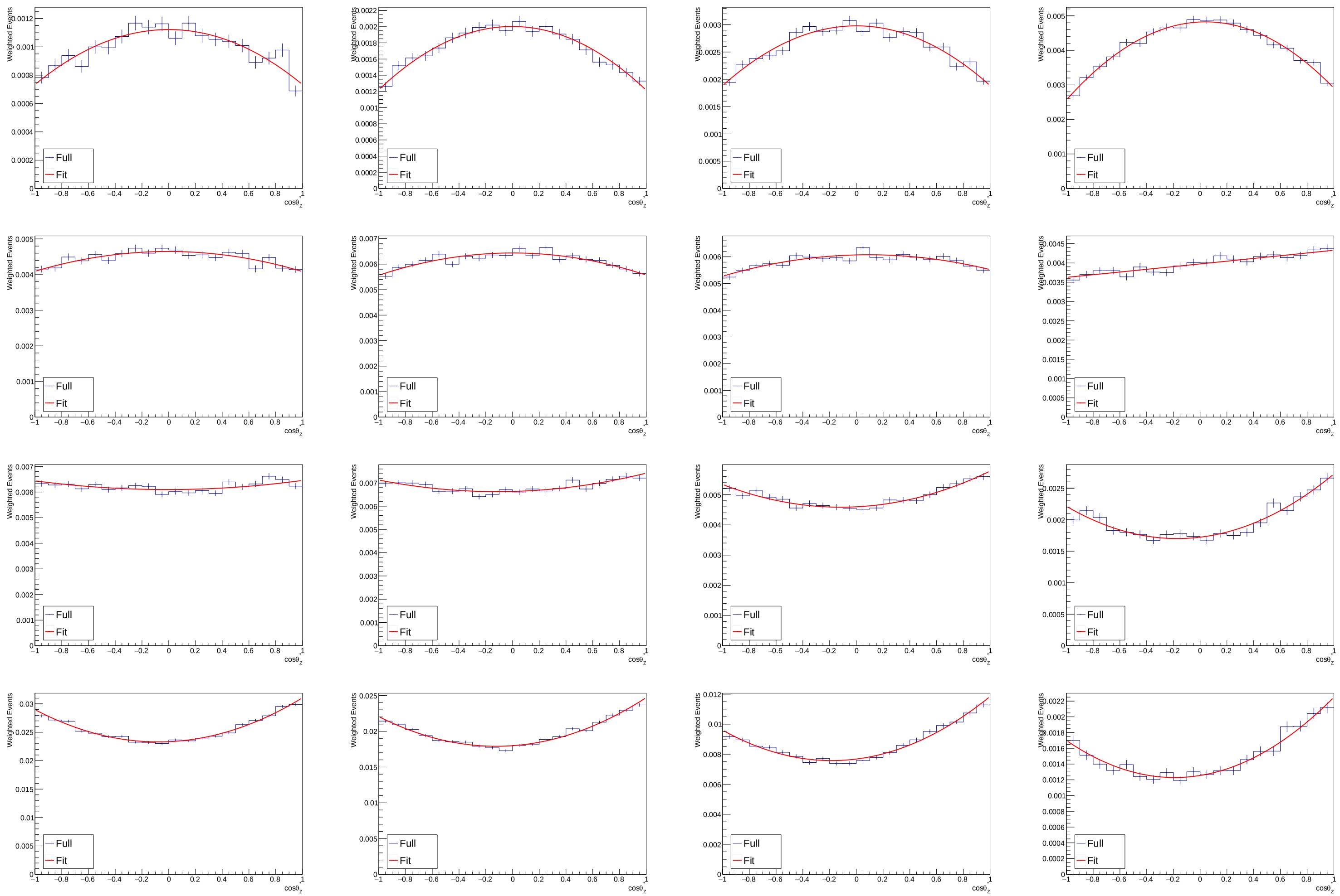

Figure A.16: Decay angle distributions of the Z alongside the fit to it for the sample of the full process. From top to bottom the transverse momentum of the boson is between $0 - 30\,\text{GeV}$, $30 - 60\,\text{GeV}$, $60 - 90\,\text{GeV}$, $90 - \infty\text{GeV}$. From left to right the absolute value of the pseudo-rapidity is between $0 - 1$, $1 - 2$, $2 - 3$, $3 - \infty$.

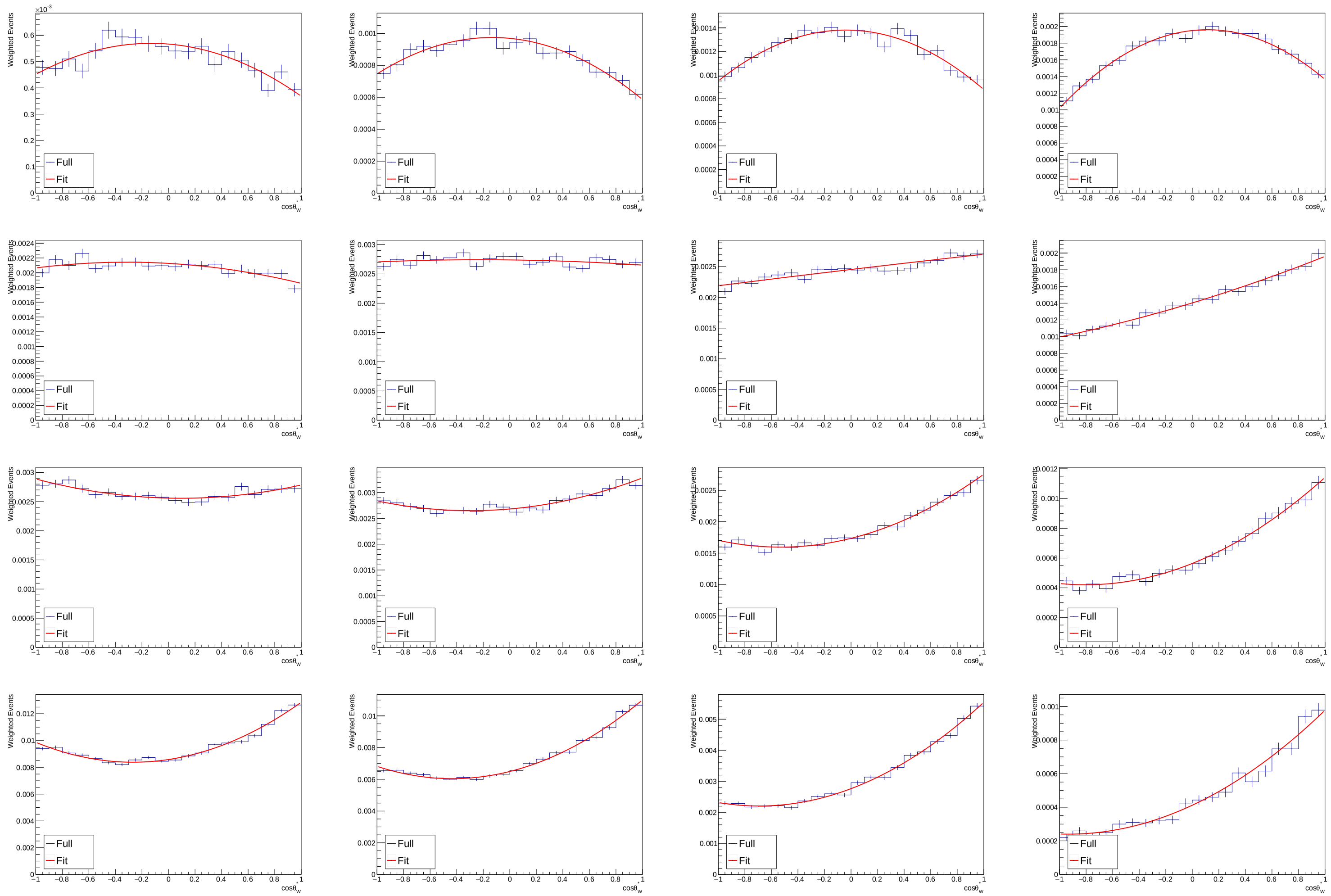

Figure A.17: Decay angle distributions of the W^- alongside the fit to it for the sample of the full process. From top to bottom the transverse momentum of the boson is between $0-30\,\mathrm{GeV}$, $30-60\,\mathrm{GeV}$, $60-90\,\mathrm{GeV}$, $90-\infty\mathrm{GeV}$. From left to right the absolute value of the pseudo-rapidity is between $0-1$, $1-2$, $2-3$, $3-\infty$.

List of Figures

List of Tables

Bibliography

[1] *What is Medical Physics*. https://www.efomp.org/index.php?r=pages&id=public. Accessed: 17.10.2019.

[2] *Biophysics*. https://www.britannica.com/science/biophysics. Accessed: 17.10.2019.

[3] Marvin L. Cohen. "Essay: Fifty Years of Condensed Matter Physics". In: *Phys. Rev. Lett.* 101 (25 Dec. 2008), p. 250001. DOI: 10.1103/PhysRevLett.101.250001. URL: https://link.aps.org/doi/10.1103/PhysRevLett.101.250001.

[4] B. Pullman and A.R. Reisinger. *The Atom in the History of Human Thought*. Oxford University Press, 2001. ISBN: 9780195150407. URL: https://books.google.de/books?id=IQs5hur-BpgC.

[5] Katherine Garrett and Gintaras Duda. "Dark Matter: A Primer". In: *Adv. Astron.* 2011 (2011), p. 968283. DOI: 10.1155/2011/968283. arXiv: 1006.2483 [hep-ph].

[6] P. J. E. Peebles and Bharat Ratra. "The cosmological constant and dark energy". In: *Rev. Mod. Phys.* 75 (2 Apr. 2003), pp. 559–606. DOI: 10.1103/RevModPhys.75.559. URL: https://link.aps.org/doi/10.1103/RevModPhys.75.559.

[7] C. N. Yang and R. L. Mills. "Conservation of Isotopic Spin and Isotopic Gauge Invariance". In: *Phys. Rev.* 96 (1 Oct. 1954), pp. 191–195. DOI: 10.1103/PhysRev.96.191. URL: https://link.aps.org/doi/10.1103/PhysRev.96.191.

[8] Sheldon L. Glashow. "Partial-symmetries of weak interactions". In: *Nuclear Physics* 22.4 (1961), pp. 579–588. ISSN: 0029-5582. DOI: https://doi.org/10.1016/0029-5582(61)90469-2. URL: http://www.sciencedirect.com/science/article/pii/0029558261904692.

[9] F. Englert and R. Brout. "Broken Symmetry and the Mass of Gauge Vector Mesons". In: *Phys. Rev. Lett.* 13 (9 Aug. 1964), pp. 321–323. DOI: 10.1103/PhysRevLett.13.321. URL: https://link.aps.org/doi/10.1103/PhysRevLett.13.321.

[10] Peter W. Higgs. "Broken Symmetries and the Masses of Gauge Bosons". In: *Phys. Rev. Lett.* 13 (16 Oct. 1964), pp. 508–509. DOI: 10.1103/PhysRevLett.13.508. URL: https://link.aps.org/doi/10.1103/PhysRevLett.13.508.

[11] Steven Weinberg. “A Model of Leptons”. In: *Phys. Rev. Lett.* 19 (21 Nov. 1967), pp. 1264–1266. DOI: 10.1103/PhysRevLett.19.1264. URL: https://link.aps.org/doi/10.1103/PhysRevLett.19.1264.

[12] ATLAS Collaboration. “Observation of a new particle in the search for the Standard Model Higgs boson with the ATLAS detector at the LHC”. In: *Physics Letters B* 716.1 (Sept. 2012), pp. 1–29. ISSN: 0370-2693. DOI: 10.1016/j.physletb.2012.08.020. URL: http://dx.doi.org/10.1016/j.physletb.2012.08.020.

[13] CMS Collaboration. “Observation of a new boson at a mass of 125 GeV with the CMS experiment at the LHC”. In: *Physics Letters B* 716.1 (Sept. 2012), pp. 30–61. ISSN: 0370-2693. DOI: 10.1016/j.physletb.2012.08.021. URL: http://dx.doi.org/10.1016/j.physletb.2012.08.021.

[14] Lyndon Evans and Philip Bryant. “LHC Machine”. In: *JINST* 3 (2008), S08001. DOI: 10.1088/1748-0221/3/08/S08001.

[15] ATLAS Collaboration. “The ATLAS Experiment at the CERN Large Hadron Collider”. In: *JINST* 3 (2008), S08003. DOI: 10.1088/1748-0221/3/08/S08003.

[16] ATLAS Collaboration. “Observation of electroweak W±Z boson pair production in association with two jets in pp collisions at s=13 TeV with the ATLAS detector”. In: *Physics Letters B* 793 (June 2019), pp. 469–492. ISSN: 0370-2693. DOI: 10.1016/j.physletb.2019.05.012. URL: http://dx.doi.org/10.1016/j.physletb.2019.05.012.

[17] Carsten Bittrich. “Study of Polarization Fractions in the Scattering of Massive Gauge Bosons $W^{\pm}Z \to W^{\pm}Z$ with the ATLAS Detector at the Large Hadron Collider”. MA thesis. Dresden, Tech. U., 2015-04-27.

[18] E. Noether. “Invariante Variationsprobleme”. ger. In: *Nachrichten von der Gesellschaft der Wissenschaften zu Göttingen, Mathematisch-Physikalische Klasse* 1918 (1918), pp. 235–257. URL: http://eudml.org/doc/59024.

[19] H. David Politzer. “Reliable Perturbative Results for Strong Interactions?” In: *Phys. Rev. Lett.* 30 (26 June 1973), pp. 1346–1349. DOI: 10.1103/PhysRevLett.30.1346. URL: https://link.aps.org/doi/10.1103/PhysRevLett.30.1346.

[20] David J. Gross and Frank Wilczek. “Ultraviolet Behavior of Non-Abelian Gauge Theories”. In: *Phys. Rev. Lett.* 30 (26 June 1973), pp. 1343–1346. DOI: 10.1103/PhysRevLett.30.1343. URL: https://link.aps.org/doi/10.1103/PhysRevLett.30.1343.

[21] Jeff Greensite. “An introduction to the confinement problem”. In: *Lect. Notes Phys.* 821 (2011), pp. 1–211. DOI: 10.1007/978-3-642-14382-3.

[22] M. Tanabashi et al. “Review of Particle Physics”. In: *Phys. Rev. D* 98 (3 Aug. 2018 and 2019 update), p. 030001. DOI: 10.1103/PhysRevD.98.030001. URL: https://link.aps.org/doi/10.1103/PhysRevD.98.030001.

[23] C. S. Wu et al. “Experimental Test of Parity Conservation in Beta Decay”. In: *Phys. Rev.* 105 (4 Feb. 1957), pp. 1413–1415. DOI: 10.1103/PhysRev.105.1413. URL: https://link.aps.org/doi/10.1103/PhysRev.105.1413.

[24] Philipp Anger. “Probing Electroweak Gauge Boson Scattering with the ATLAS Detector at the Large Hadron Collider”. Presented 01 Sep 2014. June 2014. URL: https://cds.cern.ch/record/1753849.

[25] W. J. Stirling and E. Vryonidou. “Electroweak gauge boson polarisation at the LHC”. In: *Journal of High Energy Physics* 2012.7 (July 2012). ISSN: 1029-8479. DOI: 10.1007/jhep07(2012)124. URL: http://dx.doi.org/10.1007/JHEP07(2012)124.

[26] Dieter Zeppenfeld. “Vector Boson Scattering: overview and prospects”. VBS Polarization Workshop LLR. 2018. URL: %5Curl%7Bhttps://indico.cern.ch/event/744263/contributions/3112025/attachments/1731352/2798335/VBS-Workshop-Paris-2018.pdf%7D.

[27] CMS Collaboration. “The CMS experiment at the CERN LHC”. In: *JINST* 3 (2008), S08004. DOI: 10.1088/1748-0221/3/08/S08004.

[28] The ALICE Collaboration et al. “The ALICE experiment at the CERN LHC”. In: *Journal of Instrumentation* 3.08 (Aug. 2008), S08002–S08002. DOI: 10.1088/1748-0221/3/08/s08002. URL: https://doi.org/10.1088%2F1748-0221%2F3%2F08%2Fs08002.

[29] The LHCb Collaboration et al. “The LHCb Detector at the LHC”. In: *Journal of Instrumentation* 3.08 (Aug. 2008), S08005–S08005. DOI: 10.1088/1748-0221/3/08/s08005. URL: https://doi.org/10.1088%2F1748-0221%2F3%2F08%2Fs08005.

[30] Julie Haffner. “The CERN accelerator complex. Complexe des accélérateurs du CERN”. In: (Oct. 2013). General Photo. URL: http://cds.cern.ch/record/1621894.

[31] T Gleisberg et al. “Event generation with SHERPA 1.1”. In: *Journal of High Energy Physics* 2009.02 (Feb. 2009), pp. 007–007. ISSN: 1029-8479. DOI: 10.1088/1126-6708/2009/02/007. URL: http://dx.doi.org/10.1088/1126-6708/2009/02/007.

[32] Wolfgang Kilian, Thorsten Ohl, and Jürgen Reuter. “WHIZARD—simulating multi-particle processes at LHC and ILC”. In: *The European Physical Journal C* 71.9 (Sept. 2011). ISSN: 1434-6052. DOI: 10.1140/epjc/s10052-011-1742-y. URL: http://dx.doi.org/10.1140/epjc/s10052-011-1742-y.

[33] Mauro Moretti, Thorsten Ohl, and Juergen Reuter. *O’Mega: An Optimizing Matrix Element Generator*. 2001. arXiv: hep-ph/0102195 [hep-ph].

[34] J. Alwall et al. “A standard format for Les Houches Event Files”. In: *Computer Physics Communications* 176.4 (Feb. 2007), pp. 300–304. ISSN: 0010-4655. DOI: 10.1016/j.cpc.2006.11.010. URL: http://dx.doi.org/10.1016/j.cpc.2006.11.010.

[35] Matt Dobbs and Jørgen Beck Hansen. "The HepMC C++ Monte Carlo event record for High Energy Physics". In: *Computer Physics Communications* 134.1 (2001), pp. 41–46. ISSN: 0010-4655. DOI: https://doi.org/10.1016/S0010-4655(00)00189-2. URL: http://www.sciencedirect.com/science/article/pii/S0010465500001892.

[36] J. Alwall et al. "The automated computation of tree-level and next-to-leading order differential cross sections, and their matching to parton shower simulations". In: *JHEP* 07 (2014), p. 079. DOI: 10.1007/JHEP07(2014)079. arXiv: 1405.0301 [hep-ph].

[37] Torbjörn Sjöstrand et al. "An introduction to PYTHIA 8.2". In: *Comput. Phys. Commun.* 191 (2015), p. 159. DOI: 10.1016/j.cpc.2015.01.024. arXiv: 1410.3012 [hep-ph].

[38] M. Bähr et al. "Herwig++ physics and manual". In: *Eur. Phys. J. C* 58 (2008), p. 639. DOI: 10.1140/epjc/s10052-008-0798-9. arXiv: 0803.0883 [hep-ph].

[39] Johannes Bellm et al. "Herwig 7.0/Herwig++ 3.0 release note". In: *Eur. Phys. J. C* 76.4 (2016), p. 196. DOI: 10.1140/epjc/s10052-016-4018-8. arXiv: 1512.01178 [hep-ph].

[40] ATLAS Collaboration. "Measurement of the polarisation of W bosons produced with large transverse momentum in pp collisions at $\sqrt{s} = 7$ TeV with the ATLAS experiment". In: *The European Physical Journal C* 72.5 (May 2012). ISSN: 1434-6052. DOI: 10.1140/epjc/s10052-012-2001-6. URL: http://dx.doi.org/10.1140/epjc/s10052-012-2001-6.

[41] CMS Collaboration. "Measurement of the Polarization of W Bosons with Large Transverse Momenta in W+jets Events at the LHC". In: *Physical Review Letters* 107.2 (July 2011). ISSN: 1079-7114. DOI: 10.1103/physrevlett.107.021802. URL: http://dx.doi.org/10.1103/PhysRevLett.107.021802.

[42] ATLAS Collaboration. "Measurement of $W^{\pm}Z$ production cross sections and gauge boson polarisation in pp collisions at $\sqrt{s} = 13$TeV with the ATLAS detector". In: *The European Physical Journal C* 79.6 (June 2019), p. 535. ISSN: 1434-6052. DOI: 10.1140/epjc/s10052-019-7027-6. URL: https://doi.org/10.1140/epjc/s10052-019-7027-6.

[43] E. Mirkes. "Angular decay distribution of leptons from W bosons at NLO in hadronic collisions". In: *Nucl. Phys.* B387 (1992), pp. 3–85. DOI: 10.1016/0550-3213(92)90046-E.

[44] Carsten Bittrich. *WZDecay*. https://github.com/carstenbittrich/WZdecay. 2015.

[45] Jan-Eric Nitschke. *WZDecay*. https://github.com/JanEricNitschke/WZdecay. 2019.

[46] D. Berdine, N. Kauer, and D. Rainwater. “Breakdown of the Narrow Width Approximation for New Physics”. In: *Phys. Rev. Lett.* 99 (11 Sept. 2007), p. 111601. DOI: 10.1103/PhysRevLett.99.111601. URL: https://link.aps.org/doi/10.1103/PhysRevLett.99.111601.

[47] Peter Richardson. “Spin correlations in Monte Carlo simulations”. In: *Journal of High Energy Physics* 2001.11 (Nov. 2001), pp. 029–029. DOI: 10.1088/1126-6708/2001/11/029. URL: https://doi.org/10.1088%2F1126-6708%2F2001%2F11%2F029.

[48] Andy Buckley et al. *Rivet user manual*. 2010. arXiv: 1003.0694 [hep-ph].

[49] Glen Cowan et al. “Asymptotic formulae for likelihood-based tests of new physics”. In: *The European Physical Journal C* 71.2 (Feb. 2011). ISSN: 1434-6052. DOI: 10.1140/epjc/s10052-011-1554-0. URL: http://dx.doi.org/10.1140/epjc/s10052-011-1554-0.

[50] I. Antcheva et al. “ROOT — A C++ framework for petabyte data storage, statistical analysis and visualization”. In: *Computer Physics Communications* 180.12 (2009). 40 YEARS OF CPC: A celebratory issue focused on quality software for high performance, grid and novel computing architectures, pp. 2499–2512. ISSN: 0010-4655. DOI: https://doi.org/10.1016/j.cpc.2009.08.005. URL: http://www.sciencedirect.com/science/article/pii/S0010465509002550.

[51] *TFractionFitter Class Reference*. https://root.cern.ch/doc/v606/classTFractionFitter.html. Accessed: 22.10.2019.

[52] *Multi-Boson Simulation for 13 TeV ATLAS Analyses*. Tech. rep. ATL-PHYS-PUB-2016-002. Geneva: CERN, Jan. 2016. URL: https://cds.cern.ch/record/2119986.

[53] Tanju Gleisberg and Stefan Höche. “Comix, a new matrix element generator”. In: *JHEP* 12 (2008), p. 039. DOI: 10.1088/1126-6708/2008/12/039. arXiv: 0808.3674 [hep-ph].

[54] Fabio Cascioli, Philipp Maierhofer, and Stefano Pozzorini. “Scattering Amplitudes with Open Loops”. In: *Phys. Rev. Lett.* 108 (2012), p. 111601. DOI: 10.1103/PhysRevLett.108.111601. arXiv: 1111.5206 [hep-ph].

[55] Steffen Schumann and Frank Krauss. “A Parton shower algorithm based on Catani-Seymour dipole factorisation”. In: *JHEP* 03 (2008), p. 038. DOI: 10.1088/1126-6708/2008/03/038. arXiv: 0709.1027 [hep-ph].

[56] Stefan Höche et al. “QCD matrix elements + parton showers: The NLO case”. In: *JHEP* 04 (2013), p. 027. DOI: 10.1007/JHEP04(2013)027. arXiv: 1207.5030 [hep-ph].

Danksagungen

Ich möchte allen danken, die mir während meines Studiums und speziell dieser Arbeit bei Seite standen. Ein großer Dank richtet sich allen voran an Prof. Dr. Michael Kobel, der es mir ermöglicht hat diese Arbeit zu einem so interessanten und aussichtsreichen Thema zu schreiben. Ein ebenso großer Dank gebührt Carsten Bittrich, der meine praktische Arbeit im letzten Jahr begleitet hat und mich jeder Zeit mit Rat und Tat unterstützt hat. Ebenso bedanke ich mich bei der gesamten VBS-Gruppe für das wöchentliche Feedback während der Meetings und für das Korrekturlesen der Arbeit, vielen Dank an Joany Manjarres, Stefanie Todt, Tim Herrmann, Abhishek Nag, Max Stange und Lilly Wüst.

Ebenso danke ich meinen Eltern, meiner Schwester und dem Rest meiner Familie, die immer ein offenes Ohr für mich hatten.

Zuletzt auch einen herzlichen Danke an Antonia. Danke für das Korrekturlesen aber vor allem dafür, dass du mir das letzte Jahr in allen Belangen beiseitegestanden hast. Danke, dass es dich gibt!

Erklärung

Hiermit erkläre ich, dass ich diese Arbeit im Rahmen der Betreuung am Institut für Kern- und Teilchenphysik ohne unzulässige Hilfe Dritter verfasst und alle Quellen als solche gekennzeichnet habe.

Jan-Eric Nitschke
Dresden, November 2019